LBL-29960

Center for Advanced Materials

CAM

Micromechanisms of Friction in Electrogalvanized Sheet Steel with Emphasis on the Role of Texture

S.J. Shaffer
(Ph.D. Thesis)

December 1990

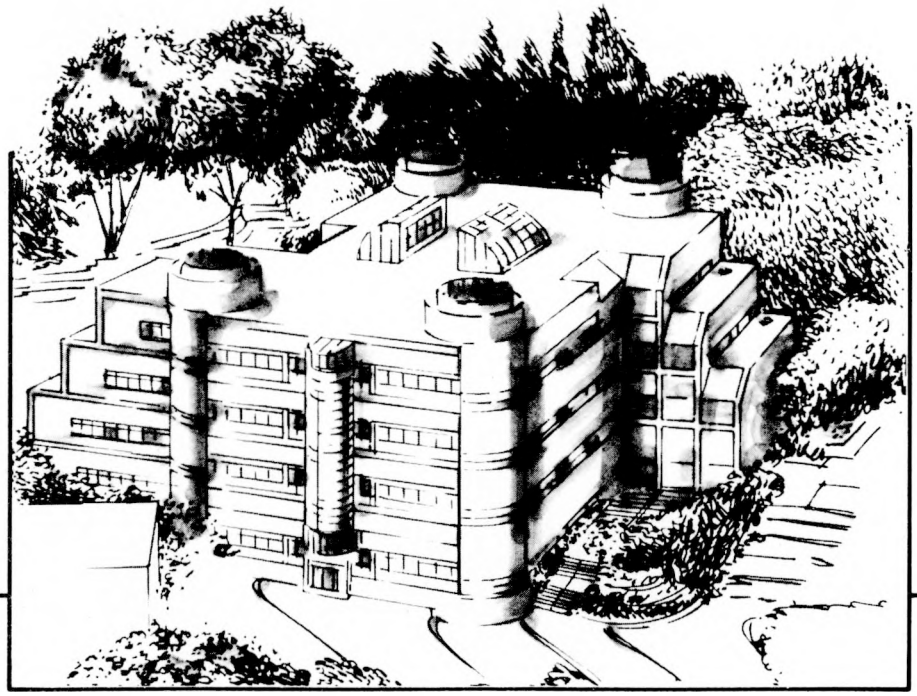

Materials and Chemical Sciences Division

Lawrence Berkeley Laboratory • University of California

ONE CYCLOTRON ROAD, BERKELEY, CA 94720 • (415) 486-4755

Prepared for the U.S. Department of Energy under Contract DE-AC03-76SF00098

LBL--29960

DE91 009113

MICROMECHANISMS OF FRICTION IN ELECTROGALVANIZED SHEET STEEL WITH EMPHASIS ON THE ROLE OF TEXTURE

Steven Jay Shaffer

Ph.D. Dissertation

Department of Materials Science and Mineral Engineering
University of California, Berkeley

and

Center for Advanced Materials
Materials Sciences Division
Lawrence Berkeley Laboratory
1 Cyclotron Road
Berkeley, California 94720

December 1990

This work was jointly supported by the Director, Office of Energy Research, Office of Basic Sciences, U.S. Department of Energy, under Contract No. DE-AC03-76SF00098, and by The Ford Motor Company, Rouge Steel Company, and LTV Steel Company.

Micromechanisms of Friction in Electrogalvanized Sheet Steel with Emphasis on the Role of Texture

By

Steven Jay Shaffer

ABSTRACT

The role of texture (preferred crystallographic orientation) of the zinc coating in friction of electrogalvanized steels is investigated. Samples of sharp 1) basal (fine grained and coarse grained), 2) low angle pyramid, 3) high angle pyramid, and, achieved through the addition of cadmium to the electrolyte, 4) prism textures, which were produced via laboratory electrodeposition, were friction tested using both a drawbead simulator (DBS) and a one-sided straight stripdraw test.

It was found that the initial texture of the samples did not influence friction through the zinc's anisotropic response to loading. However the fine grained basal samples did exhibit unusually high friction, which was attributed to a rapid increase in contact area fraction due to easy shearing of the individual zinc crystallites. In an opposite manner, the prism textured samples exhibited exceptionally low friction as a result of low contact area fraction, which was attributed to a combination of higher hardness and a rougher topography. It was found that DBS-μ correlated well with contact area fraction in both the laboratory samples and a set of commercial samples. It is concluded that those factors within the coating which dictate contact area fraction control friction. The two most prominent are surface roughness and hardness.

It was found through pole figure measurements that large changes in the texture of the zinc, restricted to a depth of about 1μm, take place as a result of friction testing. Progression toward a common texture is the result of plastic deformation, with strong evidence of recrystallization. In addition, there is evidence of some twinning for the low angle pyramid and prism textures. Calculations of resolved shear stresses for slip on the basal system corroborated this through predicted difficulty in deformation for orientations whose basal poles lie along a trace perpendicular to the macroscopic shearing direction.

Finally, techniques for rapid in-sheet-plane texture measurement and for deconvolution of textures as a function of depth and contact area fraction are proposed.

CONTENTS

LIST of FIGURES

INTRODUCTION

EXPERIMENTAL DETAILS

RESULTS

DISCUSSION

APPENDICES

Acknowledgements

Without question, the completion of this work would not have been possible without the constant support and encouragement of my wife Katie, who through the example of caring for our four children, as well as myself, during the 8 year course of my graduate study, including many many late nights at the lab, showed that hard work, patience, and perseverance do eventually pay off.

Beyond that, I owe my introduction to, and early tutoring in the field of sheet metal formability to Drs. Robin Stevenson, Stu Keeler, and Sig Hecker. I am greatly indebted to Prof. H. Rudy Wenk for his help in my education in the field of texture and deformation studies. Insightful discussions on tribology with Prof. John Schey and Mr. Mark Smith must also be acknowledged.

I could not have achieved either membership in the NADDRG or the level of satisfaction from my interaction with these colleagues without the encouragement and freedom to pursue my chosen field of interest from my advisor Prof. J.William Morris, Jr.. Bill's unwavering faith and support throughout my graduate "career" were remarkable.

I am grateful to those same colleagues in the NADDRG: Mr. Harmon Nine, Dr. Jim Story, Mr. Bob Hilsen, Dr. Dave Mueleman, Mr. Wayne Granzow, Mr. Carl VanKuren, and others too numerous to mention, for their advice and encouragement.

Mr. Norbert Izworski of the Ford Motor Company was instrumental in both encouraging the work undertaken and, more importantly, initiating the financial support necessary to complete such work, and I am deeply indebted. I am also grateful to my other "advisors": Mr. Peter Urcheck, also of Ford, Drs. Ron Miner, Joe Franklin, Jim Schrader, Jim Sprong, and Mr. Fritz Reis of LTV Steel, and Mssrs. Ron Hughes, Chuck Martin, and Mike Bingamin of Rouge Steel, for providing the industrial guidance necessary to attack this project. The formability testing equipment in the Advanced Technology and Materials Engineering Laboratory at Ford under Mr. Izworski and the experimental laboratory electrodeposition facilities at LTV Steel under Dr. George Eierman, were also indispensable in this work.

The helpful comments of my Thesis committee members, Professor J. W. Morris, Jr., Professor R. O. Ritchie, and Professor H.-R. Wenk are greatly appreciated.

Finally, I am indebted to The Ford Motor Company, Rouge Steel Company, and LTV Steel Company, who have jointly supported this work, along with the Director, Office of Energy Research, Office of Basic Sciences, U.S. Department of Energy, under Contract No. DE-AC03-76SF00098.

I INTRODUCTION

1. BACKGROUND

1.1 Electrogalvanized Steel : Use and Problem

Under aggressive environmental conditions, automotive body panels made from low carbon steel often suffer rapid deterioration due to corrosion which results in premature loss of service life (figure I1). The commitment to achieve the "ten year vehicle", combined with the increasing use of de-icing salts, has recently led to the widescale substitution of electrogalvanized (EG) steel for use in automotive body panels. The zinc layer provides both barrier protection, having a lower corrosion rate than bare steel due to the natural formation of oxides and hydroxides[I1], and, in the event of perforation of the zinc layer, sacrificial anodic protection of the steel[I2].

Unfortunately, the direct substitution of EG steel for bare steel has led to problems in the automotive stamping plants. Interestingly, EG steel is essentially the same low carbon steel which was previously used for autobody panels, now with the addition of a 5 to 10 μm thick layer of electrodeposited zinc on one or both sides. As such, the current specifications for EG steel are the same as those for the bare steel (i.e. mechanical properties and surface roughness) with the additional specification of zinc coating weight.

It is clear however that coating weight alone is inadequate for describing the differences found in pure zinc EG coated steels where large variations in coating attributes are found[I3]. The electrodeposition parameters[I4-I7] have been shown to have a large influence on the coating microstructure, morphology, and texture, which in turn affect its properties. As such, two nominally identical coils of steel with respect to specifications are sometimes found to possess very different forming characteristics.

Stamping failures are manifested by tearing or splitting of the sheet during forming. Results of mechanical testing however showed that no significant degradation of the mechanical properties of the bare steel base metal has occurred due to either hydrogen embrittlement or consumed elongation during the electrodeposition process (Table 1). Thus the stamping problems were determined to be a result of variations in frictional properties.

Typically a slight increase in friction is found with EG steels over bare steels[I8]. However extremely high friction is sometimes encountered resulting in excessive restraint in the binder and drawbead area of the die which leads to tearing of the sheet either at the die radius, in the unsupported region between the binder and the punch, or, less frequently, over the nose of the punch (figure I2). Occasionally, unexpectedly low friction is encountered which allows too much metal to flow into the die cavity and results in wrinkling. This research work was undertaken in order to determine the factors relevant to such variations.

The most critical problems with the application of EG steels for automotive use are: 1) variability in frictional properties, and 2) the current inability to specify parameters which will guarantee successful stampings.

Table 1 : Mechanical Properties of Bare Steel vs. EG Steel

	Y_s (MPa) / (ksi)	UTS (MPa) / (ksi)	e_{tot} (%)	n	$\bar{r}$
Good DQ Steel	172-207 25-30	290-317 42-46	42-48	.21-.23	1.5-2.0
Electrogalvanized Steels (11 samples, 8 manufacturers) (μ : .10 -.27)	199 28.8	310 45.0	42.1	.213	1.88

Y_s = Yield Strength in Uniaxial Tension UTS = Ultimate Tensile Strength

e_{tot} = Total Elongation of 2" gage length σ = stress ε = strain

n = strain hardening coefficient for material which can be described by : $\sigma = K \varepsilon^n$

r = plastic anisotropy ratio = $\varepsilon_3 / \varepsilon_2$ $\bar{r} = \frac{r_0 + 2r_{45} + r_{90}}{4}$

1.2 EG Steel and Lubricants

It is not uncommon, when frictional problems are encountered, to approach a solution from the standpoint of the lubricant. To date however, attempts to solve the frictional problem through the use of lubricants have been largely unsuccessful for several reasons. First, the present body of lubricant knowledge for automotive sheet forming has been gathered primarily from experience on bare steel and has proven inapplicable to EG steel. These same lubricants have been shown to reverse the rankings of several galvanized steels[I9] in drawbead simulation (DBS) tests. Such DBS tests have been shown to have excellent correlation with press shop performance[I10].

Further, the production of an automobile entails an interdependent system. Subsequent to forming the part, it must be cleaned for downline operations such as welding and painting. As such, any lubricant which is applied to facilitate formability must not adversely affect later production stages. In addition, lubricant application in the press shop is both costly and messy, and it is the current desire of some automotive companies to eliminate additional lubricant application in the stamping plants[I11].

2 DIRECTION of RESEARCH

2.1 Overall Objective

It is apparent that what is lacking is an understanding of the determinants of friction in EG steel. The overall goal of research in this field is to determine the factors, both metallurgical and morphological, which control friction during forming of EG sheet steels. Once these factors are defined and their relative importance determined, measures can be

taken either in the steel sheet production or during the electrodeposition process, or both, to help insure consistent and predictable frictional values.

Early in this investigation, a comparison of bare steel versus EG steel was made with the goal of identifying significant areas of research to pursue(I3). The results of that study indicated three major differences between bare steel and EG steel : 1) topographical - due to the zinc micro-roughness (figures I3, I4), 2) chemical - through possible reactions with lubricant additives, and 3) mechanical - through the highly anisotropic slip characteristics and relative softness of the zinc.

The role of this third feature was of prime interest to this investigator with regard to friction and the role of texture shall be the main focus of this work. Here we restrict the use of the word texture to that describing the preferred crystallographic orientation of the ploygranular zinc coating as opposed to its surface topography, which is also sometimes referred to as texture.

It has become common to categorize the texture of a zinc coating by referring to the predominant type of plane which is parallel to the surface of the sheet, for example : basal, low angle pyramid, high angle pyramid, or prism textures. Alternative references, such as the tilt angle of the basal plane to the sheet plane, or specific plane indices are sometimes used. These are shown schematically in figure I5.

2.2 Present Objective

This thesis will focus on the role of the texture of the coating and address the issue of how and whether the anisotropic mechanical properties of zinc may affect friction in quasi-hydrodynamically lubricated stripdrawing of strongly textured coatings.

In addition, other factors such as surface macro-roughness, micro-roughness (zinc crystallite morphology), hardness, and ease of material transfer, all of which contribute to the coefficient of friction, will be considered and discussed.

While a complete model, which would allow the prediction of coefficients of friction in EG steel, requires the understanding and consideration of the interaction of many dozens of variables within the tooling/lubricant/workpiece system (figure I6)(I12), such a theoretical predictive model, if possible, is far down the road. This work will be restricted to investigation solely of the influence of factors within the zinc coating itself. As such, this will be an applied research study, within the scope of identifying the micromechanisms and controlling parameters of friction in EG steel. It is intended that the results of this study will add a piece or two to the larger puzzle and thus will assist in determining the proper direction for further studies.

3 FRICTION

Webster's defines friction as : 1) the rubbing of one body against another, or 2) the resistance to relative motion between two bodies in contact. It is the second definition with which we are concerned regarding the mechanisms in EG steel.

There are a great many factors which dictate this resistance to relative motion. As such, early tribologists have, in an attempt to simplify the situation, divided friction up into a number of regimes, each of which has it's own controlling factors and characteristic range of μ (coefficient of friction). This simplified categorization scheme, along with some

friction models, is reviewed in appendix A to which the reader is referred for details. Included below are the points relevant to this work.

3.1 The Friction "Surface"

The friction "surface" of a material (or system) is comprised of both its physical (topographical and mechanical properties) state and chemical state. Each of these, along with the lubricant properties, contribute to the operational friction regime.

3.1.1 Physical State

Nominally "flat" contacting surfaces are microscopically very rough, and are composed of many peaks and valleys which are the result of prior processing stages (figures I3 and I7). Under incomplete hydrodynamic conditions, two surfaces in nominal full contact actually touch only at the asperities, or high points. The topography, mechanical properties of the surface (principally hardness), and the presence of, and viscous properties of a lubricant, in concert with the loading conditions, are the main determinants of the extent of contact area.

3.1.2 Chemical State

Many of the fundamental experimental works on friction have been performed under extremely careful, high vacuum conditions, on "atomically clean", single crystal surfaces. The work of Buckley[I12] is the best known. Under these circumstances, substantial junction formation (adhesion via cold welding) takes place, and the results of tests can be interpreted readily in terms of the physical properties of the materials being tested.

Under ordinary "atmospheric" conditions, the surface of a metal is far from clean, and typically possesses a thin oxide, adsorbed gases (including water vapor), and for automotive sheet steel, the residue of one or more "protective" and "cleaning" oils, and the "stamping" lubricant (which usually contains an additive to promote the formation of boundary compounds). These "contaminants" dictate the extent of junction formation.

For this study, we make use of only a light, rust preventative, napthenic oil, containing no boundary compound forming additives - a mineral seal oil (MSO). MSO of viscosity 60 SUS provides a medium in which some limited local hydrodynamic lubrication takes place, yet is otherwise considered a "poor" lubricant. We use this in order to distinguish frictional differences due to variations in coating properties only. "Good" lubricants can mask such differences.

3.2 The Role of Plastic Deformation

Examination of the surface of a piece of EG steel which has undergone simulative friction testing (or a production part as well) reveals extensive plastic deformation of the zinc on the macroroughness asperities, or high spots, while in the valleys, the micro-roughness remains apparently undeformed (figure I8). As such, one might expect the plastic deformation characteristics of the zinc to play an important role in friction. Indeed, several models for frictional resistance to sliding are based on plastic deformation of soft asperities by hard ones, or of shearing of cold welded junctions at the interface[I14-I17].

4 PROPOSED EFFECT OF TEXTURE

There are two primary ways in which texture may be seen to affect friction: 1) anisotropic plastic response to loading, and 2) ease of transfer of zinc to the tooling.

4.1 Anisotropic plastic response to loading

Zinc has anisotropic plastic properties. Its hexagonal close-packed (hcp) structure and high c/a ratio (1.856) lead to slip restricted to the basal plane and twinning as the primary deformation modes. In comparison, face centered cubic (fcc) metals have 12 equivalent slip systems, while body centered cubic (bcc) metals have 48 slip systems.

Since the surface of the zinc coating is severely deformed during strip drawing or sheet forming, it would seem to follow that the anisotropy of plastic properties would manifest itself in some way during these processes. As such one might expect strong textures to influence the frictional response in EG steels. This might particularly be expected in light of the extremely sharp textures which are found in the zinc coatings of EG steels. In a simple single crystal model, it would be easiest to deform zinc by simple shear for basal textured zinc and more difficult for all other orientations. As such, basal oriented EG coatings would appear, at first thought, to be desirable for low friction.

4.1.1 Prior Work Proving Effect of Structure and Anisotropy

Indeed the work of Buckley[I18] showed that hcp metals had lower friction than fcc metals of similar hardness (due to restricted slip) and that for titanium (hcp, c/a = 1.587) friction on prism planes in the close packed direction was lower than that on the basal planes[I19]. In extending these results to zinc (on which Buckley did not perform experiments), one would expect the opposite case; lower friction on the basal planes compared to the prism planes, since zinc has a high c/a ratio and hence more closely packed basal planes than the prism planes, and correspondingly the opposite slip planes.

However, the applicability of that extremely high vacuum, low strain rate work, where actual junctions were formed and sheared, is questionable to "terrestrial" or production situations, where as previously discussed, the surfaces are covered with several layers of contaminant films. This point holds true for all models which emphasize shearing of welded junctions.

4.1.2 Applicability of Prior Friction Modelling Work and Anisotropy

In all of the asperity "deformation" models, whether or not the premise of junction formation is made, the assumption of an isotropic "shear strength" is used. This is necessarily true of all slip line field analyses. The anisotropic slip characteristics of zinc give rise to questioning the validity of such analyses for EG steel. Recent analysis by Rangarajan, et. al.[I20] makes use of the Wandheim and Bay[I17] model, taking into account the anisotropy of zinc. Using such analysis, they conclude that basal oriented zinc should provide the lowest resistance to "shearing", and therefore it should have the lowest coefficient of friction. This was not experimentally confirmed for EG coatings in their work however.

Despite these simplified, intuitively appealing viewpoints of low expected friction for basal textured coatings, in experiments on laboratory samples of strong basal texture by Lindsay, et. al.[I21], as well as some of our early tests on commercial samples[I22],

significantly higher coefficients of friction have been found on some basal oriented electrodeposits.

4.2 Transfer of Zinc

The second way in which texture may be seen to influence friction is through the possible role it may play in the transfer of zinc to the tooling. This may occur through either flaking or adhesion and shearing. Indeed, for the same reason one might expect low friction (easiest shear) for basal oriented zinc, one might also expect this orientation to be the most prone to removal via complete shearing of an individual crystallite.

Alternatively, the phenomenon known as powdering, manifested by intracoating cracking may be influenced by texture. This typically occurs in alloy coatings containing brittle intermetallics such as the Γ phase in Zn/Fe galvannealled coatings[I23,I24]. In the case of pure zinc coatings, where no intermetallics are present, powdering might be promoted by orientations such as prismatic textures, where easy flow parallel to the surface is not possible by slip on the basal planes.

Both these possible phenomena have been the subject of research as well as debate at recent symposia[I25,I26].

5 DESIGN of EXPERIMENTS

In this work the goal was to both document the effect of texture on friction of EG steels, and to investigate the frictional mechanisms operating during stripdrawing.

It was necessary to first obtain samples of sharp textures. One-sided electroplating of samples was accomplished at the LTV Steel Co. Research Center in Independence, Ohio. All characterization was performed at U.C. Berkeley and Lawrence Berkeley Laboratory.

Subsequently, it was desired to test them in a manner in which measured frictional differences could be distinguished in an environment similar to that in which they are used. Thus the drawbead simulator (DBS), modified to restrict the differences in measured friction to the zinc coated side only, or one-sided drawbead simulation, was chosen.

Additionally, a test from which some fundamental information could be obtained regarding the mechanisms of friction within the coating itself, without any influence of the substrate, was desired. One-sided stripdrawing was chosen for this test. In this test a series of loads was determined in which the changes in contact area fraction, as a function of load, of the zinc alone could be monitored. DBS friction testing and stripdrawing were done at the Advanced Technology and Materials Engineering Laboratory of Ford Motor Company in Dearborn, Michigan. Details of the deposition and testing procedures are given in Part II.

6 INTERPRETATION of RESULTS

6.1 DBS : Coefficient of Friction

The derivation for computing the coefficient of friction using a DBS makes use of several simplifying assumptions. The most significant of these are: 1) that the normal force is distributed uniformly over the contact area, and 2) that friction is constant and independent of normal load (Coulombic Friction). Whether these are strictly valid will influence the absolute value of the calculated coefficient of friction. As such, numbers

obtained, particularly in the one-sided modification of the test, cannot be compared to values obtained in another type of friction test. The relative values however, for a series of similar strips tested under identical conditions, do not depend on the validity of these assumptions and can be used for internal comparison, as was done in this work.

6.2 Stripdraw : Dependent Variables

In straight stripdrawing, where the coefficient of friction concept is used and the area fraction deformed is measured, it is important to recognize the proper dependence of variables. For example, take two materials which are tested in a series of straight stripdrawing type test under a range of normal loads. During the tests the normal load and resulting pulling load are monitored and recorded, and after testing, the area fractions for each normal load are measured. In such a test, for two materials with similar plastic properties and surface topographies, the area fraction will depend on the normal load, while the pulling load will depend on the area fraction. As such, the pulling load will depend on the normal load and the slope of a plot of normal load versus pulling load will give the coefficient of friction. These relationships are shown schematically in figure I9.

If a given normal force gives rise to a constant contact area fraction, then on a plot of area fraction versus pulling force the material with the higher slope should correspond to a higher coefficient of friction. This is shown schematically in figure I10. This approach is similar to the one used by Nakamura, et. al.[I27], in experiments in which they investigated the effect of drawing velocity and lubricant oiling weights on various types of zinc alloy coatings.

7 SUMMARY of WORK

In this work we show that the texture of the zinc is not a dominant controlling factor of friction through its anisotropic plastic response to loading. This is a result of rapid evolution to a common texture of a very thin surface layer, due primarily to recrystallization of the zinc in the deformed region. The contact area fraction was found to correlate well with coefficient of friction in the DBS test. As such, hardness and surface roughness are the most influential factors in determining friction in EG steels.

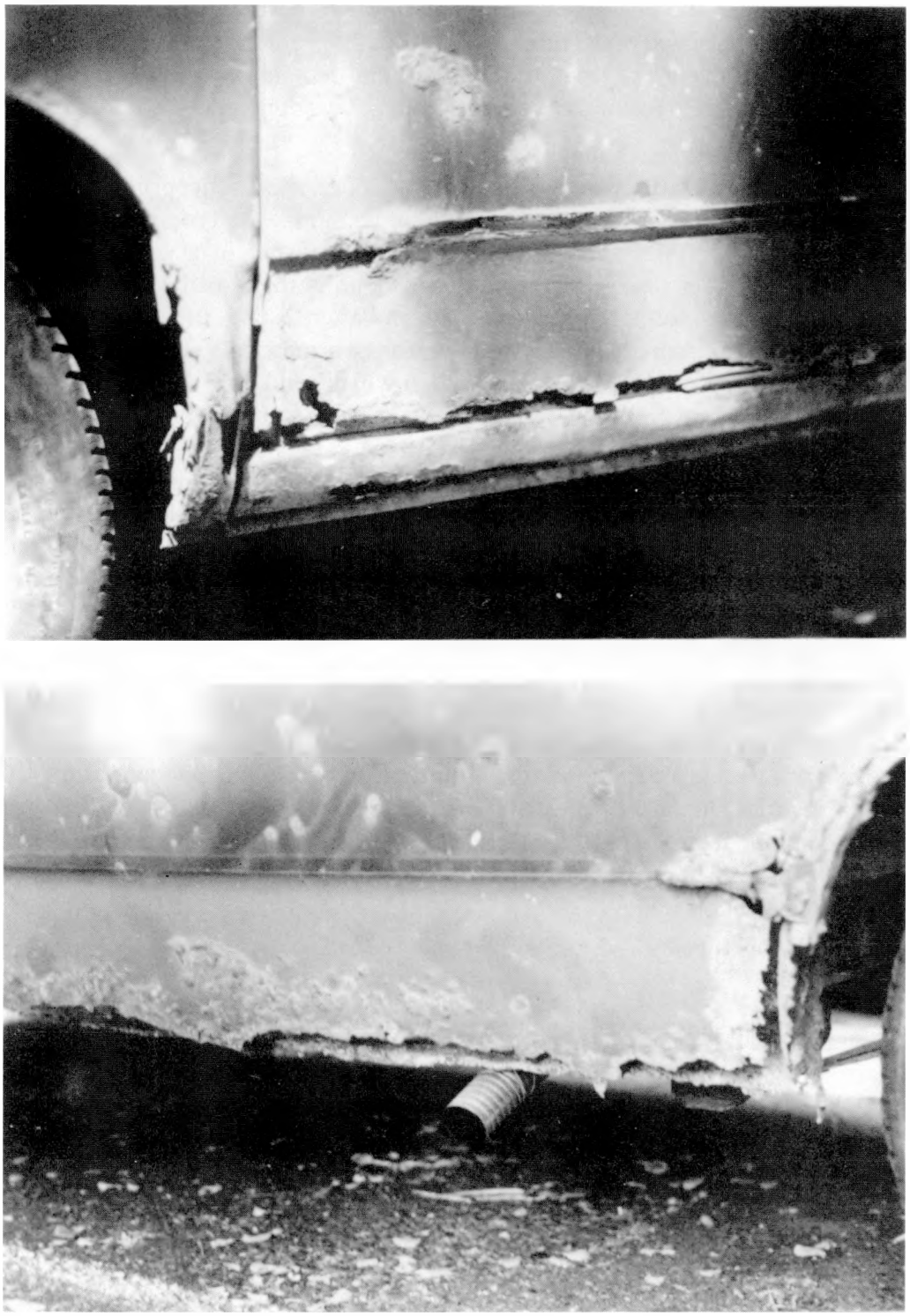

XBB 900-8637

Figure I1) Accelerated deterioration of automotive outer body panels due to aggressive environmental conditions induced by the use of de-iceing road salt.

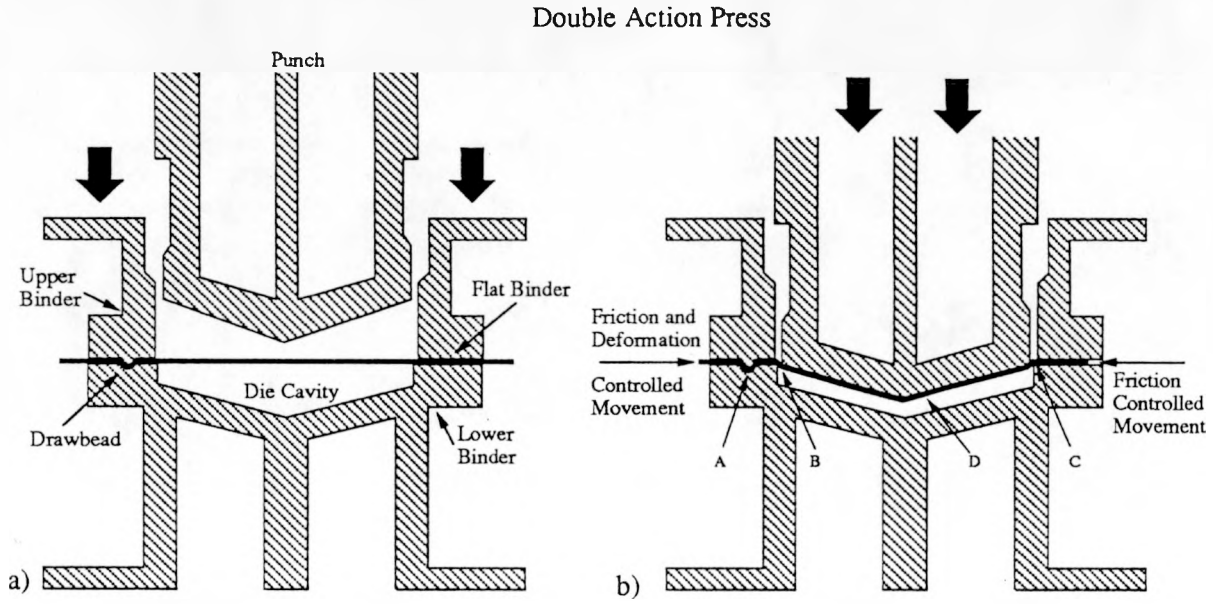

Figure I2) Schematic cross-section of a dual-action stamping press. a) The outer binder first clamps the sheet in place. b) The punch subsequently comes down and deforms the sheet into the die cavity. Failures are seen to occur A) in the drawbeads, B) in the unsupported region between the binder and the punch, C) at the die radius or punch shoulder, or D) over the nose of the punch. Figure adapted from reference I10.

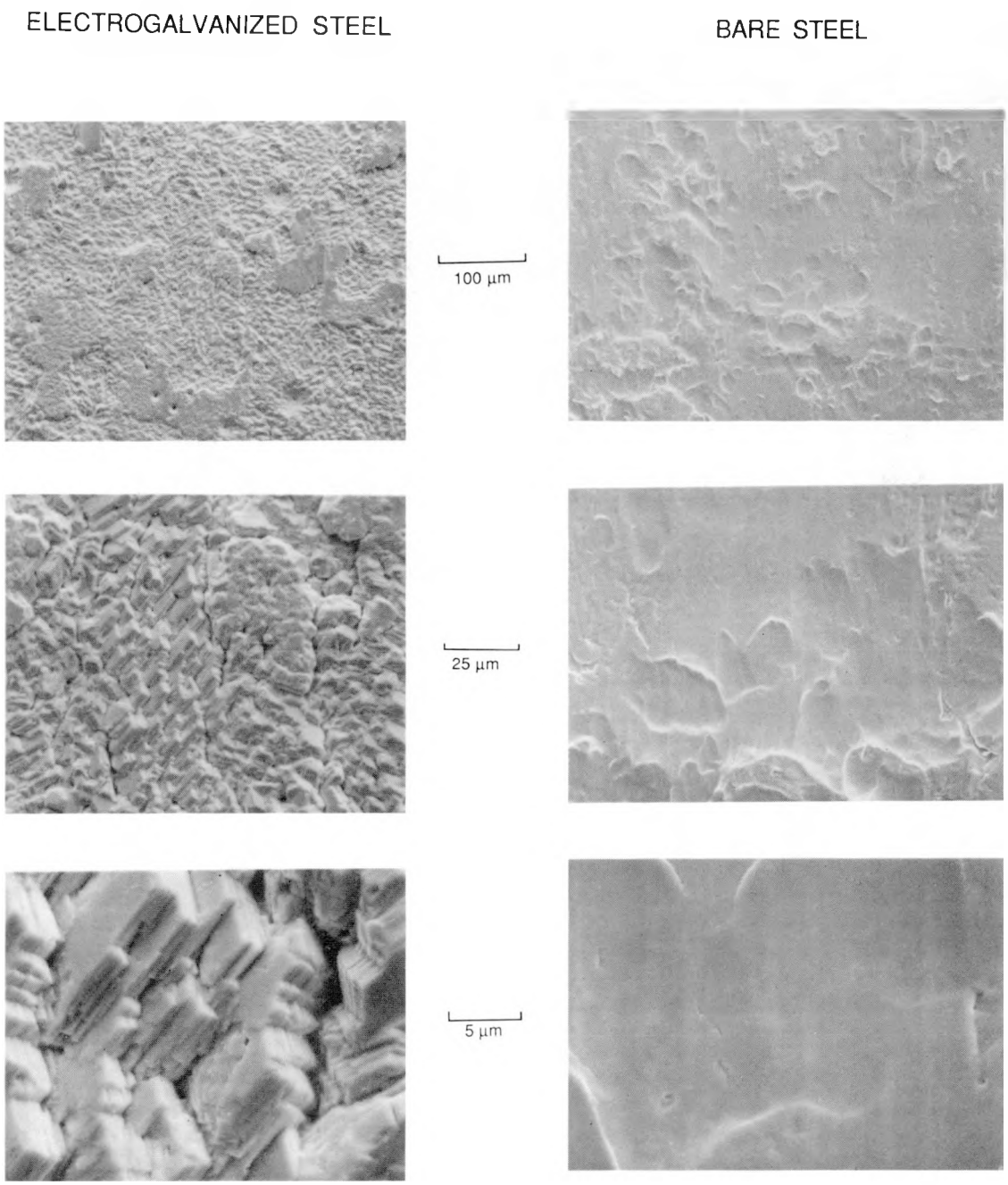

Figure I3) Graphical definition of microroughness is shown in these surface SEM micrographs of a commercial EG steel and bare steel. Between the asperities and dimples of the macroroughness (resulting from temper rolling) the bare steel is extremely smooth, while that of the EG steel can be remarkably rough.

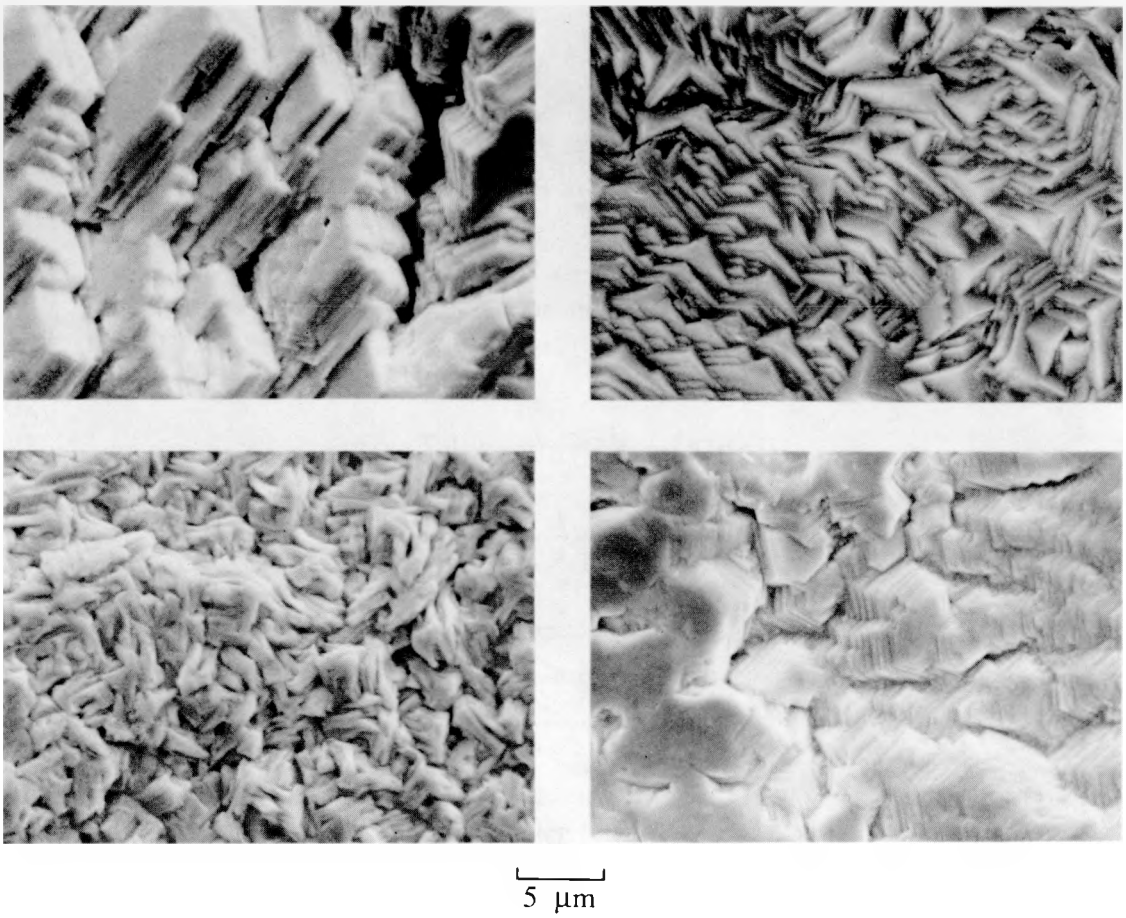

XBB 887-7145

Figure I4) Examples of the variations of microroughness which can be found in commercial EG steel. The microroughness is a result of the zinc crystallite morphology and is determined by the electrochemical deposition conditions. (SEM micrographs)

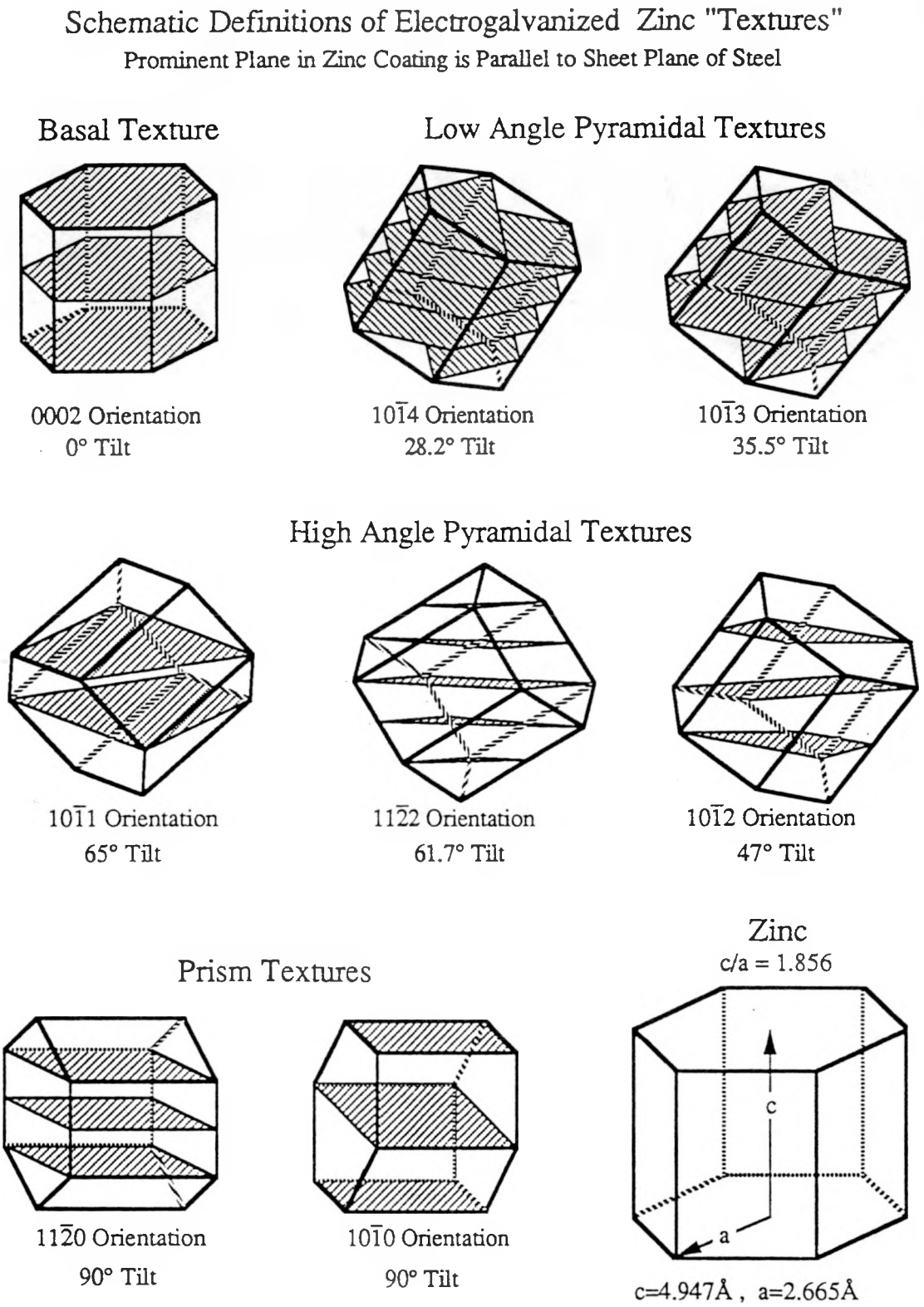

Figure I5 Schematic examples of "textures" in zinc crystals. Texture can be defined by either the type of plane parallel to the sheet, by the angle of the basal plane to the sheet plane, or by the specific plane parallel to the sheet.

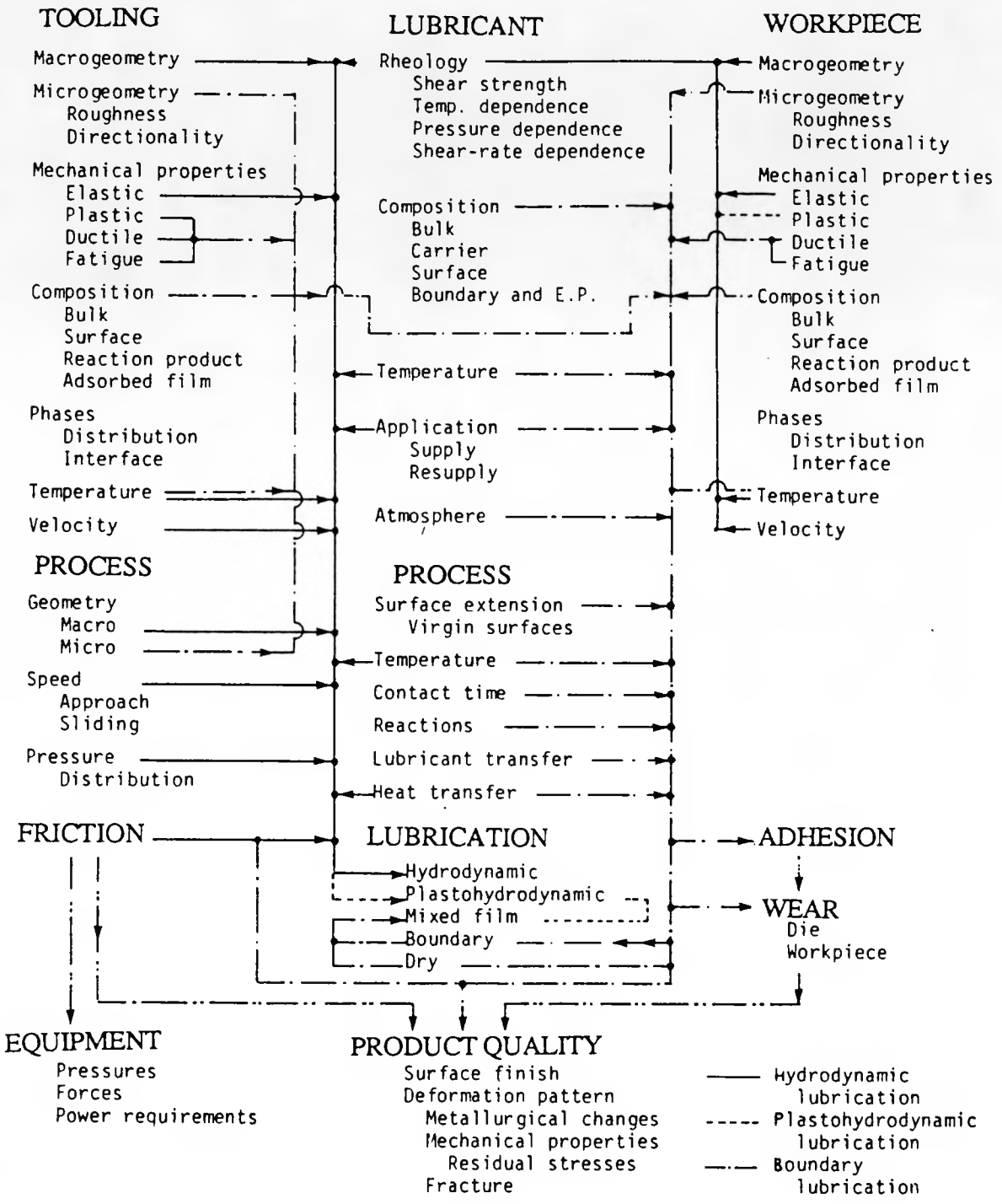

Figure I6) Frictional resistance is determined by a complicated inter-relationship of many parameters within the tooling/lubricant/workpiece system. (Adapted from reference I12)

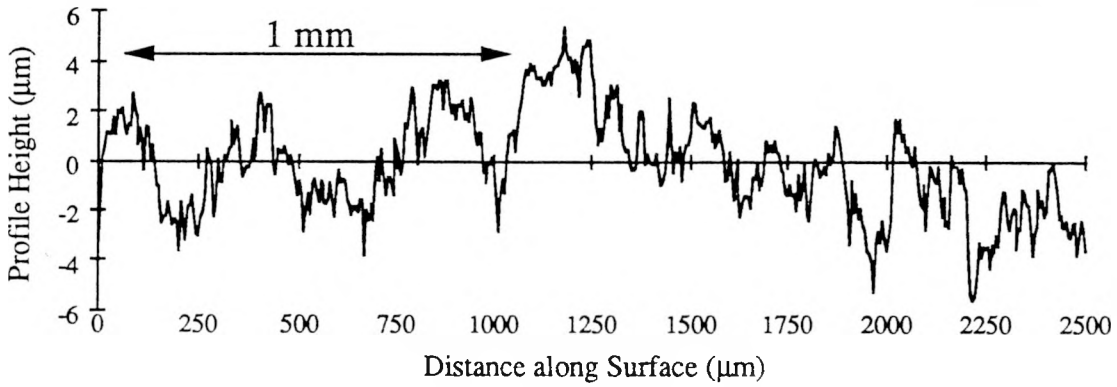

Figure I7) Example of surface profile obtained from a mechanical stylus profilometer trace of an electrogalvanized steel surface. Note that the vertical magnification is 64 times that of the horizontal. The topography results from the superposition of the cold rolling, temper rolling, and electrogalvanizing processes.

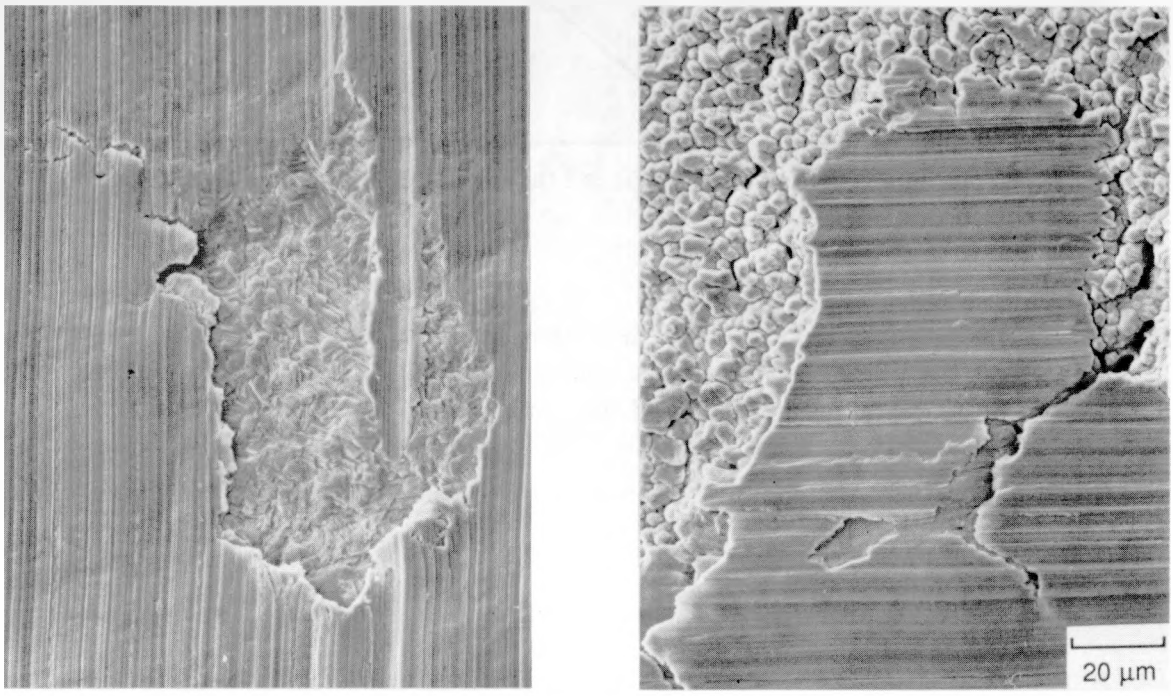

a)

b)

XBB 880-11499

XBB 891-318

Figure I8) The severe deformation of the zinc surface on the contacting asperities is shown by these high magnification SEM micrographs of the surface of two different EG surfaces after strip draw friction testing. In each case the microroughness in either a) an isolated valley, or b) a low area surrounding an isolated mesa, is left undisturbed.

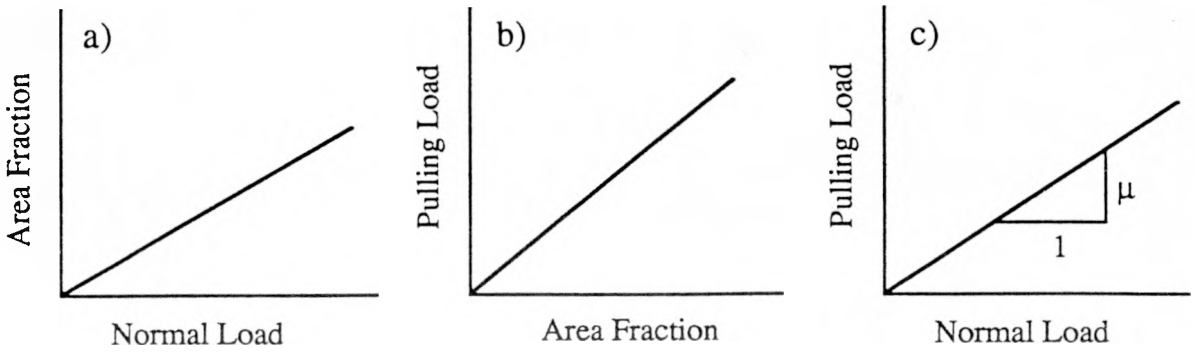

Figure I9) Schematic illustrations of the dependence of a) contact area fraction on normal load, b) pulling load on area fraction, and hence c) pulling load on normal load. The slope of the pulling load vs. normal load plot gives the coefficient of friction - μ.

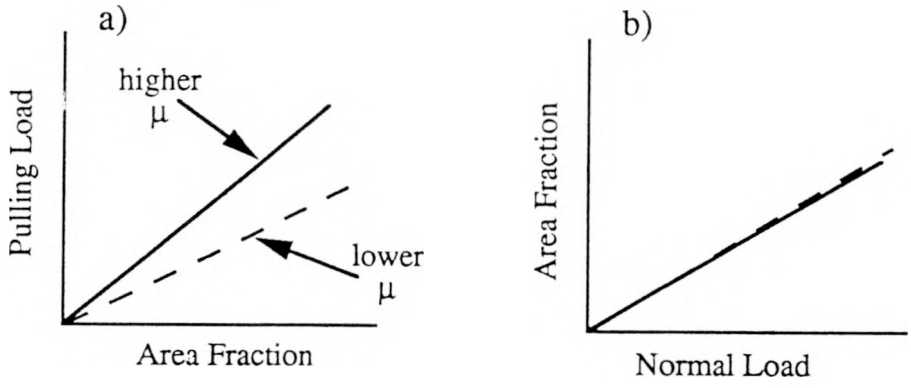

Figure I10) Schematic illustration of two materials which exhibit a) different dependence of pulling load on area fraction, for b) similar dependence of area fraction on normal load. The steeper the slope, the higher the expected coefficient of friction.

II EXPERIMENTAL DETAILS

Commercial EG sheets from different manufacturers have variations in practically every aspect, from substrate mechanical properties and surface roughness, to zinc crystallite morphology, texture, and hardness. Since friction may depend on all these factors, it has, up to now, proven extremely difficult to determine why one sheet may have a lower (or higher) coefficient of friction than another. As such, investigations utilizing single parameter variations, such as texture, are only possible using laboratory prepared samples.

In order to isolate variables, sheets of a typical commercial aluminum killed drawing quality (AKDQ) steel, cut from a single coil, were electroplated with zinc in a laboratory simulator in which various electrodeposition parameters could be controlled. Using such a simulator, the substrate mechanical properties and surface topography could be fixed, and differences due only to the coating properties could be investigated.

1 SPECIMEN ELECTRODEPOSITION

A rotating cathode electrodeposition simulator, constructed and operated by the LTV Steel Research Center in Independence, Ohio was used to obtain samples of widely varying textures. A 150mm by 600mm (6" x 20") sheet of drawing quality cold rolled steel was rolled into a cylinder. This was then mounted such that the cylinder axis was vertical and was immersed into a reservoir of electrolyte containing a 25mm by 150mm insoluble anode. The cell configuration is shown schematically in figure E1. In the sulphate bath, the temperature, flow rate, line speed, pH, current density, and zinc concentration were varied between two extreme values, giving a total of 64 different process conditions. (The precise values of the parameters are propriatary to LTV steel.) In addition, other inorganic and organic additives could be incorporated in the electrolyte. One-sided deposits corresponding to a G70 coating ($\approx$10μm thick) were made for all conditions.

The resulting deposits from the 64 different conditions were characterized for texture and microstructure. From these, samples of sharp basal (both fine grained and coarse grained), low angle pyramid, and high angle pyramid were selected for testing. After no prism oriented samples were obtained with pure zinc, trace metallic additions were made to the electrolyte and it was found that the addition of cadmium produced samples with a near prism orientation. The surface morphology and textures, represented by percentage of planes in the sheet plane, are shown in figure E2 along with schematic drawings of zinc crystals oriented corresponding to the measured textures. These specimens, labelled A through E, were used in the friction studies.

2 CHARACTERIZATION

2.1 Texture Measurements

Two different methods of texture measurements were used in this work. The first method, described in detail in Appendix B, was used to survey the series of experimental electrodeposits to identify sharp textures. The results of this normalization technique can be plotted in such a manner as to quickly identify the general "texture" of the coating as

shown schematically in figure E3. This method however, gives only the relative proportions of grains with a particular plane parallel to the sheet surface with no information about rotational distributions - hence a fiber texture is assumed. For applications such as paint adhesion[E1] or corrosion resistance[E2], this method may be sufficient. However for quantitative modelling and deformation studies, a more complete description of oriention distributions, and hence a different method of measurement, is required.

The second method for texture determination is the standard Schultz[E3] reflection pole figure method. Here, the distribution of a particular "pole" (the normal to a plane) is measured and described relative to the specimen coordinates. The geometry is depicted in figure E4[E4]. Since the reflection method is only accurate out to a tilt angle ($90-\chi$) of about 70°, the measurement of several pole figures and subsequent computation of the orientation distribution function (ODF) is necessary for truly quantitative results. In this work, the 0002, $10\bar{1}0$, $10\bar{1}1$, and $10\bar{1}2$ pole distributions in the zinc coatings were measured and the ODF was computed using the POPLA[E4] software package. The recomputed 0001 pole figures are presented in this work.

Measurements were made in the U.C. Berkeley Structural Geology Laboratory of Prof. H.-R. Wenk using a Scintag/Nonius diffractometer system with Fe K_α radiation. Intensities were collected for ten seconds at each position for ($90-\chi$) from 0° to 85° and ϕ from 0° to 355° with a step spacing of 5 degrees.

2.2 Friction Testing

Every computed "coefficient of friction" depends on the type of test in which it was measured. There still exists debate as to which is the "best" test for sheet metal forming. Variations include pulling a strip between two flat blocks, between a flat block and a cylinder, two cylinders, etc., with only elastic deformation of the sheet, as well as tests in which the substrate is plastically deformed, around single or multiple "bead" configurations of various radii. In this study, two types of tests were performed. A straight stripdraw type test and a drawbead simulation test.

For both tests, 38 mm (1.5 in.) wide samples were first cleaned in acetone, then rinsed with ethyl alchohol and finally with isopropyl alchohol to remove any residual mill oils, followed by hot air drying. Prior to testing, the strips were saturated lubricated on both sides with a 60 SUS mineral seal oil applied with a paint brush. All tests were run under stroke control at a speed of 85mm/sec (200 in/min) with a total stroke of 150mm (6 in). Pulling and clamping loads were recorded and stored digitally.

2.2.1 Stripdraw Friction Tests

To quantify the effect of plastic deformation of the zinc alone, and to gain insight into the frictional mechanisms, samples were tested using a straight stripdraw-type test. With no bending and unbending of the substrate, the use of a large "frictionless" roller against the bare steel side, and selection of the proper load ranges, frictional effects due to plastic deformation of the zinc alone was possible. The test geometry made use of a 9.5mm (3/8") diameter fixed cylindrical bead against the zinc side of the sheet and a 25.4mm (1") diameter free rolling cylinder on the back (bare steel) side as shown schematically in figure E5a. Nominal loads of 23, 45, 91, 159, 250, and 351 kg_f (50, 100, 200, 350, 550, and 775 pounds) were used. The bead material was D2 tool steel hardened

to Rockwell C62 and polished with 600 grit SiC paper, then 0000 steel wool in the longitudinal direction. The same bead was used in both the stripdraw and the one-sided DBS test (below).

2.2.2 Drawbead Simulation - DBS

The drawbead simulator, developed by Harmon Nine[I10] at General Motors in the late 70's, has lately come into broad acceptance as a reliable predictor of press shop performance of friction in the drawbead area of stamping dies. This is not surprising as the geometry, speeds, tool material, and lubricants used are all representative of those used in production. While it was originally meant to be used to rank lubricants, if the lubricant is kept constant, it can also be used to compare frictional variations among coated steels.

In this test, only a single normal load or pressure is possible, and is determined by the thickness, width, and mechanical properties of the sheet and the setting of the spacing between the sets of beads. For our tests the clamping load was typically around 363 Kg_f (800 lbs).

The idea behind the test is to simulate the geometry of the sheet in the drawbead portion of the die, and to be able to separate the restraining force due to friction from that due to plastic bending and unbending of the sheet. To accomplish this, two sets of "beads", of identical geometry and material, are used. One set is mounted on "frictionless" bearings and hence the measured pulling load is due only to the plastic deformation of bending and unbending of the strip. The other set of beads, used in subsequent tests, is fixed, and thus the measured pulling load has an additional component due to frictional sliding on alternating surfaces of the strip.

The difference in load required to pull pairs of identical strips through each set of beads is attributed to friction. The test analysis assumes Coulombic friction, i.e. friction coefficient independent of normal load, and that the normal load is uniformly distributed along the contact area. Usually three strips are tested in each fixture and the results are averaged. In this work, two roller bead and four fixed bead samples of each texture were tested. As expected, the roller bead loads for all the strips were constant, since all were on the same substrate steel. The details for the test and calculation of coefficient of friction can be found in Nine's papers[E6-E8].

In order to isolate effects due to the zinc coating alone, a modified, one-sided version of the test (figure E5b) was used in this work. In this case:

$$\text{OSDBS-}\mu = \frac{F_{Pf} - F_{Pr}}{(\pi/2)\,F_{Nf}} .$$

where F = measured force or load, P = pulling, N = normal, f = fixed beads, and r = roller beads.

2.3 Contact Area Fraction

In order to measure the contact area fraction of the surface of a strip after friction testing, it is necessary to have a technique which can distinguish the contacted versus uncontacted regions. Sufficient contrast must be present, depending on the instrument and sample, for accurate determination. Fortunately, in the case of EG steel, the microroughness due to the fine zinc crystallites on the surface provides such contrast.

When a beam of incident light is reflected off the surface of EG steel, the microroughness of the EG coating causes a significantly greater proportion of diffusely scattered compared to specularly scattered light. This is illustrated schematically in figure E6. As a result, after deformation of the strips, when viewed through a microscope under normal incident reflected light, the regions of the surface which were "burnished" or deformed (the contact area) appeared shiny in comparison to the undeformed regions, in which the microroughness still persisted. This contrast, which can be seen in figure E7, allowed the fraction of deformed (bright) to undeformed (dark) regions to be determined using a Buehler Omnimet image analyzer system. Measurements were taken directly through a microscope at a magnification of 60x.

Since the DBS-μ values represent an average of the local clamping and pulling loads over the whole specimen width and length, it was necessary to measure the contact area fraction over the entire specimen surface, and average these results. The strips were divided into a grid of 20 regions with at least 3 measurements taken in each region. These measurements were then averaged to give the area fraction for each strip at each load. For the DBS tests, the results from all four fixed bead strips were averaged.

2.4 Hardness

There is no standardized method for obtaining the hardness of thin zinc coatings which have been electrodeposited on steel. The loads required must be extremely light in order that the steel substrate does not produce an "anvil" effect. For accurate measurements, the depth of penetration must be less than one tenth the thickness (or, the diagonal less than 1.5 times the thickness)[E9]. In using loads light enough to satisfy this requirement (on the order of less than 2 grams), both the macro-roughness and micro-roughness create difficulty in obtaining well defined impressions from which the diagonal diameter may be accurately read.

One method, common among Japanese researchers[E10], has been to test the Vickers Hardness of special laboratory deposited 100μm thick coatings and assume it is the same for the thinner coatings. This has obvious drawbacks.

A second method is to make use of a "nano-indenter" and obtain a plot of load versus depth such as is common in electronics thin film research. This method requires a smoothly polished surface, thus changing the original properties through deformation of the surface. Additionally, it provides information from an extremely small area, likely to lose any relevance to the bulk coating characteristics.

Sometimes Knoop Hardness is measured in cross-section with the long diagonal parallel to the coating/substrate interface using extremely light loads on the order of 1 gram. The relevance of this method to surface deformation hardness is questionable as well, as it has been shown to vary significantly with orientation in anisotropic materials[E11]. It is clear that there is not really a good method.

In this work a compromise was made. Plane section samples were very lightly polished using 0.25 μm diamond paste. This smoothed the tops of the macroroughness asperities so that, with careful aim, a well defined pyramidal indentation could be made. At least six such measurements were taken and averaged at loads of 50, 40, 25, 20, 10, 5, and 2 gms. This allowed consistant internal comparison of specimen hardnesses.

2.5 Surface Topography

Experiments requiring surface topography measurements can account for entire research projects in themselves. In this study, to compliment the work on texture, it was necessary to characterize the surfaces of the samples for comparison purposes. Detailed theoretical analysis and interpretation was beyond the scope of this study. This section will breifly describe the techniques used in this work.

As previously noted, the surface of EG steel contains a level of roughness, the "microroughness" - due to the zinc crystallite morphology. This is at a finer scale than most stylus instruments area capable of measuring. In addition, it is now believed that longer wavelength measurements are of significance to the painted appearance of body panels.

Typical commercial instruments were previously designed to provide only that information deemed relevant by the instrument manufacturers. These instruments, as well as the "standards" which they report, were originally developed for single point tooling machined surfaces. In the past the parameters of interest were simply the " Arithmetic Average Roughness" (R_a), or the Root Mean Square Roughness (R_{rms}), the maximum peak to valley height (R_y), and the peak count (ppi). The instruments contained "filters" to exclude from the calculations any contribution from wavelengths either longer or shorter than those of interest[E12].

In order to collect data which contained all possible information of relevance, for present or future use, unfiltered profiles were collected. Using a modified Clevite Model 150 SurfAnalyzer, fitted with a 5 μm radius stylus tip (compared to the usual 25 μm diameter) and a 25 mg. load (compared with 125 mg. typical), we were able to discern some of the finer details of the microroughness tips (though not in the valleys) on top of the macroasperities while not "plowing" through the soft zinc as has been observed using traditional profilometers such as the Taylor-Hobson, Bendix, or Perthometer. The analog output signal was converted to digital and saved via floppy disk. From the raw profile, software could be written to compute any of the hundreds of descriptive parameters used in the field of metrology, as well as having the option of defining our own parameters.

In this work, it was decided to compute and report only the R_a, R_y, Area Under the Bearing Area Curve, and Area Under the Amplitude Density Function. For details on these functions and others the reader is referred to the ANSI Standard[E13], as well as several of the innumerable texts, papers, and conference proceedings on the subject[E14-E18].

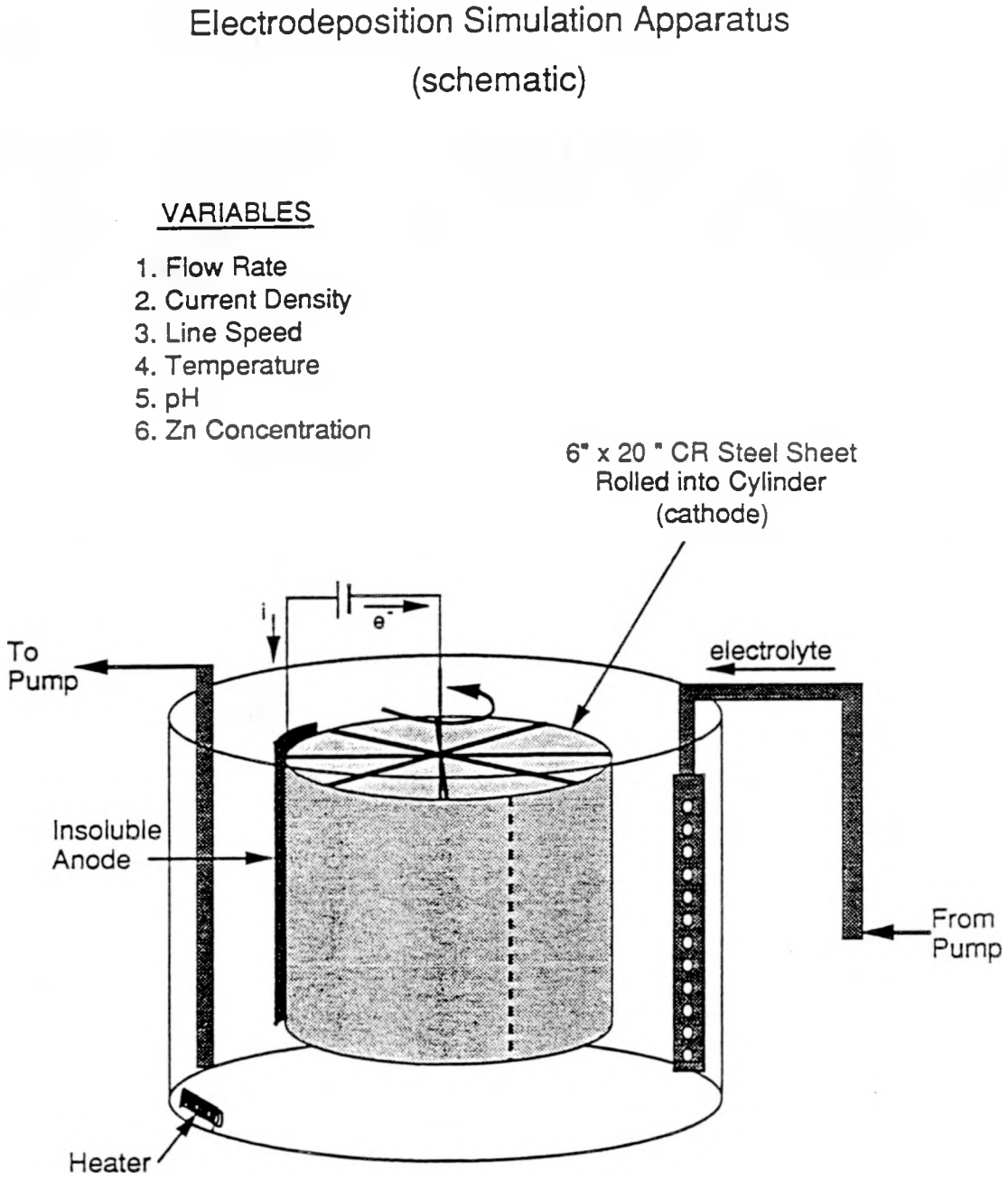

Figure E1) Schematic illustration of rotating cathode electrodeposition simulator.

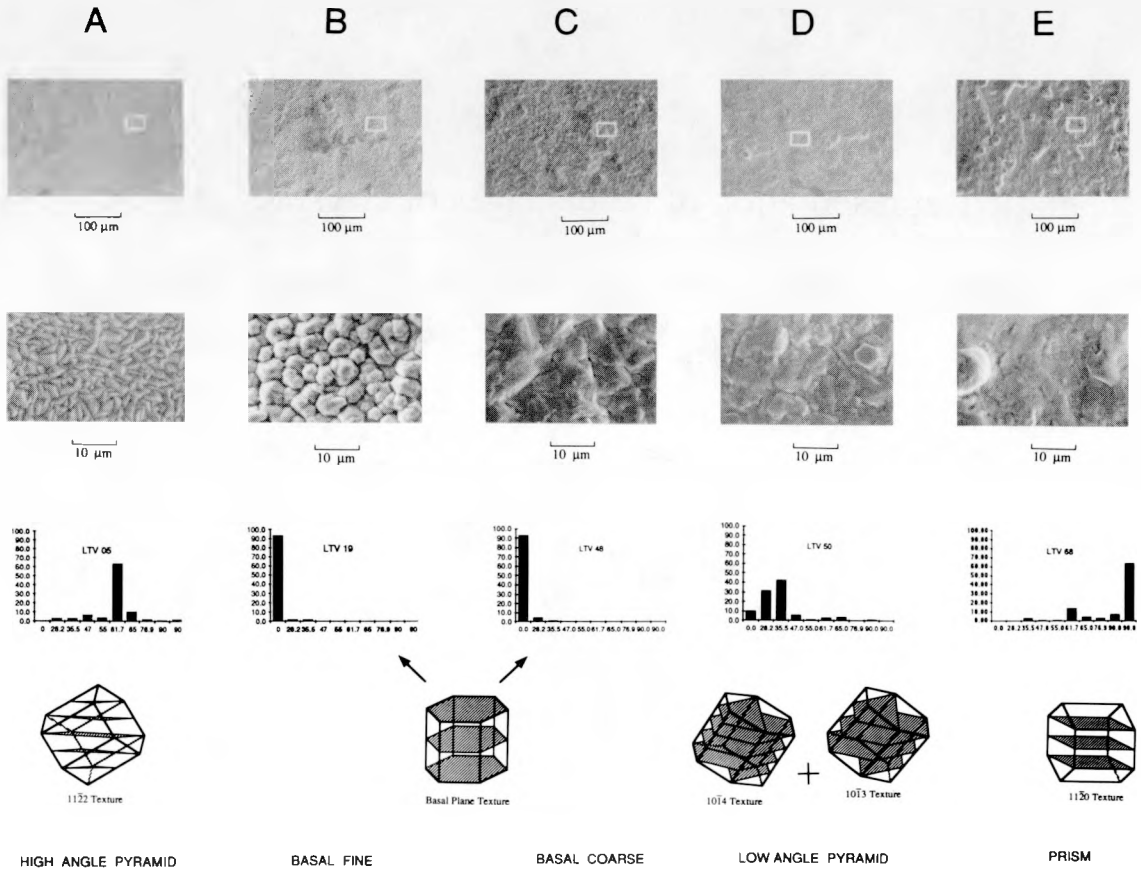

XBB 901-238

Figure E2) Resulting morphologies and textures of different electrodeposition parameters chosen for friction studies.

Schematic Representation of Percentages of Crystallographic Planes Plotted as a Function of Angle of From Basal Plane

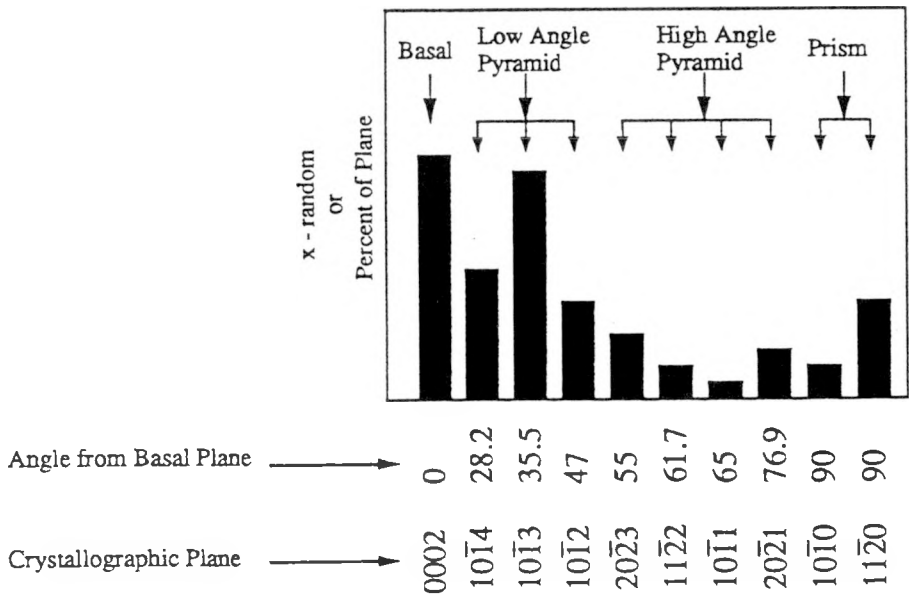

Figure E3) Schematic plotting for comparison of relative amount of zinc grains oriented with planes parallel to the sheet plane. This "texture" representation assumes a radially symmetric distribution, or fiber texture.

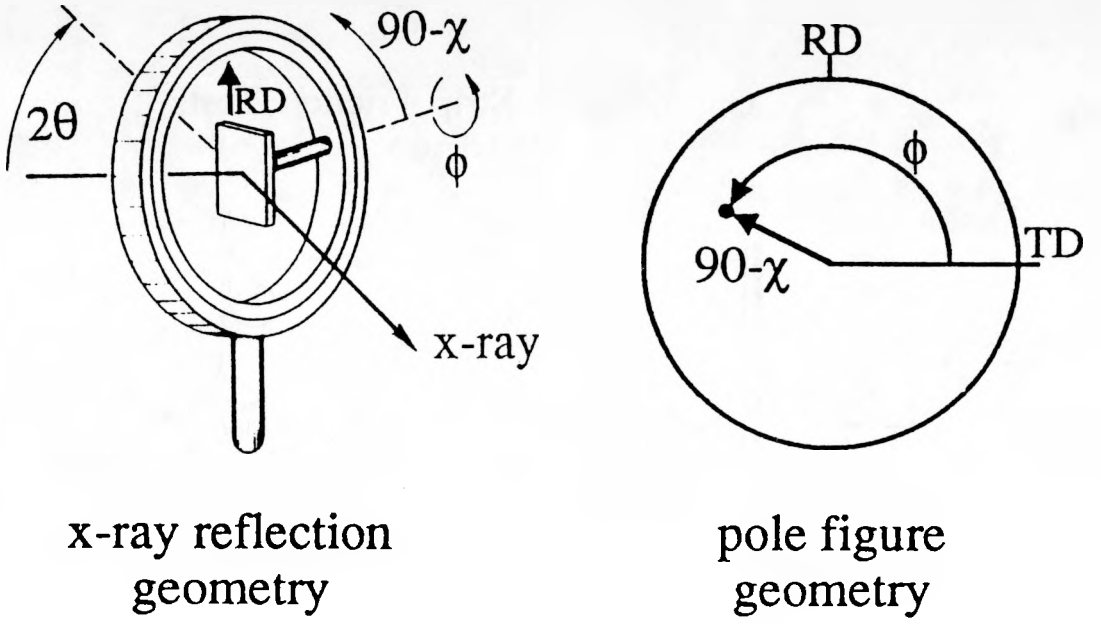

Figure E4) Geometry used for pole figure collection and display (Adapted from ref. E4).

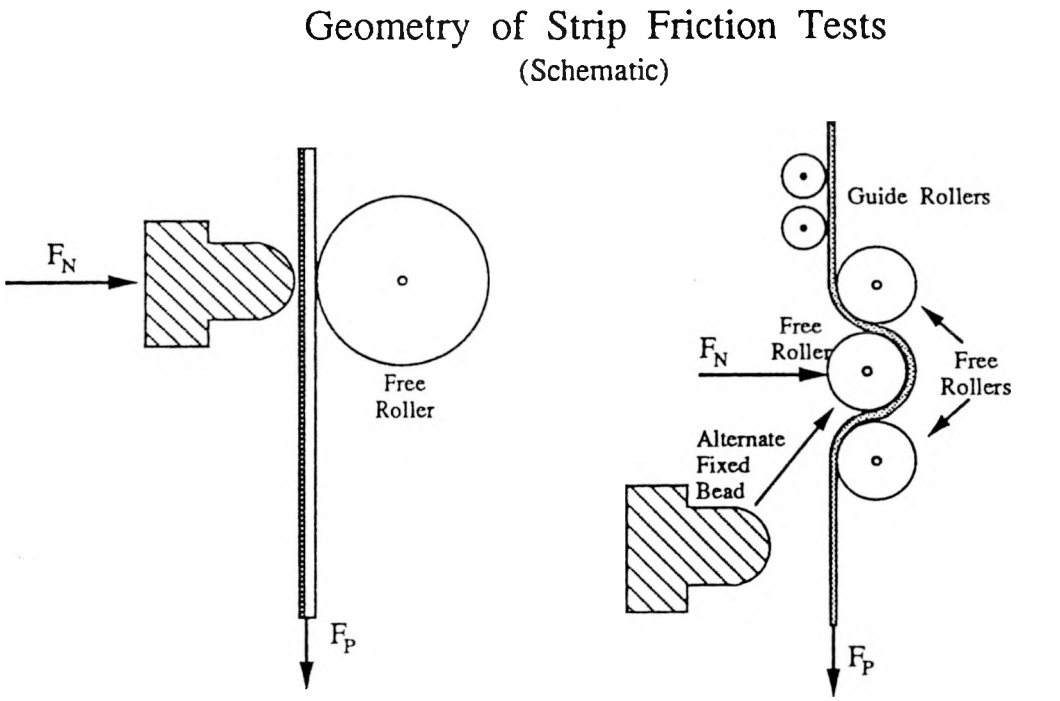

Figure E5) Schematic Illustration of a) straight stripdrawing, and b) one-sided drawbead simulation geometries.

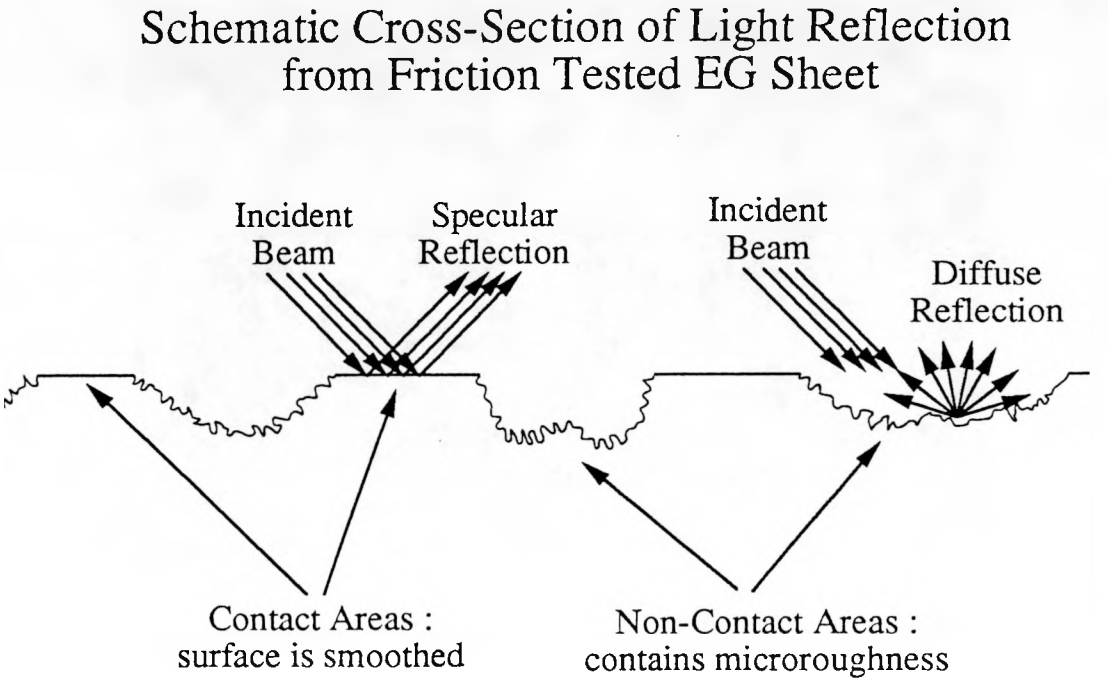

Figure E6) Light is specularly reflected from a smooth surface, while it is diffusely reflected from a rough surface as illustrated schematically above. This allows the burnished contact areas to be easily distinguished from the undeformed regions in EG steel.

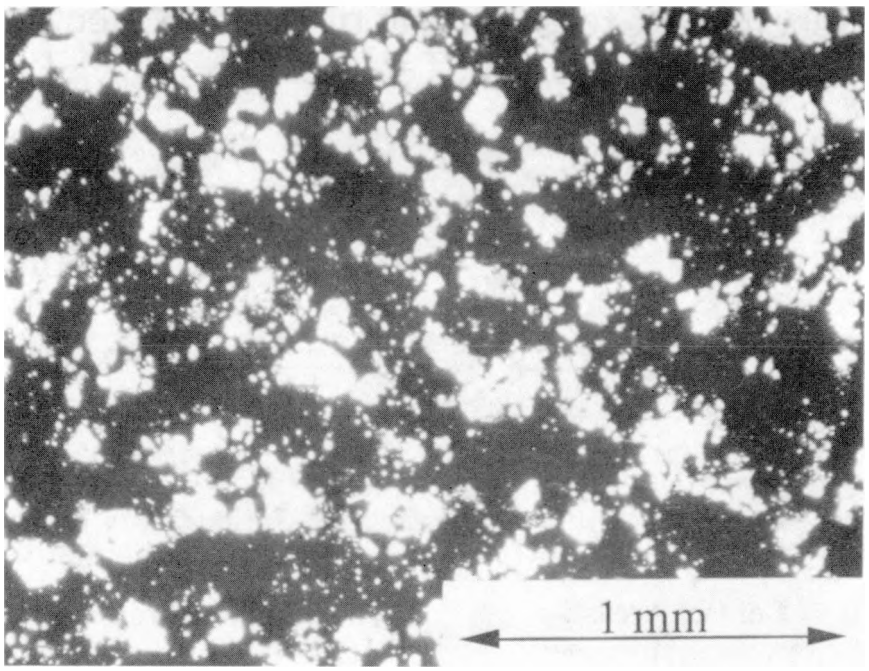

XBB 9011-9333

Figure E7) Contrast under reflected light optical microscopy from areas of contact (bright) and non-contact (dark) between the tooling and the sheet .

III RESULTS

1 THEORETICAL PREDICTIONS

The simplest view of the effect of texture on friction is that modelled by the resistance to deformation of a single crystal of zinc, under an imposed loading condition. This is somewhat analogous to the Sachs[R1] model for deformation. If the individual crystallites on an asperity (or the entire asperity itself) are considered independent single crystals, then it follows in this view that the orientation which has the lowest resistance to deformation, or alternatively, the highest resolved shear stress (RSS) for basal slip should have the lowest coefficient of friction. Since slip on the basal system is some 30 to 50 times easier than any other system[R2], looking at the RSS for basal slip only gives a reasonable comparison for ease of deformation for different orientations.

1.1 Loading Condition on an Asperity

The exact loading condition on a zinc asperity is unknown, however the use of some assumptions allows an estimate to be made based on the geometry of the tooling / asperity interface.

If plane stress loading is assumed, then one can define the full range of possible loading conditions using a parameter α, the fraction of load which is compression (as compared to shear) as depicted in figure R1 and used in the following matrix where the assumed loading condition on an asperity is :

$$\text{plane stress loading tensor} = \begin{pmatrix} 0 & 0 & 1-\alpha(\sigma_{13}) \\ 0 & 0 & 0 \\ 1-\alpha(\sigma_{31}) & 0 & \alpha(\sigma_{33}) \end{pmatrix}.$$

From this, the RSS for slip on an asperity of a given orientation (modelled as a single crystal) can be computed as a function of α. The was done for basal (0001), low angle pyramid $\{10\bar{1}3\}+\{10\bar{1}4\}$, high angle pyramid $\{11\bar{2}2\}$, and near prism $\{11\bar{2}0\}$ orientations. A listing for the program which performs the calculations can be found in Appendix C.

For loading conditions of near shear (α near 0), it is seen that basal oriented zinc has the highest RSS (figure R2), thus the least resistance to deformation, and hence would exhibit the lowest coefficient of friction. Earlier analysis however, based on the geometry of the tooling[I3] found α to be around 0.8. The results predict that for α of around 0.8, the basal textured zinc should, in fact, have a higher resistance to deformation (hence higher friction) than either of the pyramidal orientations as a result of the high proportion of compressive loading. Although this prediction is counter intuitive, high basal friction has sometimes been observed experimentally.

Additionally, for rotations of a zinc single crystal about the sheet normal (rotations about ψ), there can be large variations in RSS, depending on the tilt angle, θ. This can also be seen in figure R2 as the RSS for ψ=0°, 90°, and that corresponding to a fiber texture (rotational symmetry about the sheet normal) are shown. For the cases of $11\bar{2}2$ and basal, the RSS is not very sensitive to rotations about ψ, while for $10\bar{1}3$ and near prism, it is extremely sensitive. It is interesting to note that for both these θ orientations, the RSS

for $\psi = 90°$ is very unfavorable for deformation by basal slip, hence one might expect some other type of deformation mechanism to operate. This theoretical result will be borne out in examination of the post-friction testing texture measurements of samples D and E in section 4, where strong evidence of twinning is found.

2 FRICTION RESULTS

2.1 DBS - Coefficient of Friction

2.1.1 As Received

Figure {R3} shows the results of the one sided DBS tests on the coatings of different textures. The high-angle pyramid, low-angle pyramid, and coarse basal texture coatings had essentially the same coefficient of friction, while that of the fine grained basal coating was much higher and the Cd doped prism sample was much lower. Surprisingly, these results suggest that texture is not of primary importance in determining friction in this test. This is the first significant finding of this work. The two extreme cases warrant further discussion and will be covered in part IV.

In the case of the "cadmium added" series, which have increasing amounts of near prism textures (figure R4), it can be seen that the OSDBS-μ decreases as the amount of prism texture is increased (figure R5). However, there is also an increase in hardness for all the cadmium added samples (figure R6). These two factors may be somewhat related, owing to the plastic deformation dependence of the hardness test[E11].

Table 2 : Surface Topography Parameters of Laboratory EG Sheets

EG Sample ID	OSDBS-μ	R_a	R_y	Area Under ADF	Area Under BAC
A : High Angle Pyramid	.28	.92	9.75	.33	4.48
B : Fine Basal	.32	1.42	11.22	.37	5.16
C : Coarse Basal	.28	1.43	11.25	.38	5.30
D : Low Angle Pyramid	.275	1.08	11.71	.39	5.24
E : Prism (500 ppm Cd)	.21	2.15	18.95	.63	8.27
150 ppm Cd	.23	1.77	14.77	.49	7.78
50 ppm Cd	.28	1.23	13.29	.44	7.38
Zn Standard	.28	1.00	9.10	.31	4.14

R_a = Arithmetic Average Roughness (μm)
R_y = Maximum peak-to-valley height (μm)
ADF = Amplitude Density Function
BAC = Bearing Area Curve

However, since there is little difference in texture for the pure zinc control and the 50 ppm Cd added sample, which have identical coefficients of friction while the 50 ppm Cd added sample is somewhat harder, it appears that hardness alone is not the dictating parameter, at least at an increase in hardness of this slight level. There may, additionally,

be some compensating effect due to surface roughness as the 50 ppm Cd sample also had a slightly rougher surface as described by various surface profilometry measurements (Table 2). Separation of the contribution from surface topography would require further investigation with samples of controlled surface roughness.

2.1.2 Microroughness Removed

To investigate the role of the zinc microroughness on friction, a comparison was made between samples in which the microroughness was chemically removed, and those in the as-deposited condition. Removal of the microroughness was accomplished by a 15 to 20 second immersion in a 5% HCl / 95% distilled H_2O etchant. Results of such a treatment are shown in figure R7 for three of the textures. While complete removal of the microroughness was impossible, the resulting surfaces were much more similar than before the treatment.

The results of the OS-DBS tests are shown in figure R8, along with the as-deposited results where it can be seen that removal of the microroughness in every case led to an increase in friction. As there was no change in plastic properties of the zinc due to the removal of the microroughness, this must therefore be a lubricant related effect. One interpretation is that the role of the microroughness is to serve somewhat as a lubricant reservoir, forming microhydrostatic pockets, on the tops of the macro asperities, between the zinc crystallites.

Alternatively, the presence of the microroughness might be viewed as having the effect of increasing the "effective viscosity" of the lubricant in the macrovalleys, in a manner analogous to the flow of a fluid along a smooth versus a rough conduit[R3]. In both these views the lubricant is more effective in helping to maintain hydrostatic pressure, thus relieving some of the load on the zinc asperities and lessening the extent of metal to metal contact.

2.2 Stripdraw - Area Fraction Relations

Examination of the plot of pulling load versus area fraction (figure R9) reveals that all samples have nearly the same slope except for sample B, the fine grained basal coating. This sample had a lower pulling load for a given area fraction which, according to earlier analysis, would imply a lower coefficient of friction. This agrees with the asperity deformation models, not surprisingly since they assume simple shear, as well as with the RSS calculations for the case of near $\alpha=0$ (mostly shear). However it is in disagreement with the experimentally measured DBS-μ values.

Figure R10 shows the change in area fraction as a function of normal load for the straight stripdraw samples. In this case, the fine grained basal sample showed an exceptionally high area fraction for the lower load range. The stripdraw normal load which would produce a pressure equivalent to that in the DBS test lies in this range of 100 to 200 lbs. (See Appendix D). Conversely the near prism sample showed a lower rate of area growth with normal load.

The combined effect of these two plots is shown in figure R11 where surprisingly, the coefficient of friction as defined by the pulling load divided by the normal load, is seen to be nearly the same for all the pure zinc coatings but considerably lower for the cadmium added, prism texture sample.

It seems that the ease of shearing a given area for the fine grained basal oriented zinc is compensated for by the increased rate of area growth, leading to a coefficient of friction, as measured by this type of test, which is the same as the other samples. For the prism oriented sample, although the pulling load for a given area was similar to the other samples, the increase in area fraction per normal load was lower. This led to the lower coefficient of friction as measured by the slope of the normal vs. pulling load plot.

3 AREA FRACTION - DBS TEST

Examination of both the trend in contact area with normal load from figure R10 in the strip draw test and the rankings from figure R3 in the DBS friction test, suggested that there may be a correlation between contact area fraction and coefficient of friction as measured by the DBS test. Subsequently, area fraction measurements were performed on the DBS tested samples and such a correlation was investigated.

Figure R12 shows SEM micrographs of deformed area fractions for the laboratory samples of strong textures. Contact area fraction measurements were made and the results are plotted as a function of OSDBS-μ in figure R13. It seems that contact area fraction does indeed correlate fairly well with coefficient of friction in this test. This is the second significant finding of this work.

As part of an ongoing companion investigation, the area fractions from a series of commercial samples from several manufacturers (varying textures, roughnesses, microroughnesses, etc.) was also measured and plotted against DBS-μ (figure R14). Here too, good correlation was found.

4 TEXTURE RESULTS

4.1 Change in Texture with DBS Testing

As shown via the basal pole figures in figure R15, the initial texture of the coatings is changed via deformation of the coating as a result of the DBS test. The basal poles are "displaced" away from the drawing direction, which corresponds to the direction in which the zinc asperities would be deformed via shear. Irrespective of starting texture, all of the coatings approach a similar final texture, with the peak density of basal planes occurring at about 40 degrees from the sheet plane and in the direction of forward shear. This is the third significant finding.

Another noteworthy feature is that all of the coatings show a decrease in pole density for grains whose c-axes lie along the N/S trace, or perpendicular to the drawing direction. This corresponds to ψ=90° in figures R1 and R2. It is apparent that grains oriented in this direction require a considerably greater stress for deformation by slip than those grains oriented along ψ=0°.

This is evident in both sample D (low angle pyramid) and particularly in sample E (near $11\bar{2}0$ prism) where there is seemingly a large, or even discontinuous "rotation" observed of the basal planes in going from a N/S concentration to a high density at 90 degrees from this (again at a tilt angle of about 40° from the sheet normal) in the direction of forward shear. Neither moderate slip on the basal systems nor prism slip can account for such rotation. However, twinning in zinc on $\{10\bar{1}2\}\langle 10\bar{1}1\rangle$ can partially account for such changes (figure R16).

Due to the c/a ratio of 1.856, the $\{10\bar{1}2\}$ planes in zinc lie at 47° from the basal plane. As a consequence, the basal poles in each of the six twin variants lies at 86° to the original basal plane pole, in a direction defined by the common $<10\bar{1}1>$ direction. Figure R17 shows the position of the six variants for the basal poles after twinning for grains with orientations corresponding to samples D and E.

In addition to the apparent twinning of those grains unfavorably oriented for slip under shear loading, both the fine grained and coarse grained basal samples also exhibit evidence of twinning due to compressive loading. This is manifested by the appearance of a higher than random distribution of basal poles in positions inclined "into" the shearing direction. These clearly could not occur via slip and thus must have come from either twinning followed by rotation due to shear, or recrystallization.

4.2 Change in Texture with Stripdrawing

The post-stripdrawing textures are shown, again via basal pole figures, in figure R18. In this test as well, sample E, the near prism texture, exhibits a final texture related to the as-deposited texture through twinning. The other samples all show a rotation of the basal poles towards the direction of forward shear, as might be expected. Qualitatively, the same changes, though apparently much less in magnitude, are seen to have taken place in these samples as in the DBS samples. These measurements were taken from the highest load stripdraw samples. It appears clear that the significantly shorter sliding distance in the stripdraw test, despite the higher load, compared with the DBS test is the reason for the smaller evolution of texture. It also seems that the bending/unbending of the DBS test does not have a significant effect on the resultant textures, except for possibly contributing to the twinning in the basal samples in the DBS test.

4.3 Region of Meaningful Texture Measurement

It must be noted that the entire sample surface has not been deformed, only some 45%-70% in the DBS test where the asperities were contacted. Since the x-ray beam covers a rather large area (on the order of 1 cm^2 due to sample translation), a considerable fraction of the x-ray signal contributing to the "after drawing" texture comes from the surface regions which have not seen any deformation due to the drawing.

In addition, for those regions which have been deformed, the measured texture is a "composite" of the texture through the entire coating thickness. This is a two-layer structure consisting of (1) the surface layer which has been deformed in the regions of contact with the tooling, and (2) the remaining lower portion of the coating. As observed via cryogenically fractured cross sections (figure R19) the apparent depth of the deformed layer is on the order of one micron or less.

Due to absorption, the signal received at the detector is not representative of the entire coating thickness, but is weighted with a preference toward the top layers. Figure R20a shows the effect of absorption through the ratio of incident versus reflected intensity as a function of depth for the 0002 reflection for zinc for several different x-ray sources. Note that even for soft x-rays from a Ti tube, there is considerable penetration compared with the apparent 1 micron depth of deformation.

Integration of this function gives the fraction of signal coming from a given depth (or volume if the beam size is known). For example, figure R20b shows that 33% of the signal comes from the top 1 μm of the coating using an Fe x-ray source as in this work.

Due to these two factors, the measured post-friction testing pole figures only qualitatively represent the "after deformation" textures. The texture changes of the surface must be considerably sharper than those presented in figure R15. If quantitative information regarding the change in texture due only to the frictional deformation is desired, the measured pole figures must be modified by somehow subtracting the contributions from both the uncontacted regions and the undeformed subsurface.

For the extreme texture changes in sample E, this was done. Using a solution of 3% HCl in distilled H_2O, the top 4 μm was chemically etched away and the texture was remeasured. A return to the original texture can be seen in figure R21, which proves that such a technique is feasible. The task now remains to develop algorithms for deconvolution of textures when much smaller fractions are removed. In this way, textures as a function of depth may be obtained from very thin sections. Such a technique is under development and is presented in Appendix E.

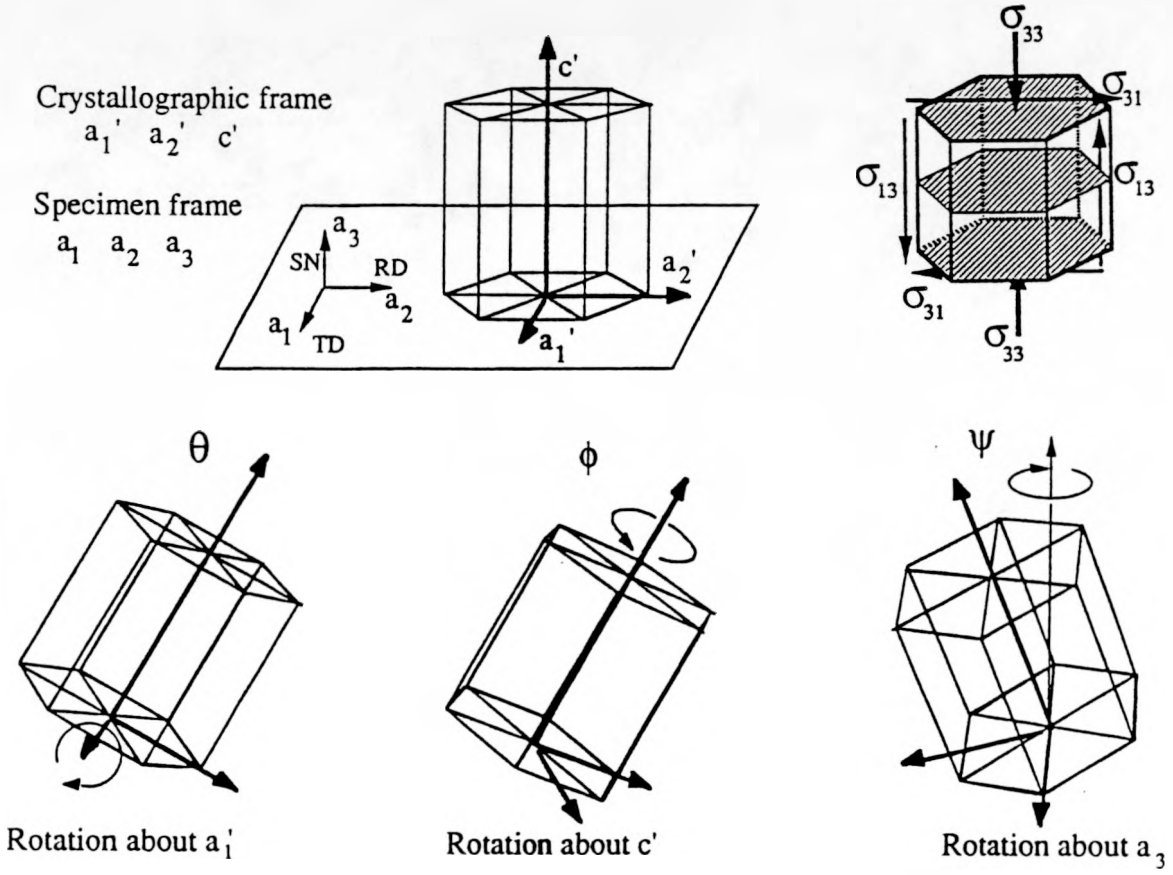

Figure R1) Axes which define loading system and angles used to define textures.

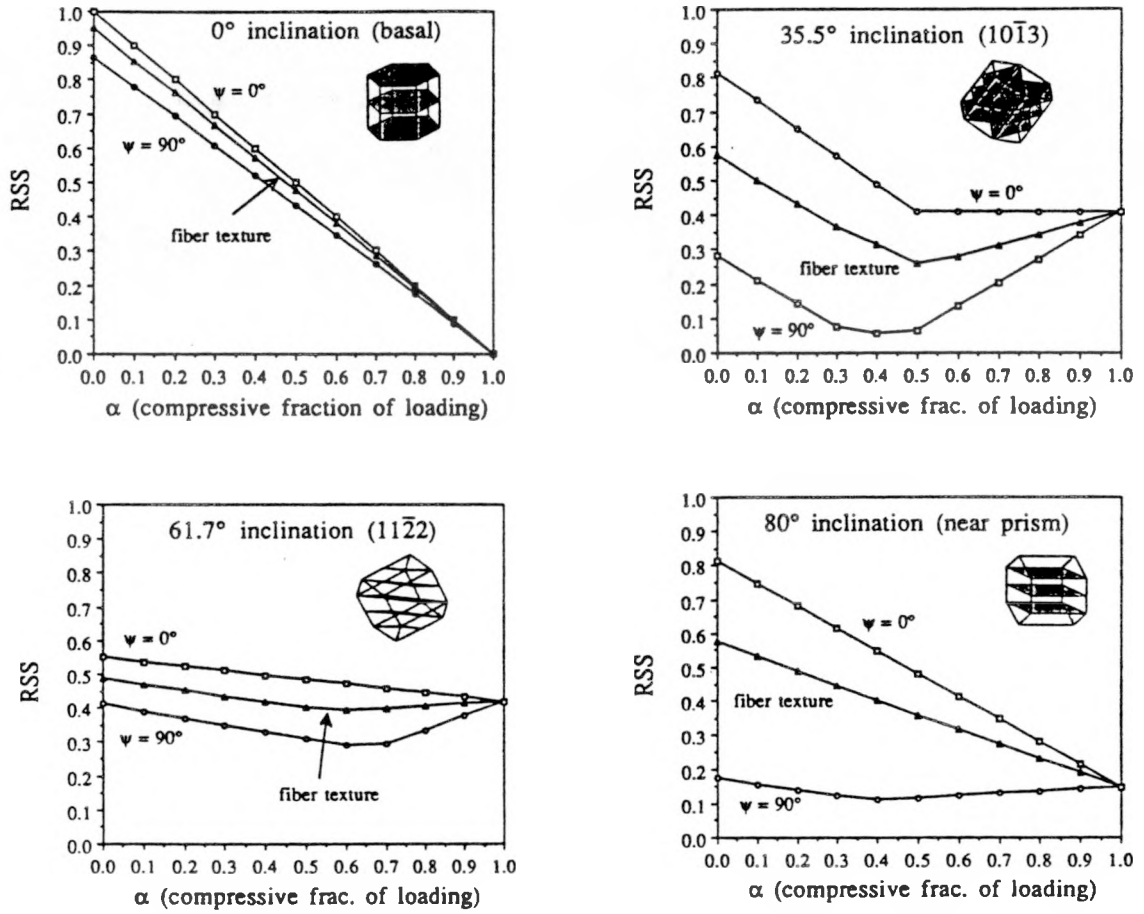

Figure R2) Results of resolved shear stress (RSS) calculations for four model textures. The basal sample exhibits a strong dependence on loading condition (α) only, while the high angle pyramid (11$\bar{2}$2) texture is rather insensitive to α, but somewhat sensitive to orientation of loading (as defined by ψ). Both the low angle pyramid (10$\bar{1}$3) and near prism textures are sensitive to both orientation and type of loading.

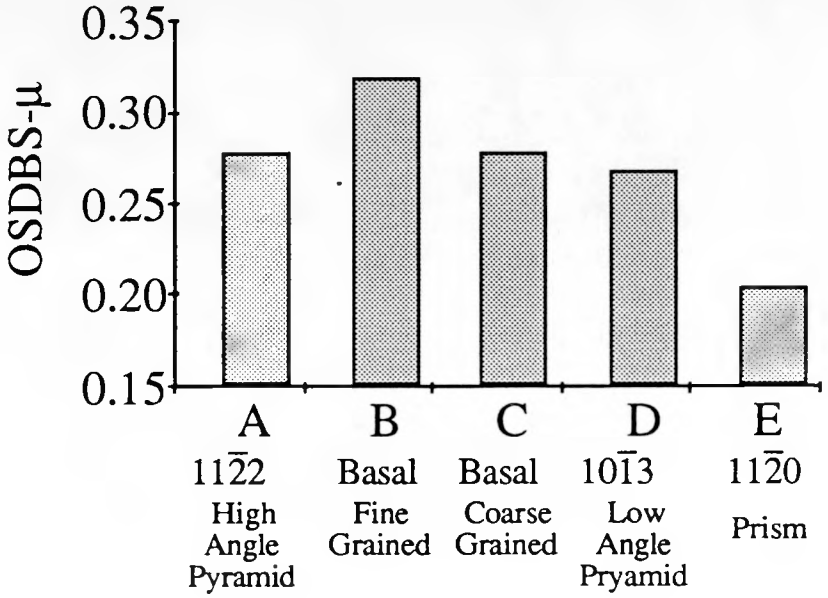

Figure R3) Results of one-sided drawbead simulator (OSDBS) tests. Results indicate no consistent dependence on texture. Only the fine grained basal and the Cd doped, near prism samples exhibit differences.

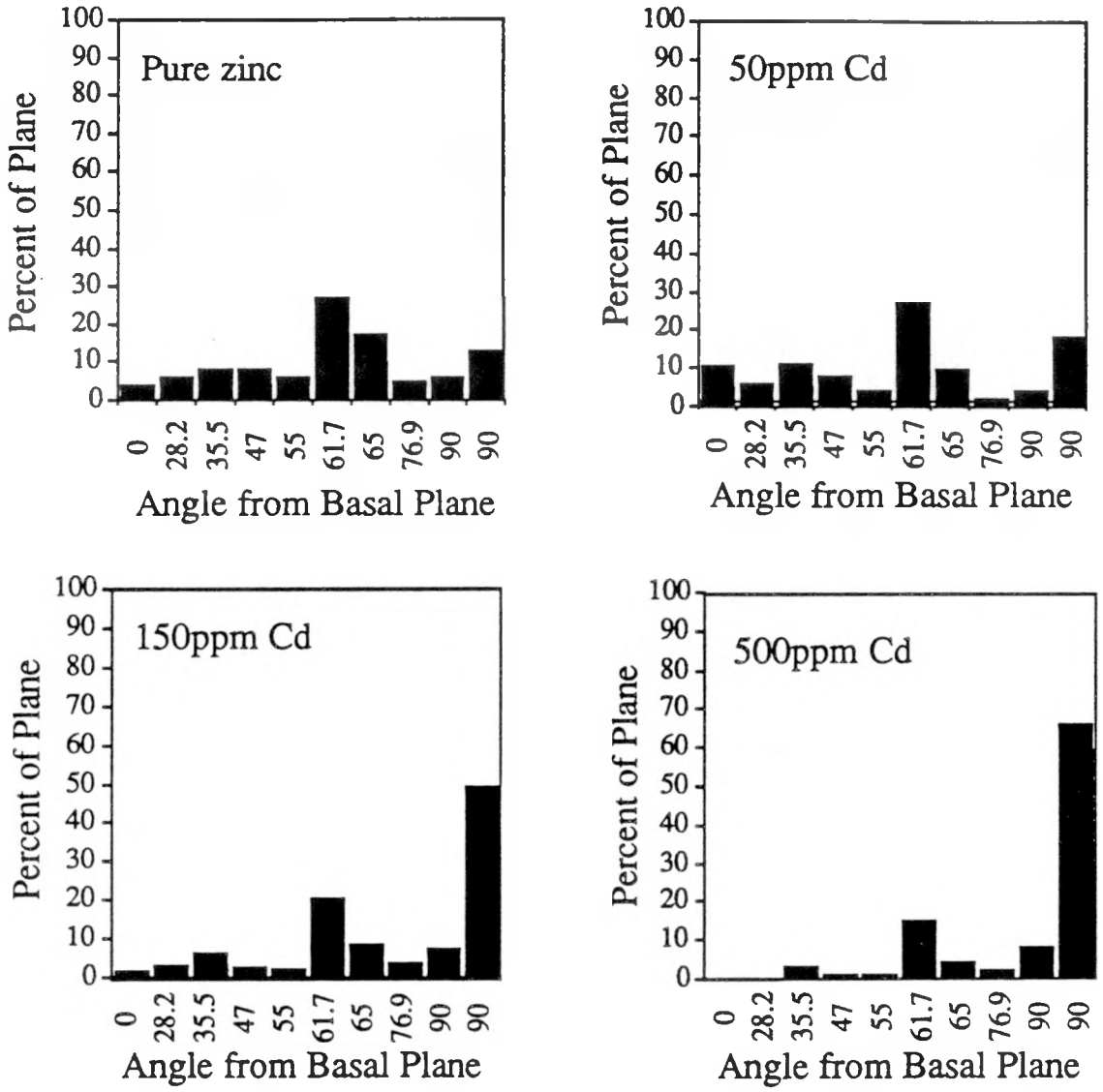

Figure R4) Strength of prism component is seen to increase with Cd additions to the electrolyte bath.

COEFFICIENTS OF FRICTION FROM ONE-SIDED DRAWBEAD SIMULATOR TEST

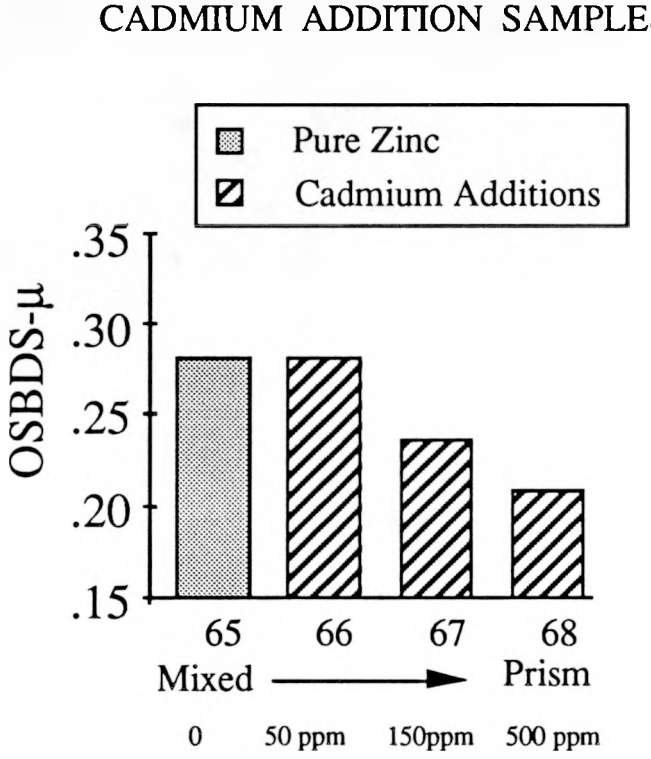

Figure R5) Results of OSDBS testing of Cd doped samples. μ decreases with increase in proportion of prism texture.

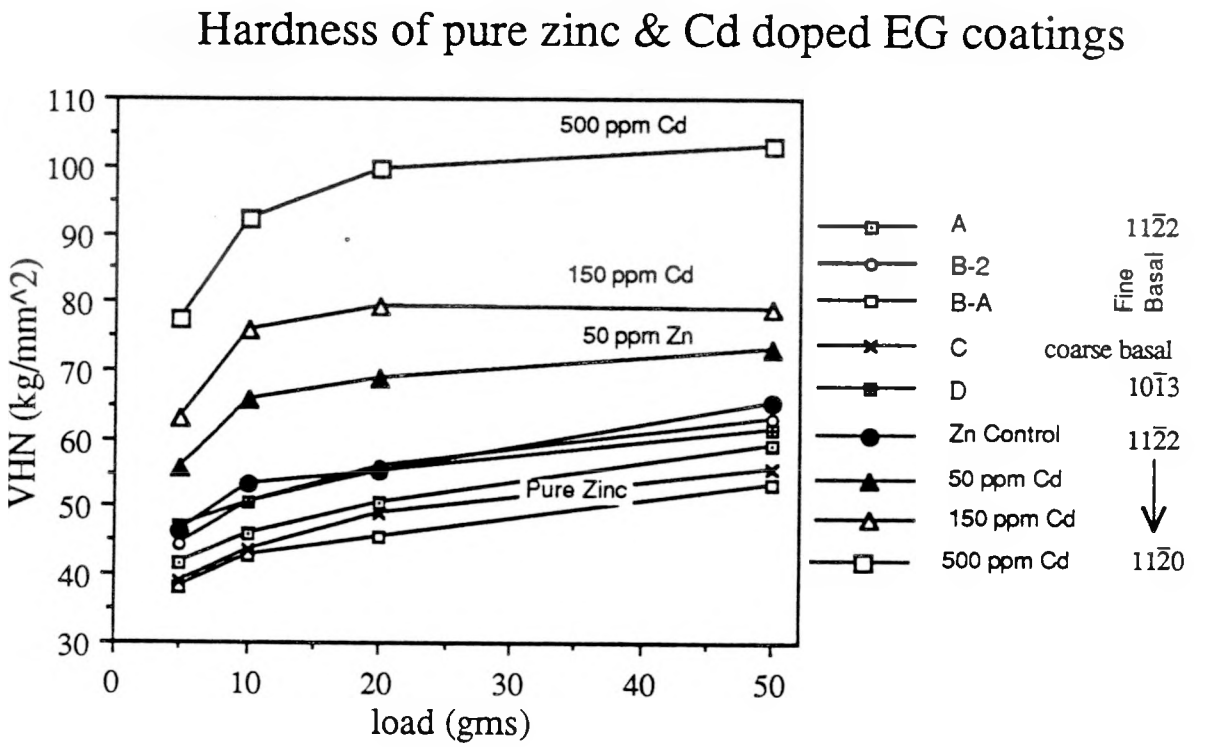

Figure R6) Vickers hardness measurements of EG samples as function of load. All pure zinc samples fell within the same range, while the addition of Cd resulted in a monotonic increase in hardness.

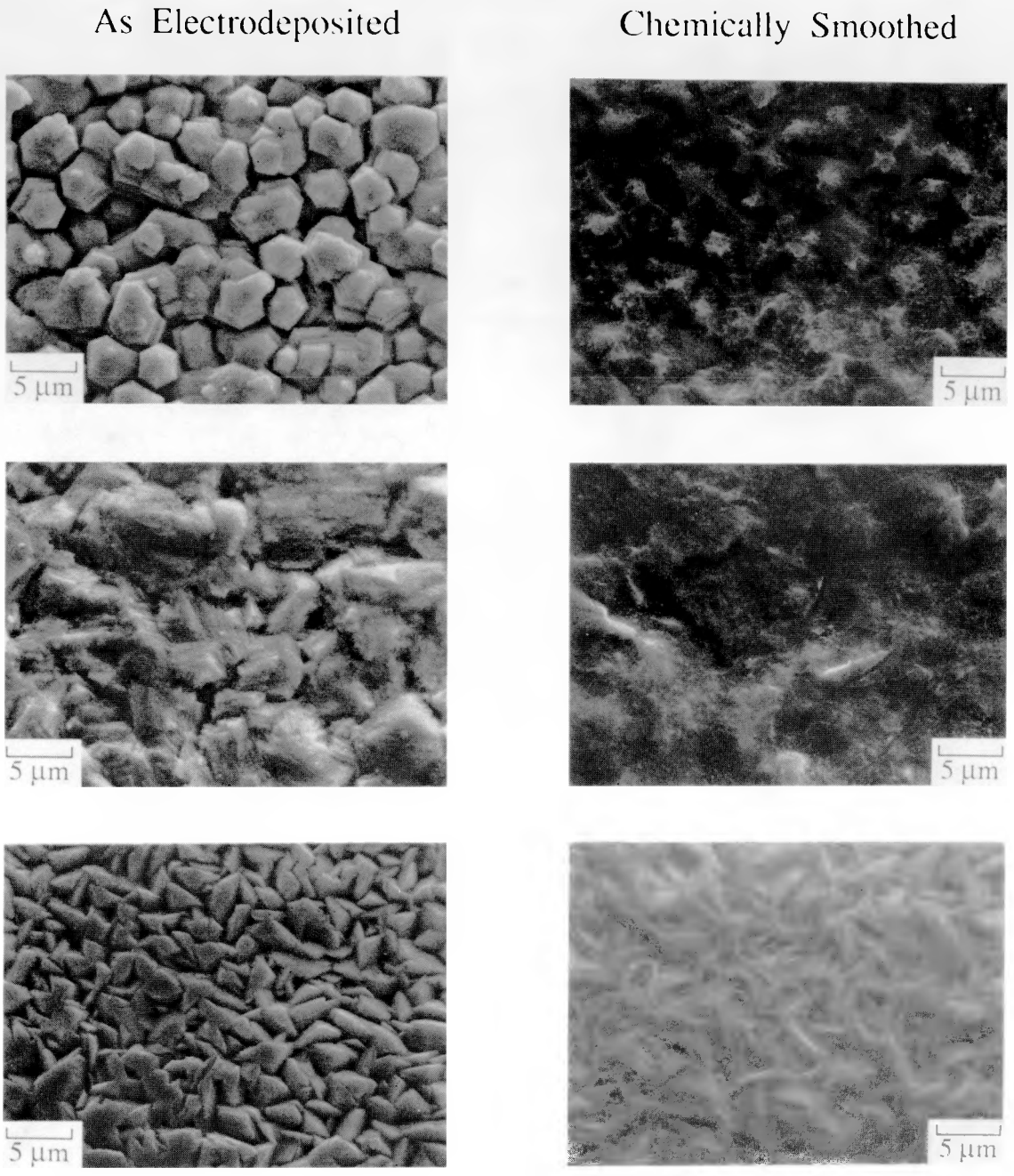

Figure R7) Removal of microroughness through chemical etching is shown in these SEM micrographs.

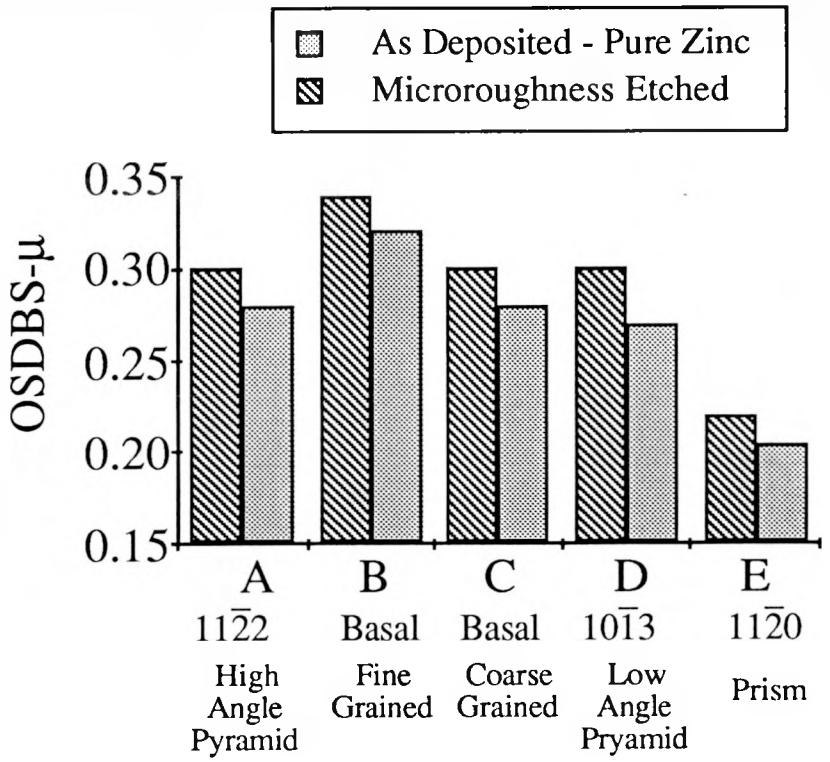

Figure R8) OSDBS test results indicate that removal of microroughness increases coefficient of friction. This is suspected to be through an effect of the lubricant's "effective viscosity".

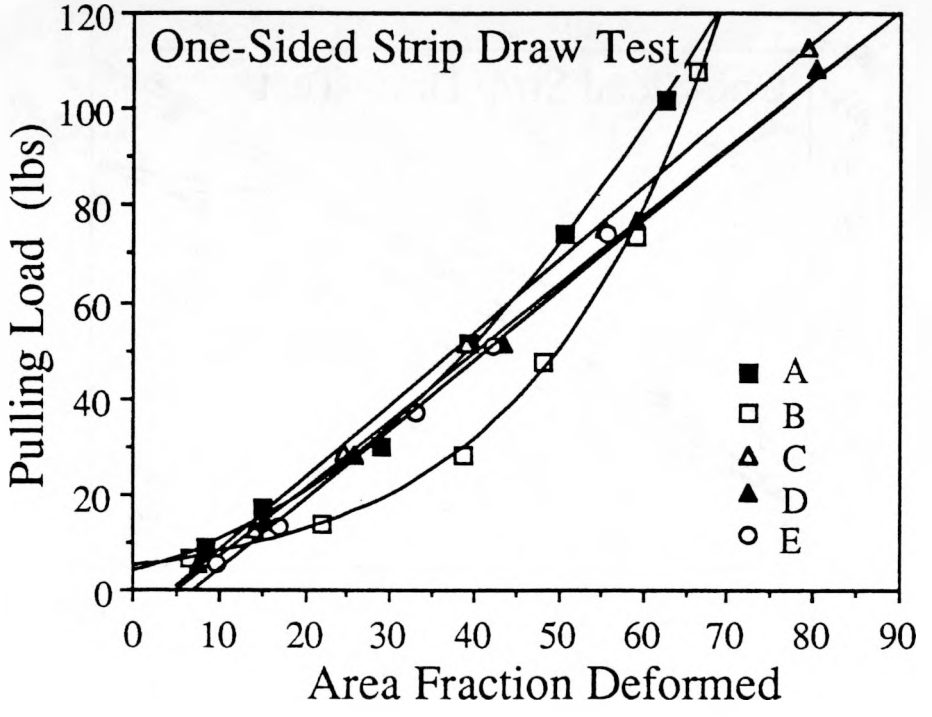

Figure R9) Dependence of pulling load on area fraction in straight stripdraw test.

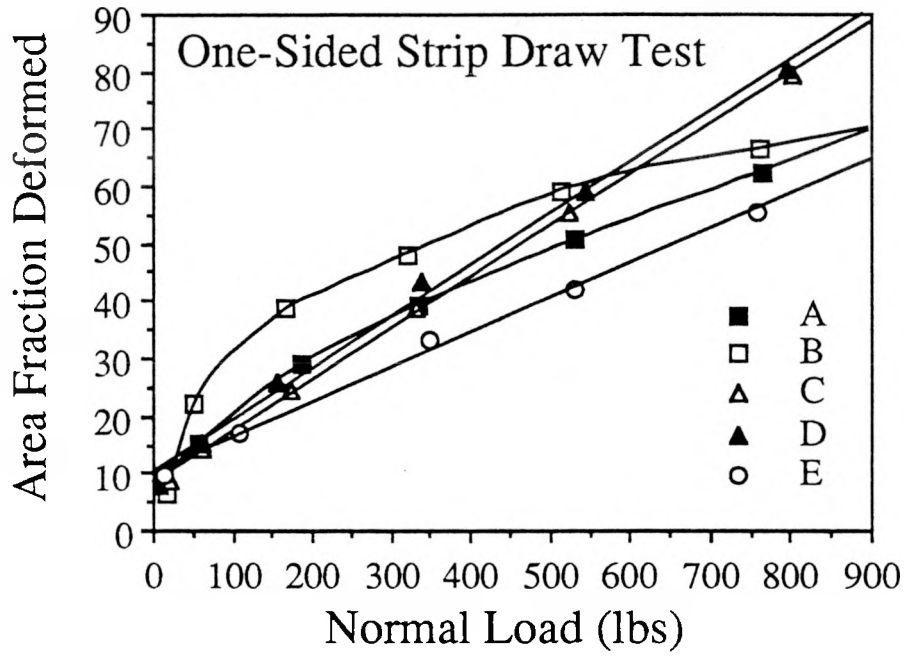

Figure R10) Dependence of area fraction on normal load in straight stripdraw test.

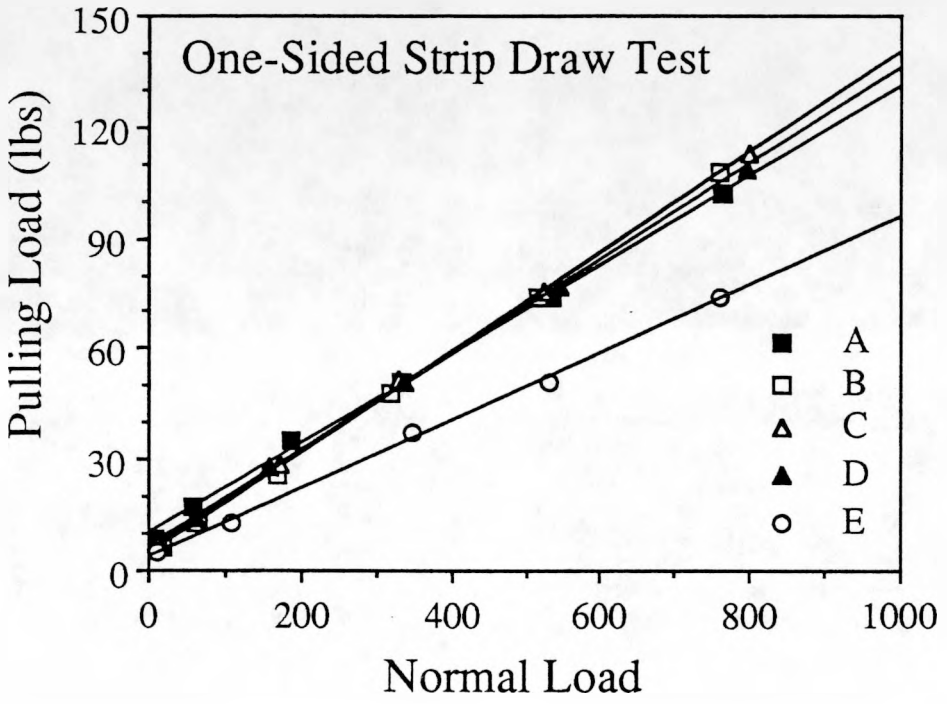

Figure R11) Dependence of pulling load on normal load in straight stripdraw test.

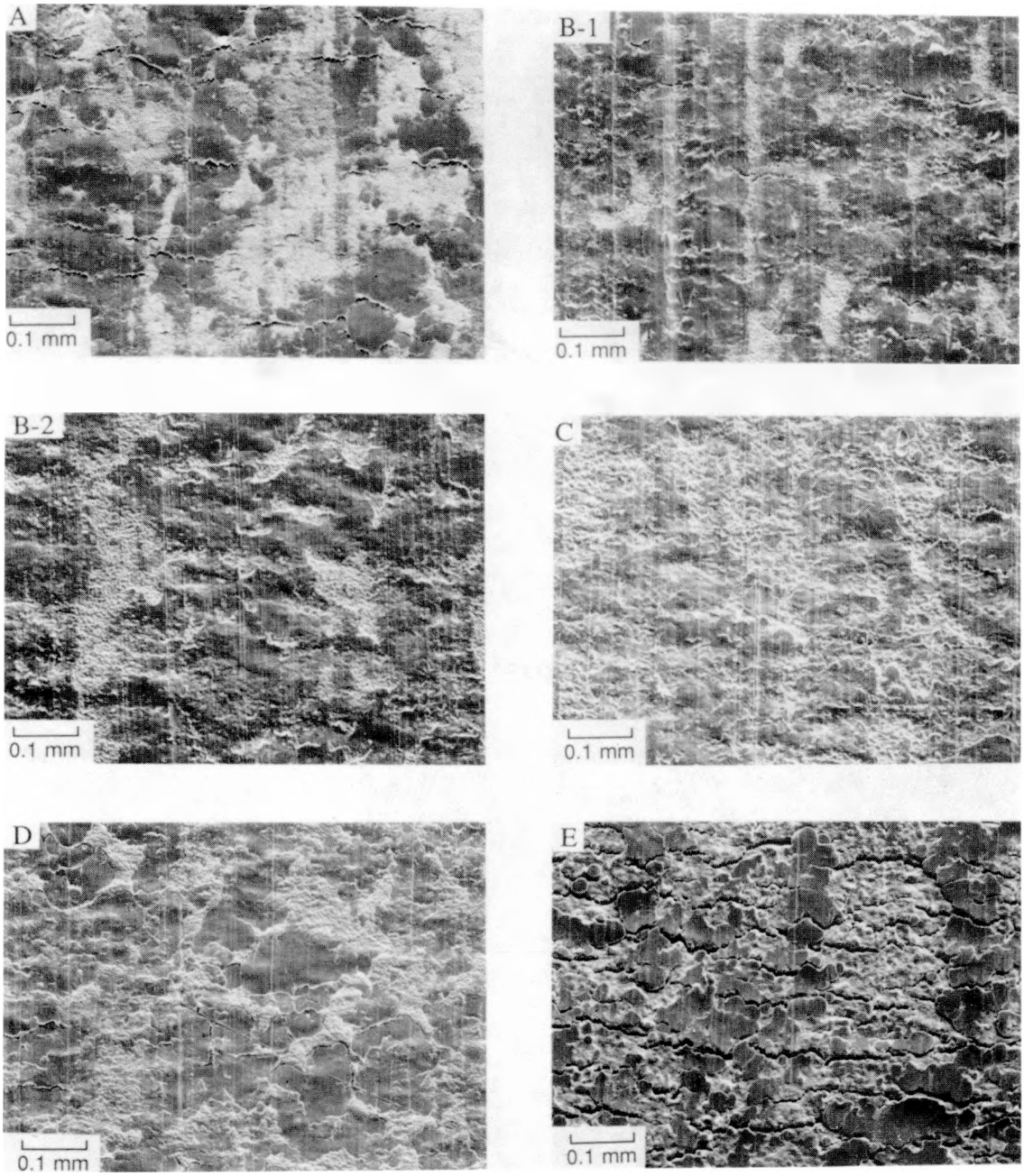

XBB 908-6161

Figure R12) SEM micrographs of surface contact area for various samples.

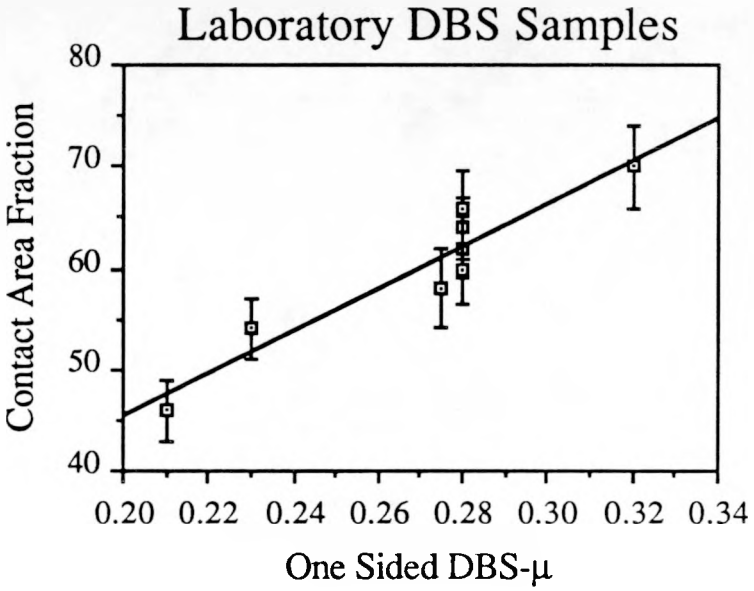

Figure R13) Dependence of coefficient of friction on contact area fraction for laboratory prepared samples of different textures.

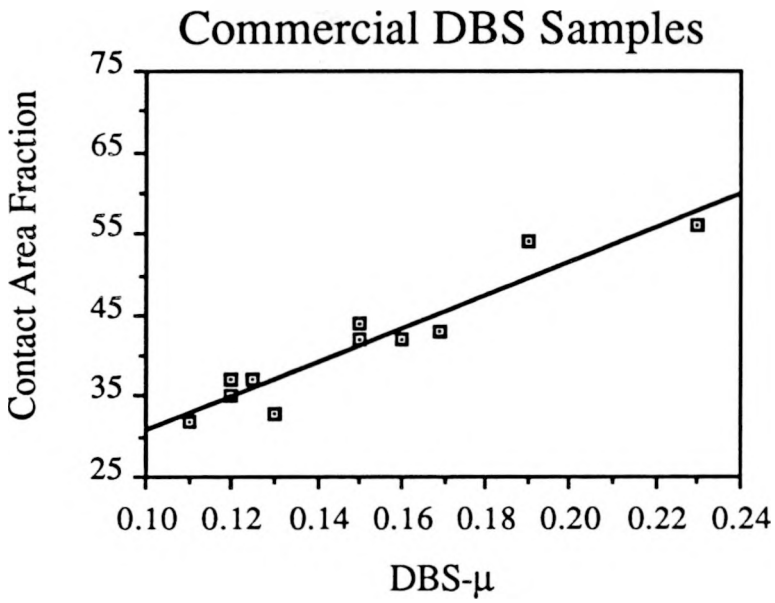

Figure R14) Dependence of coefficient of friction on contact area fraction for commercial samples.

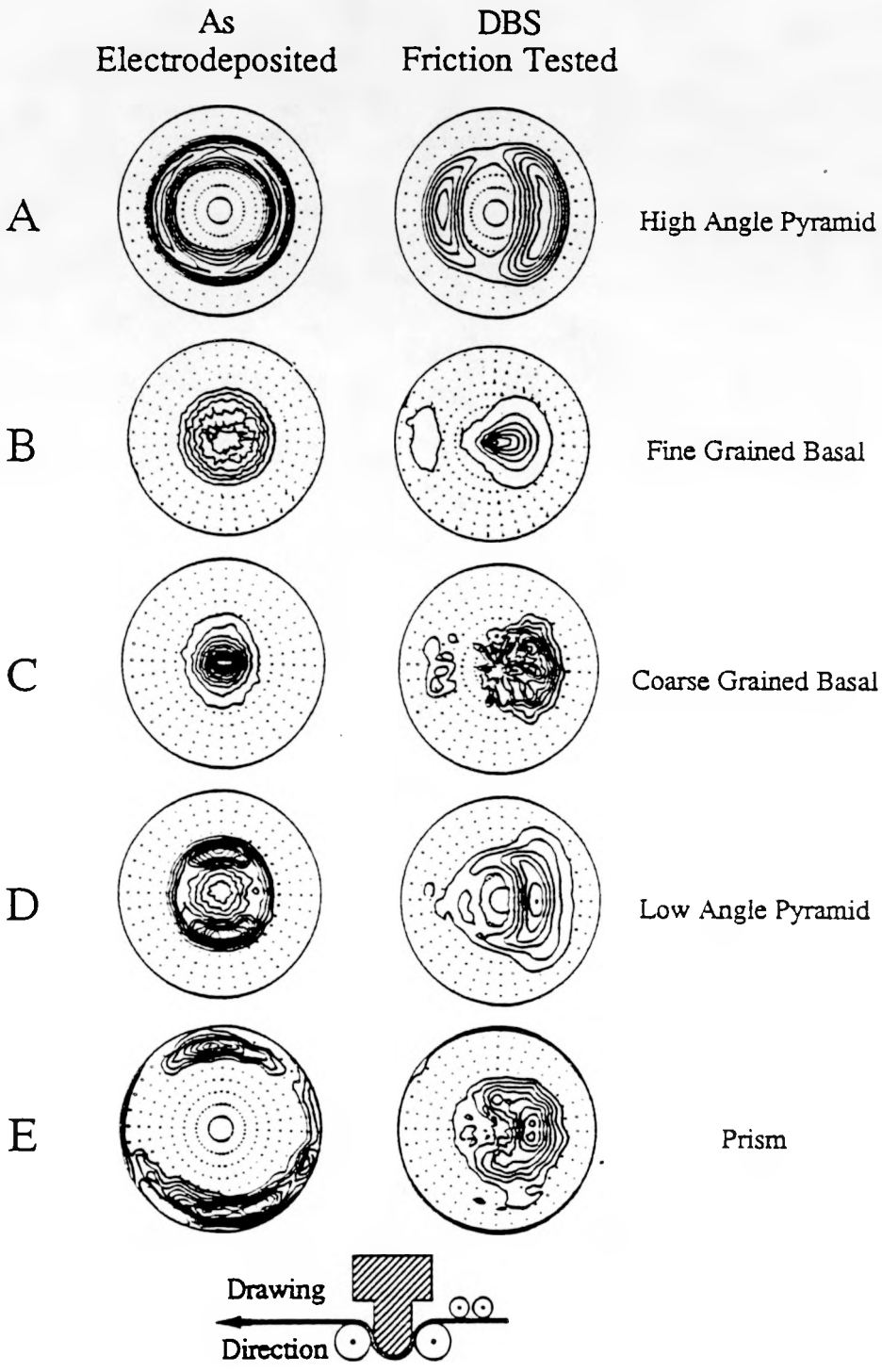

Figure R15) 0002 pole figures for EG coatings show change of texture of coatings after DBS friction testing. The surface of all coatings evolves to nearly the same final texture as noted by the position of the peak intensity.

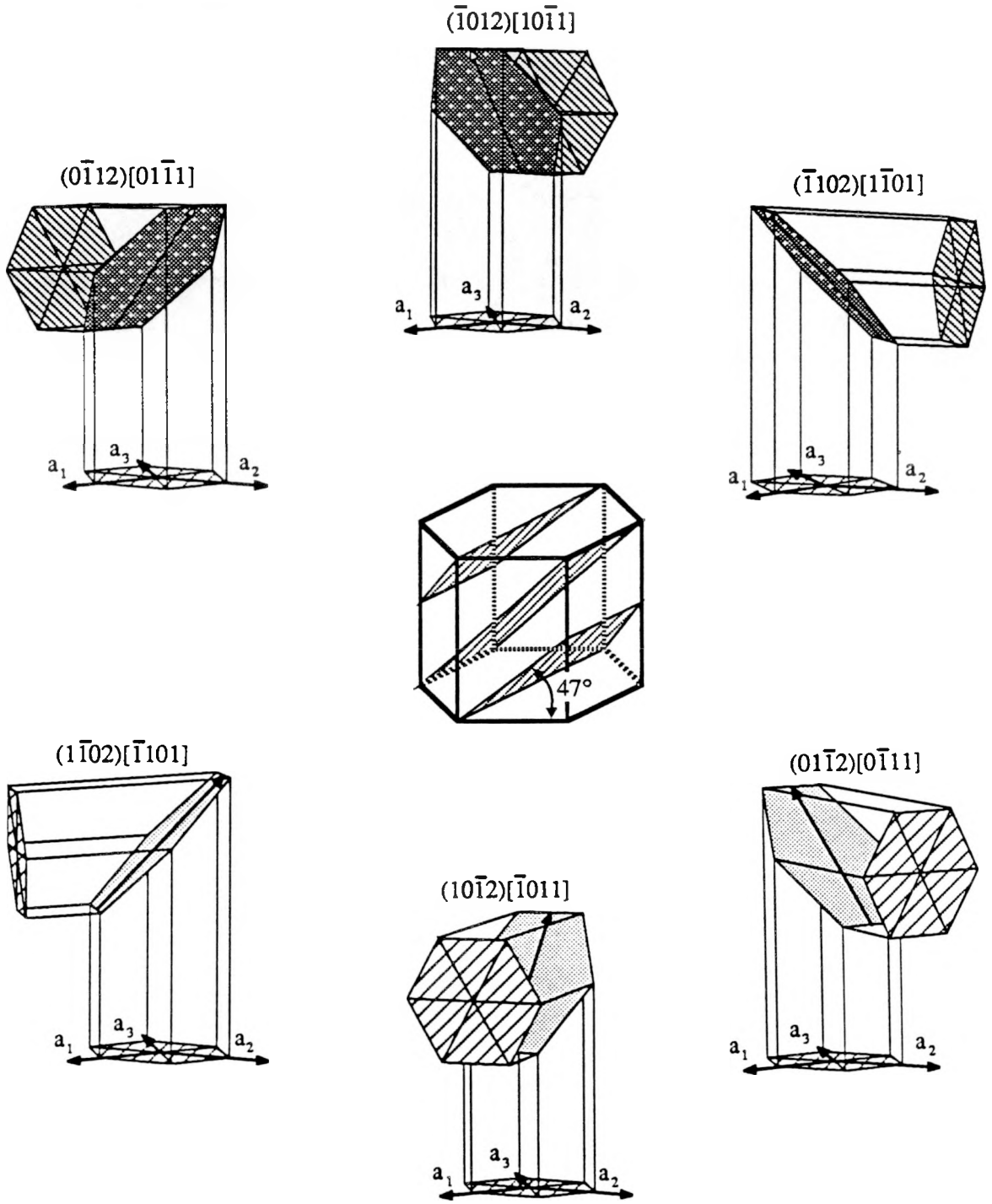

Figure R16) Twinning on $\{10\bar{1}2\}\langle 10\bar{1}1\rangle$ in zinc. The c/a ratio of 1.856 dictates that the $\{10\bar{1}2\}$ planes lie at 47° from the basal plane (center). As a consequence, the basal plane in each of the six crystallographically equivalent twin variants (periphery) lies at 86° to the original basal plane, with a common $\{10\bar{1}2\}$ plane and $\langle 10\bar{1}1\rangle$ direction between matrix and twin.

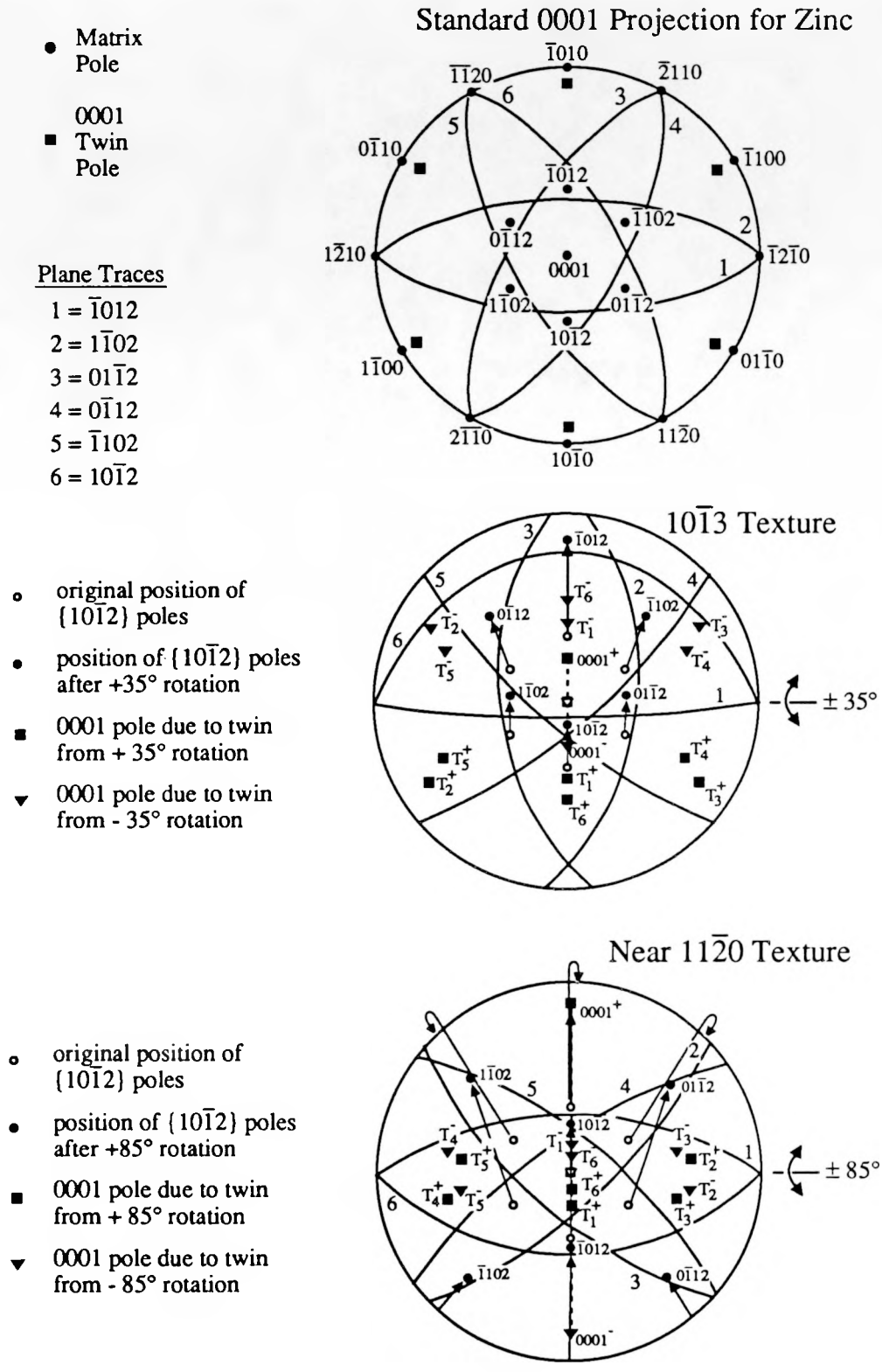

Figure R17 Schematic pole figures for zinc showing position of basal poles after twinning on $10\bar{1}2$ planes. a) Zinc crystal in basal orientation b) ± 35° rotation corresponding to sample D ($10\bar{1}3$ texture), c) ± 85° rotation corresponding to sample E (near $11\bar{2}0$ texture).

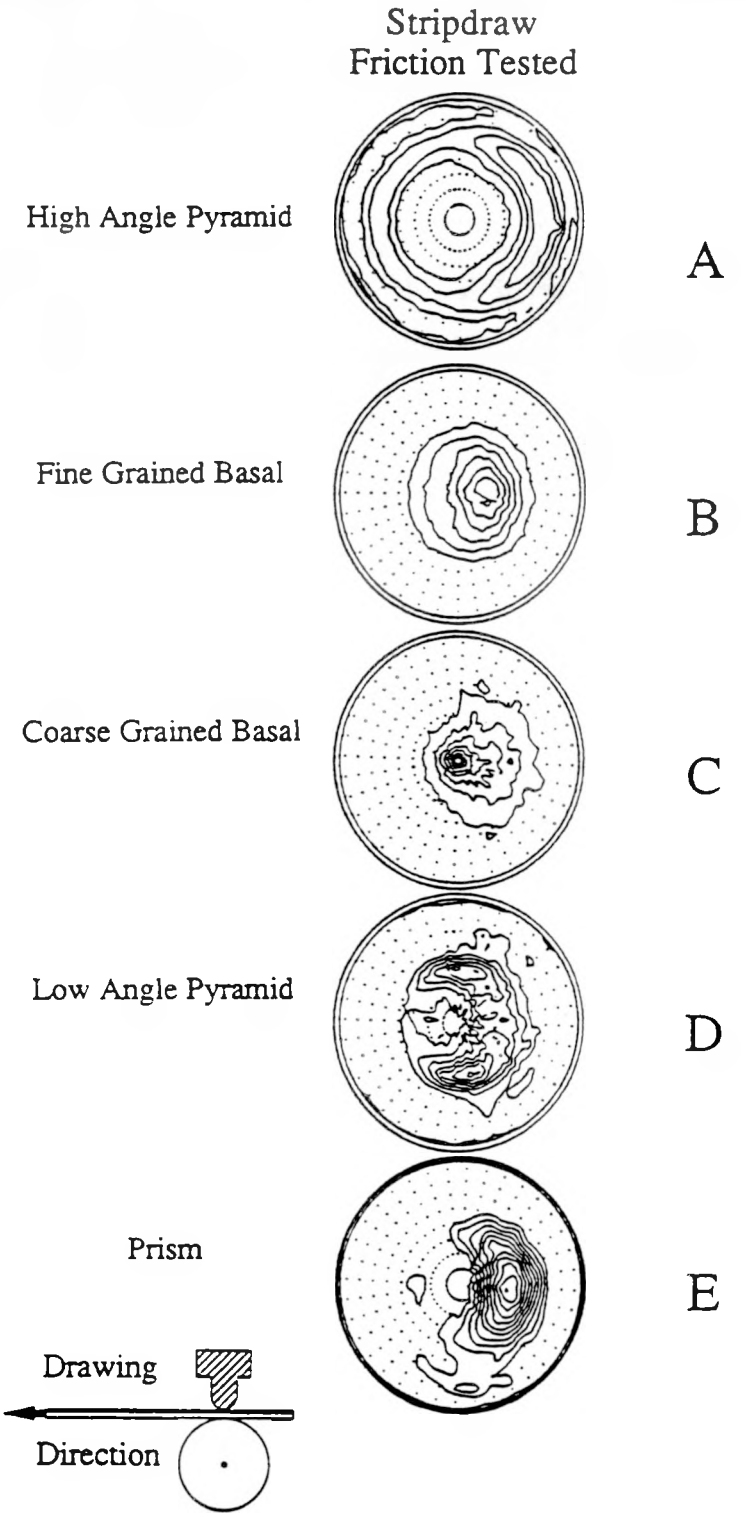

Figue R18) 0002 pole figures for EG coatings show change of texture of coatings after stripdraw friction testing. As in DBS testing, but to a lesser extent due to a shorter sliding distance, the surface of all coatings evolves toward the same final texture.

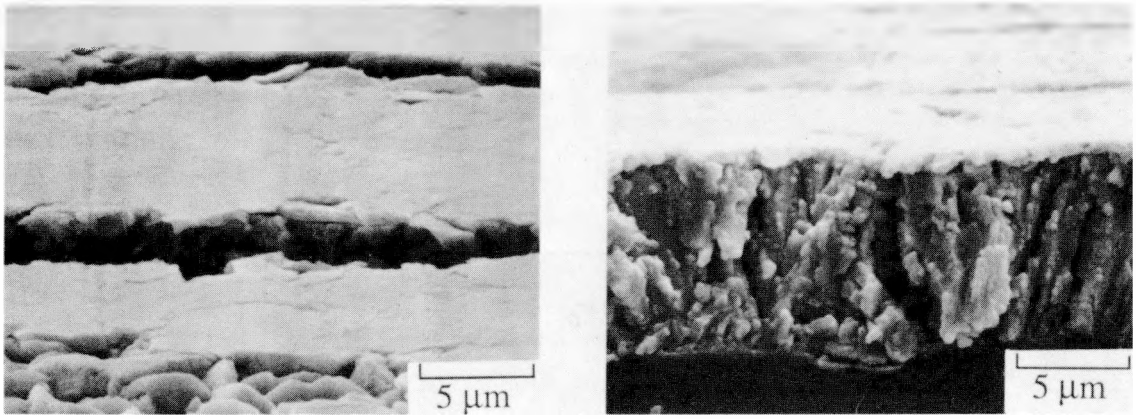

XBB 905-3533

Figure R19) The apparently shallow depth of deformation is seen in these cryogenically fractured cross-sections of EG coatings A (left) and E (right). (SEM micrographs)

a)

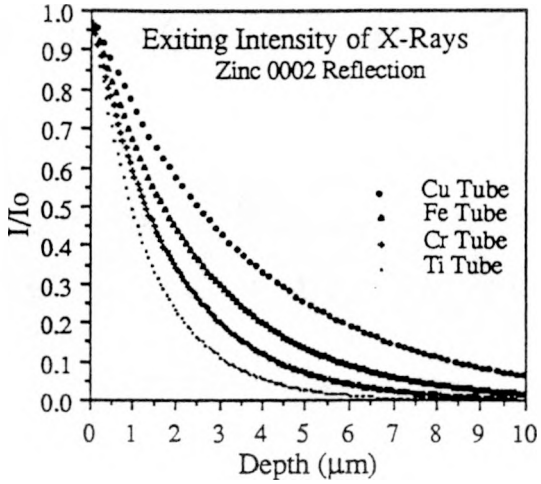

b)

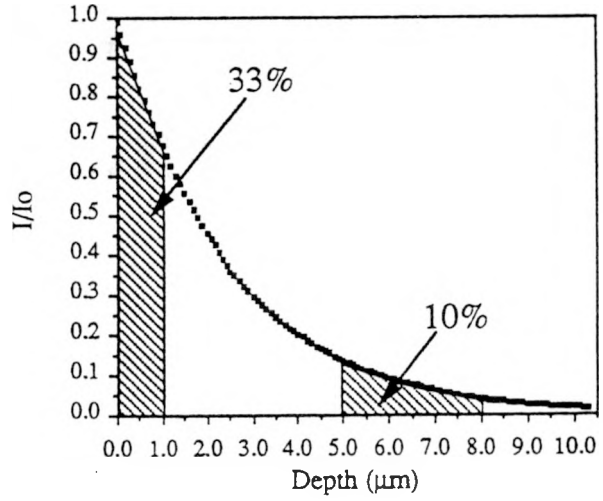

Figure R20) a) Reduction in intensity of reflected signal due to absorption as a function of depth for several x-ray sources. b) Volume contributing to the signal is given by the area under the curve. Note, for example, that for an Fe x-ray tube, one third of the signal is due to the top 1 μm, while only 10% is contributed from the depth of 5 to 8 microns.

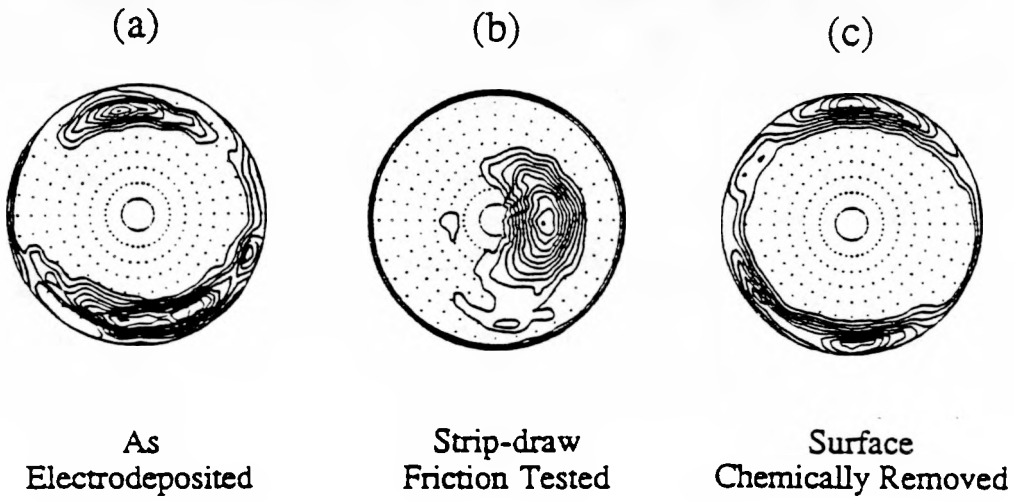

Figure R21) The texture at the surface after friction testing is distinct from that in the bulk of the coating as revealed by surface etching. a) As deposited b) after friction testing c) after etching away 4 μm of coating.

IV DISCUSSION

The three main results of the friction experiments in this study are as follows: 1) The texture of the zinc coating does not control friction as predicted through its anisotropic mechanical response to imposed loading or deformation conditions. 2) The contact surface area correlates with coefficient of friction in DBS testing. 3) Large changes in texture, restricted to a thin layer at the surface, take place as a result of friction testing and approach a similar final texture.

Each of these points as related to friction in EG steels merits further discussion, as well as some related issues. Finally, some preliminary modelling work will be discussed.

1 TEXTURE and FRICTION

1.1 TEXTURE and ANISOTROPIC MECHANICAL PROPERTIES

Contrary to the high vacuum, single crystal work of Buckley[I18,I19], no self-consistent correlation between texture and measured coefficient of friction was found in this work. Neither does our simple RSS based predictions provide agreement with the experimentally measured coefficients of friction in the DBS test. In particular, the anomalous behaviors of the fine grained basal textured sample and the Cd doped, near prism textured sample warrant further discussion.

1.1.1 Fine Grained Basal Texture

We turn to the straight stripdraw test for some insight. In examining the correlation between pulling load and area fraction (figure R9), the behavior of the fine grained basal samples does appear to agree with asperity deformation friction model predictions based on deformation by shear, i.e. least resistance for a given area. However it must be noted that the coarse grained basal samples behaved identically with the other zinc textures, as did the prism textured sample.

One plausible explanation is that under the lower loads, the morphology of the fine grained samples could be considered as individual single crystals compared with the coarse grained samples (figure D1). Simple shear of basal oriented single crystal zinc is predicted to be the easiest. The initial rapid increase in area fraction as a function of normal load in figure R10 may be due to the ease of shear of the individual crystallites of the fine grained basal oriented grains in the loading direction as compared with either the more constrained surface grains of the coarse grained basal samples or with the other orientations.

Alternatively, if the loading conditions were to move more towards the $\alpha=0$ end, this could further explain the behavior of sample B in figure 9. A significant change from the geometrically predicted compressive loading conditions to those of shear might occur under two possible conditions: 1) sticking at the interface, or 2) mechanical locking of asperities. However a slight change in conditions may not even be necessary to promote basal slip in the case of unconstrained grains, as the RSS may be large enough. Nevertheless, under the incomplete hydrodynamic lubrication conditions of the test, both of these events are possibilities to varying small extents. In particular, any slight transfer of zinc to the tooling then has the effect of promoting mechanical locking of asperities, which in turn would promote further sticking; an accelerating effect.

1.1.2 Other Views

The work of Lindsay, et. al.[I21] proposes that high friction in basal textured EG samples may be due to larger contact area on the flat faces of the basal oriented crystallites compared with the "tips" of the inclined pyramidal textured deposits. They model this as rows of bricks either lying flat with broad faces exposed (basal texture) and a large contact area, or bricks tilted on their edges with the opposite edges exposed, hence a small contact area. This would be classified as a "microroughness" effect. However, owing to the obliteration of the microroughness in both cases, it was instead suggested by Nine[D1] that transfer of zinc to the tooling (galling) was the cause of higher friction in their work.

In our tests however, no noticeable transfer of zinc was observed on the tooling. This is not to say that transfer could not have occurred, we were just not able to distinguish any by visual inspection. It is also possible that a steady state is reached in which zinc is transferred from the strip to the tooling and back. This transfer-retransfer mechanism is the (as yet unsubstianted) view of Prof. Schey[D2] for one of the primary mechanisms of stripdrawing friction in EG steel.

1.1.3 Prism Texture

In the also case of the Cd doped, prism textured samples, it is not clear whether the lower measured friction is a texture effect, hardness effect, or an initial surface roughness effect. In the DBS test, clearly, the "pillows" or nodules on the surface supported the load with a smaller contact area than any of the other samples (surface effect) as shown in figures D2 and R12. However, in the stripdraw tests, the deformed area fraction grew more slowly as a function of normal load (hardness effect). Both of these could also be viewed as a texture effect.

It is noted however, that there was an extreme change in texture resulting from friction testing in these samples as well. It was shown that this change in texture is related to the original texture by twinning and that it occurred in both the stripdraw (short contact length) and the DBS tests (longer sliding distance). It appears that this orientation has the promise of beneficial frictional properties via both its resistance to normal loading and its resistance to area growth.

It is possible that the energy required for twinning had an effect on reducing the contact area per normal load, as well as increasing the resistance to deformation by slip after twinning. Bell and Kahn[D3] showed that the critical resolved stress for twinning (CRST) was at least 100 times that of basal slip, and that after twinning, the CRSS on the basal system was more than 15 times normal. It is also significant to note that the initial texture is "hard" for the entire range of α, from shear to compression, for the $\psi = 90°$ orientation, as was the orientation of our samples.

Commercial, near prismatic orientations have been observed to exhibit low frictional properties[I22]. These same samples have also been observed to exhibit cracking of the coating resulting from the tensile strains due to bending imposed during the DBS test. This cracking through the coating thickness (figure D3) is considered undesirable by some automotive engineers, although others argue that the cracks are insignificant. Cracking was not observed in the stripdraw tests.

To avoid any potential problems with coating cracking, one obvious direction to explore would be the possibility of a duplex coating structure with pyramidal texture

through the bulk of the coating for good tensile deformation characteristics, and a top layer of prismatic texture for good frictional properties. Clearly this is an area for further research.

It was attempted to have a second set of samples made, of considerably greater coating thickness (on the order of 50 μm) so that the surface roughness effect could be eliminated through mechanical smoothing. Unfortunately, within the time and resources available for this work, after several attempts, deposition of such samples was not successful.

2 TEXTURAL CHANGES with FRICTION TESTING

Zinc has never been regarded as a technologically significant metal, being primarily used as an alloying addition, for non structurally critical castings, or as monolithic sacrificial anodes for ocean going vessels. Because of this, very little, if any, mechanical properties data or deformation and texture work has been done on zinc.

Recrystallization textures as a function of different modes of deformation from cold worked zinc have not been reported in the literature. In fact, the only literature data available for deformation textures of zinc is that for cold rolling of zinc of more than fifty years ago by Caglioti, et. al.[D4] and reported in Barrett and Massalski[D5] and that of Hofmann, et. al.[D6] reported in Wassermann and Grewen[D7]. In these works, it was found that the basal planes of zinc end up at between 20 and 25 degrees from the sheet normal after rolling, but could vary depending on the amount of twinning, which was influenced by alloying. Hargreaves[D8] found that the texture at the surface differed from that in the interior.

The points for discussion are how is it possible that coatings with such widely varying starting textures could end up with the same final texture, and what significance this has with regard to friction in EG steel.

2.1 Changes due to Deformation

For a tension test (stretching in the plane of the sheet), slip on the basal plane would cause rotation of the grains such that the basal poles move "towards" the sheet normal (or center of the pole figure). For compression normal to the sheet, the same results are expected. For shearing in the plane of the sheet, the basal poles are expected to rotate toward the direction of shearing.

In materials such as steel, where the 48 slip systems available in the bcc structure allow arbitrary shape changes to occur quite readily, at high enough strains, evolution to a common texture will eventually occur, independent of starting texture. The strains necessary for such evolution may be on the order of several thousand percent, depending on the differences in starting texture.

The strains seen on the surface of the stripdraw friction samples have been estimated to be only on the order of a few hundred percent at most. Additionally, with the lower symmetry and limited slip systems of zinc, evolution toward a common texture, if possible, would require significantly greater levels of strain than those for the higher symmetry bcc or fcc structures.

The main point here is that the similar textural changes observed for all the zinc samples, given the wide variation in starting textures, are undoubtedly achieved through mechanisms in addition to slip, such as recrystallization and/or twinning.

2.2 Changes due to Recrystallization

There is still debate as to the controlling mechanisms for recrystallization textures, and whether the recrystallized texture can be predicted from the deformed texture[D9]. As a result, it is as yet unclear, depending on the deformation mode and extent, whether recrystallization of a cold worked sample can lead to a common texture, independent of the starting texture. In the case of the surface deformation of the friction tested samples, owing to the localization of deformation, it is also possible that a dynamic recrystallization process is taking place.

Certainly a major factor which would promote recrystallization is the proximity of the testing temperature to .5 T_m (half the homologous melting point). At room temperature (20° C) zinc is already at .42 T_m. Recrystallization resulting from room temperature tension testing of 80μm thick electrodeposited coatings was reported by Read, et. al.[R10]. On top of this, there is also local heating of the deformed asperities due to the friction of sliding itself. The temperature rise at contacting asperities can be estimated using the formula developed by Rabinowicz[D11], and was found to be only on the order of 15° C, giving a T_m of .45. As an alternative approach, the samples themselves were quite warm to the touch after testing, hence their temperature must have been greater than normal skin temperature (34° C), which gives a T_m of .48. The local temperature at the asperities must then have been greater than that of the bulk or very near .5 T_m.

Given the relatively high strains and high homologous temperature of the zinc during friction testing, it is likely that recrystallization occurs. As such, all of the final textures can be explained primarily on the basis of recrystallization.

Unfortunately, no direct TEM evidence of recrystallization has yet been obtained. This is primarily due to the technical difficulties in producing an "undisturbed" cross-section with the electron transparent region confined to the top two microns of the coating. Due to the severe bending of the sample along the diamond blade during sectioning, ultramicrotomy techniques for preparation of TEM samples are not possible. New sample preparation techniques utilizing mechanical back thinning and final ion polishing are currently being developed, but have not been perfected as yet.

Instead a polished and etched metallographic cross section was examined in the SEM. Figure D4 shows that the top 1 μm layer of a DBS friction tested sample is essentially devoid of structure compared with the remainder of the coating. While one may be tempted to say this layer appears amorphous, this cannot be since diffraction occurred from this layer. It is more likely that the structure is so fine that the deformed surface grains could not be resolved with this etching procedure. As such the term "recrystallized" will be used.

2.3 Changes due to Twinning

While basal slip is the primary deformation mode in zinc, there are some combinations of orientation and loading condition for which the resolved shear stress for basal slip is so low that another deformation mode must be activated. This is twinning on the $\{11\bar{2}1\}<10\bar{1}1>$ system. There are six possible variants of this system and for the bi-symmetric orientations of samples E and F, this leads to 12 possible positions for the basal poles after twinning. These were shown in figure R17. The newly oriented twinned regions are then more favorably oriented for slip, and subsequently, recrystallization.

In a columnar grain structure the depth of twinning may very well exceed the depth of deformation by shear, as was shown in figure R21 where a return to the original texture was not achieved until four microns had been etched away. As such, the texture measured for sample E (and to a lesser extent D) may very well be a composite of the deformed and recrystallized top 1 μm layer, with possibly some residual twinned region below that, and finally the undeformed and untwinned sublayer.

It has previously been reported by Mathewson[D12] that compression normal to the basal planes or tension parallel to the basal planes (in the close packed direction) are the two loading conditions under which zinc will twin. The basal oriented samples are likely candidates for twinning under compressional loading, as are the near prism samples under tension (due to bending strains in the DBS test). However, similar final textures were found in the straight stripdraw samples where there was no tension due to bending. Although twinning as a result of shear loading has not been previously reported in the literature, it appears from this work that this too is a possible mode. In addition, in samples of "fiber texture", those grains whose basal planes are oriented such that the projection of their poles are along the tensile axis (ψ=90°) are also unfavorably oriented for slip under compressive loading (α=.8). As a result, these grains most likely undergo twinning as well.

2.4 Summary of Texture Changes and Relevance

The main point of the discussion on texture changes is that whether by deformation, recrystallization, twinning, or some combination thereof, a similar final texture is achieved, and that the starting texture does not seem to be of influence. Additionally, since the starting texture is readily changed, it also does not seem to be relevant to friction through its possible anisotropic response to plastic deformation. The role of texture, if any, seems to be through the ability to resist large areal contact or increases in areal contact during sliding. As such, some promise exists for the near prism orientations and further research in this area is required. It also appears relevant to avoid textures and microstructure combinations, such as the fine grained basal texture, which might promote zinc transfer during sliding.

Finally, due to the rapid evolution to similar final textures, it appears that what were previously thought to be anisotropic mechanical properties have become, in essence isotropic. Perhaps this is the reason for the good correlation between area fraction and coefficient of friction as measured by drawbead simulation. Further, some of those previously thought to be inapplicable friction models may again hold some promise, if they can account for the possible changing conditions and transfer mechanisms during sliding.

3 SURFACE CONTACT AREA and FRICTION

It has become apparent that a correlation between contact area fraction and DBS-μ exists. As such, those factors which affect surface contact area will influence friction to the extent that they dictate contact area. A list of such factors might include: texture (easy shear vs. difficult shear), hardness (compressive resistance), original surface roughness, and lubricant properties. We have seen that friction is not controlled through the easy vs. difficult shear differences predicted by RSS computations for different textures due to possible recrystallization or twinning. Although under certain circumstances, some orientations may contribute to the differences in contact area fraction. The two other primary factors within the coating itself which dictate contact area are original surface

roughness, and hardness. There may be some additional factors due to the substrate as well, depending on the test.

3.1 Surface Roughness

The original surface roughness of nearly all the sheets was nominally identical since all coatings were deposited on pieces of steel cut from the same coil. The exception was the set of cadmium addition samples which were made after the original 64 conditions and were plated on sheets which came from a different coil. After electrodeposition of the zinc coatings, the roughnesses were changed somewhat and such changes are reflected in the surface profilometry traces (figure D5a,b) and companion calculations (table 2) of parameters which describe the distribution of peak heights.

The "cadmium added" series also shows a change in surface roughness through the appearance of nodules or pillars on the surface of the coating (figure D6). The distribution of these nodules is non-uniform and their occurrence and height increases with cadmium content. While there does seem to be a trend toward "the rougher the surface, the lower the friction", there is not a one-to-one correspondence between coefficient of friction and any of the tabulated parameters. Additionally, there are certain limitations placed on the surface topography by the automotive companies in order to meet current paint appearance standards. Finally it is not at all clear at this time, which of the many roughness descriptive parameters, or combination thereof, is the best. This aspect is the focus of continued investigation.

3.2 Hardness

That the hardness can affect friction has been well documented for other materials[D13-D15]. It has also been shown effective in lowering friction in alloy-type galvanized coatings as demonstrated by the development of the duplex 85/15 Fe/Zn surface layer deposited over the 15/85 Fe/Zn sublayer in some Japanese work[D16]. Discussion with these researchers indicate that the main effect of the hardness is to reduce the contact area fraction, and thus give better frictional properties. Additional Japanese work[I27] on different types of coatings showed a beneficial effect of hardness, however it is difficult to legitimately compare hot dipped galvanized, electrogalvanized, galvannealed, and uncoated strips due to their differences in other properties as well, most notably surface characteristics.

In the case of nominally pure zinc coatings, there may be some benefit in trying to harden the EG zinc coating through the use of additions to the electrolyte. It is clear from this work that cadmium had a beneficial influence on hardness, whether through texture or otherwise, but EPA regulations cause manufacturers to shy away from use of such heavy metals if possible. Some proprietary experimental work on hardening the coating through the use of some type of organic "grain refiner" additions to the electrolyte has been carried out. Alternatively, in looking to solid solution strengthen zinc with metallic additions, the choice of materials is rather sparse. Table 3 lists other possible candidates. Owing to the expense of gold and the toxicity of mercury, silver may be the most viable choice for these types of experiments.

Table 3 : Metallic Candidates for Solid Solution Strengthening of Zinc
(Atomic radius of zinc = 1.53Å)

SYMBOL	Element	Reported % Solubility	Atomic Radius	% Mismatch
Ag	Silver	2.6 % at 200° C	1.75	14.3
Al	Aluminum	0.6 % at 275° C	1.82	19.0
Au	Gold	≈8% at 100° C	1.79	17.0
Cd	Cadmium	0.52% at 150° C	1.71	11.8
Cu	Copper	0.3% at 100° C	1.57	2.6
Fe	Iron	none reported < 400° C	1.72	12.4
Hg	Mercury	≈5-6 % at 43° C	1.76	15.0
Ni	Nickel	none reported < 400° C	1.62	5.9

Solubility data obtained from equilibrium binary phase diagrams published in : ASM Metals Handbook, v.8, 8th edition, (1973), pp.256, 265, 269, 287, 301, 308, 311, 326.

3.3 Determinants of Contact Area

We have seen that the two major factors within the coating itself which determine the contact area are the surface topography and the coating hardness. In addition to these, there are several factors determined by the friction test method. As such, it is important to examine whether one might expect a difference in contact area fraction depending on the type of test performed. There are several significant differences between the straight stripdrawing test and the DBS test which affect contact area fraction. These will be delineated below, under the assumption of identical lubricating conditions.

3.3.1 Stripdrawing

The contact area fraction in stripdrawing is determined by :

1) the load and width of strip,
2) the geometry (e.g. radius of curvature, length of flats, etc.) of the tooling,
3) the roughness of the tooling,
4) the roughness of the sheet (including the microroughness, waviness, etc.), and
5) the "strength" of the zinc supporting the load.

3.3.2 Drawbead Simulation (DBS)

The contact area fraction in DBS is determined, as in the case of straight stripdrawing by :

1) the load and width of strip,
2) the geometry (e.g. radius of curvature) of the tooling,
3) the roughness of the tooling,
4) the roughness of the sheet (including the microroughness, waviness, etc.), and
5) the "strength" of the zinc supporting the load.

In addition the contact area fraction in the DBS test is also determined by :

6) the strength (or thickness) of the substrate
   - a higher normal load is required for higher strength (or thicker) material to achieve the correct geometry for the test - hence the soft zinc coating would be deformed more.

7) the "r-value" of the substrate
   - this dictates the amount (and direction) of grain rotation, which leads to roughening of the free (convex) surface opposite that in contact with the tooling
8) the grain size of the substrate
   - which dictates the extent of the "r-value" effect

These last three parameters, concerning the substrate "mechanical properties", are what make it difficult to predict coefficient of friction in a "bending-type" friction test on the basis of surface roughness or zinc coating parameter specifications alone. This has become particularly evident with the use of materials with soft coatings. Similarly it is dangerous, if not impossible, to predict the frictional behavior in a bending-type test on the basis of a straight strip-draw type test, as was seen in the case of the fine grained basal samples in this work. It is useful however to examine the effects these differences may have. This will also be helpful in illuminating what is needed in order that specifications for EG steel may be formulated.

4 DBS vs. STRIPDRAW

The two significant differences between the stripdraw test and the DBS test are : 1) plastic bending/unbending deformation of the substrate, and 2) significantly longer sliding distance than in the straight stripdraw test. Both of these can be seen to manifest themselves in the contact area fraction.

4.1 Effect of Substrate Bending

As mentioned earlier, the bending and unbending of the substrate may be important due to the phenomenon known as "orange peel". This refers to roughening of the sheet, as a result of deformation, with an extent on the order of the grain size. Examining the geometry of the DBS test, it is clear that this change in roughness of the substrate is due to tension via bending while passing over the outside of the first bead. This will result in a change in contact area at the second bead as compared with the original roughness of the sheet. This phenomenon has been documented on both bare steel and aluminum by Nine[E8]. Such an effect will not appear in straight stripdrawing.

While this difference may exist between the two types of tests, in our DBS tests, all coatings were on the same substrate so for internal comparison this should not give rise to differences between the sheets in a given type of test. For comparison with other investigators' work, such an effect may have to be taken into account.

Whether or not this effect is significant on comparison of commercial sheets is not presently known. An experiment is proposed which will determine the relevance of this effect. Sheets of widely differing "r" values (representing the degree of sharpness of texture) would be required. The sheets should be polished to uniform surface roughness and then tested in two different ways: 1) stretched in tension, with the change in surface roughness measured after deformation. This would serve to measure the extent of the effect as a function of "r" value. 2) If a measurable effect was detected, subsequent friction testing in drawbead simulation would determine the relevance of the effect.

4.2 Effects of Sliding Distance

The effects of sliding distance are dependent on the operational friction mechanisms. Work by Shima and Yamamoto[D17] on the effect of tool/workpiece contact length indicate an increase in coefficient of friction due to a reduction in lubricant film thickness resulting from an increase in temperature. This in turn increases the amount of metal to metal contact compared with pure hydrodynamic conditions. A similar phenomenon is likely taking place in our DBS vs stripdraw studies.

Other experiments by vonStebut and Perry[D18] on multipass vs. single pass strip testing of bare and coated steels show a increase, though at a diminishing rate, of the contact area with subsequent pass. They however report an associated decrease in measured coefficient of friction. They attribute this to less adhesive junction formation due to the lower local pressures resulting from asperity ironing with subsequent pass at constant normal load. In their work however, lubrication is minimal and junction formation is the dominant friction mechanism.

These results indicate that the increased sliding distance of the DBS test may be what distinguishes the fine grained basal from the coarse (and the pyramidal textures). The small crystallites are easily sheared, but lead to a large increase in contact area. These two effects compensate one another in the stripdraw test, while the DBS test is dominated by the contact area. The pulling load for a given area fraction for the Cd doped, prism textured samples was the same as the other pure zinc samples in the stripdraw test. At the same time, the "pillow" decorated surface roughness, combined with an increase in hardness for these samples gave rise to lower area fraction for normal load as well as low contact area in the DBS test. This led to low frictional coefficients in both the stripdraw and the DBS tests.

Basal Textured EG Deposits

a)

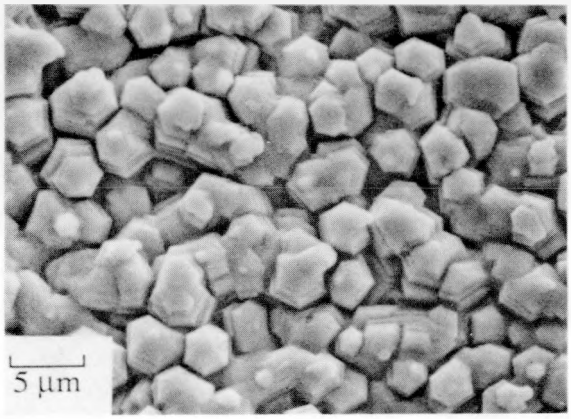

b)

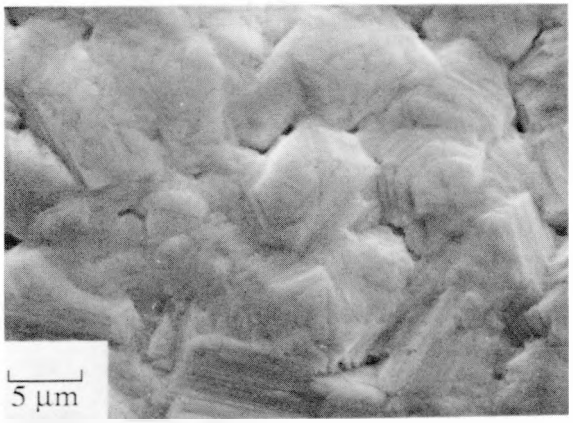

XBB 898-6995

Figure D1) Microroughness differences resulting from zinc crystallite morphology of zinc in a) fine grained, and b) coarse grained basal textured EG electrodeposits.

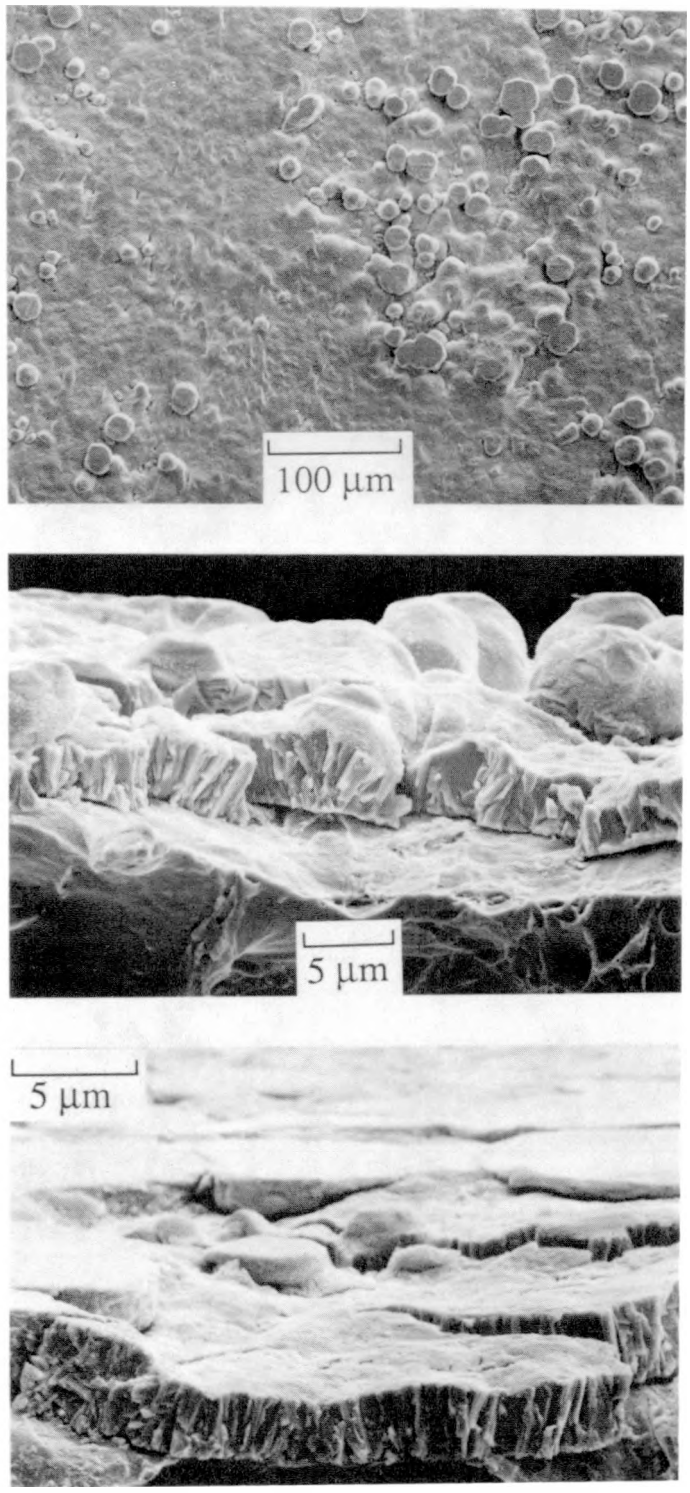

XBB 905-3534

Figure D2) Nodules on Cd added, near prism texture sample E. a) surface b) cryogenically fractured cross-section c) after DBS friction testing.

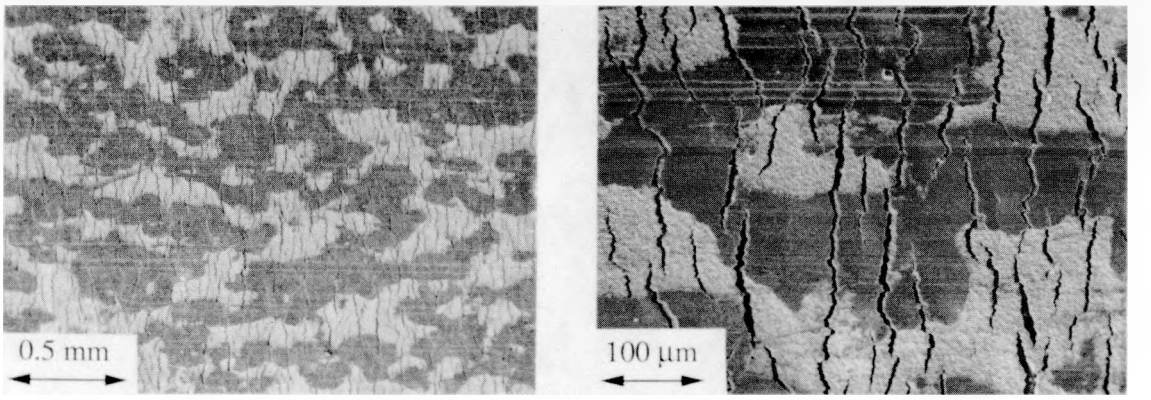

XBB 904-3480

Figure D3) Cracking through the thickness of the coating is observed after DBS testing in this commercial, near prism textured EG steel.

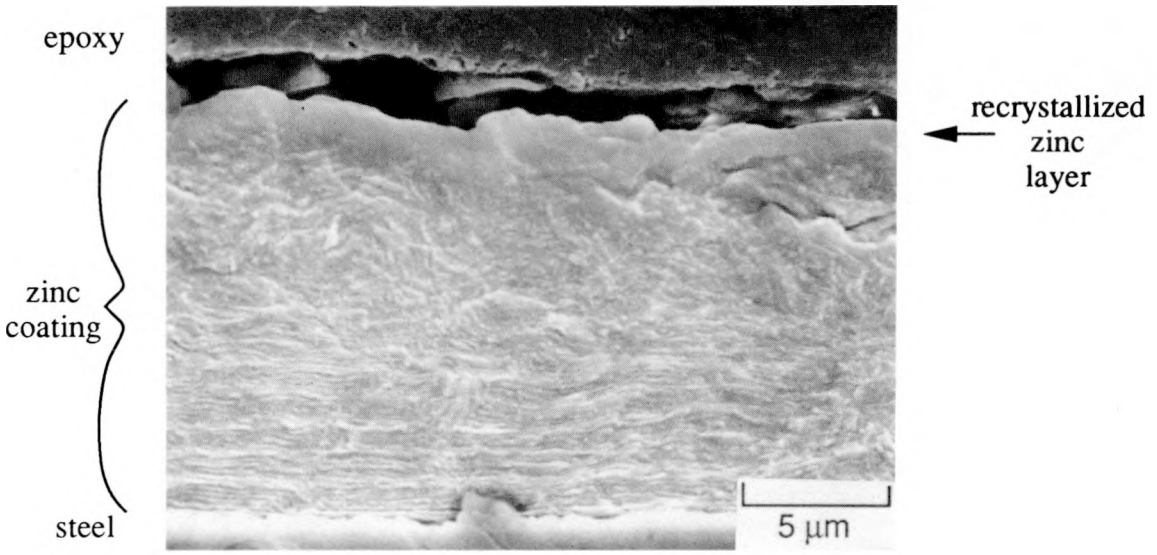

Figure D4) Polished and etched cross-section of DBS-Tested sample showing recrustallized region at the surface.

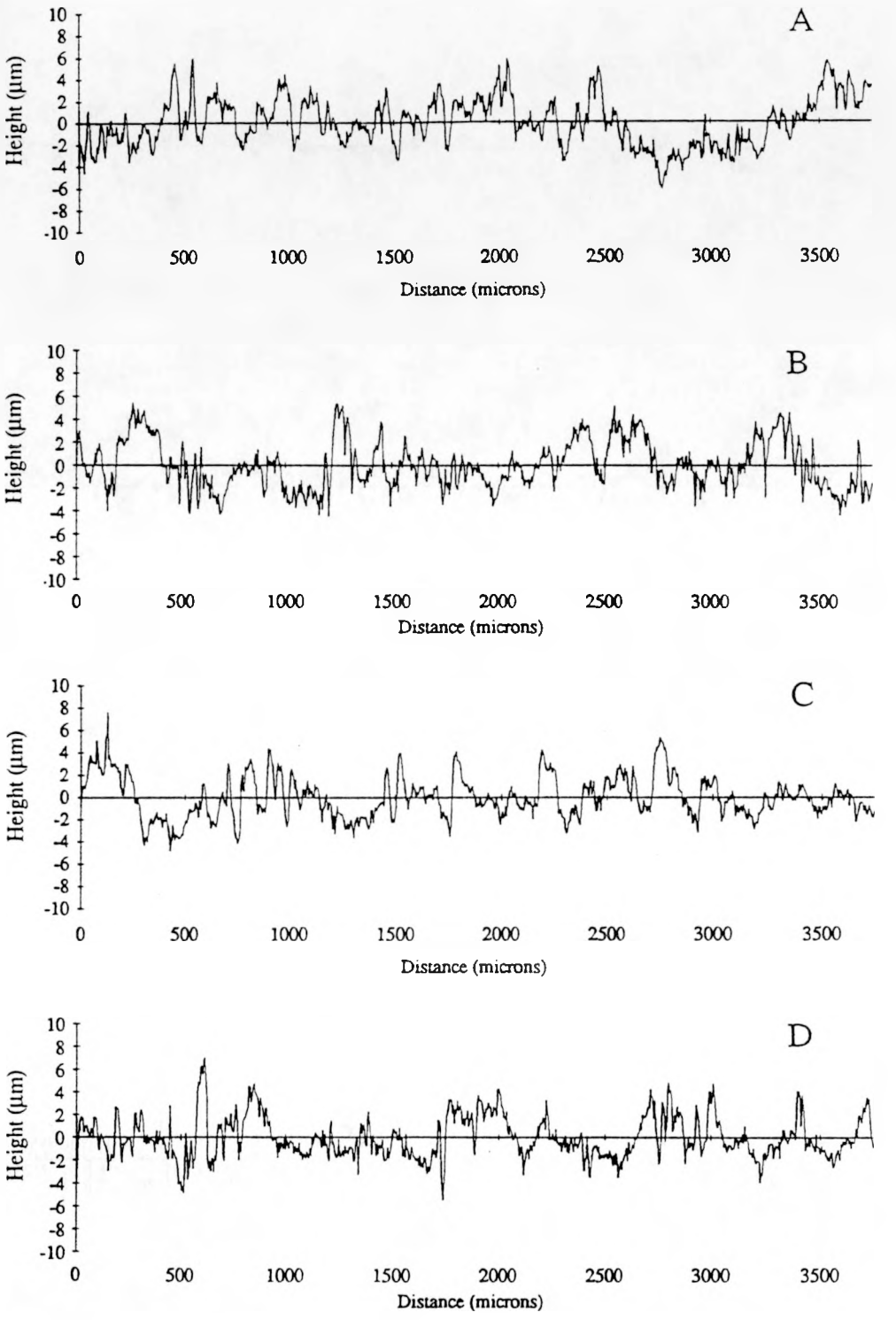

Figure D5a) Surface profilometry traces of laboratory EG samples of pure zinc, different textures used in this work.

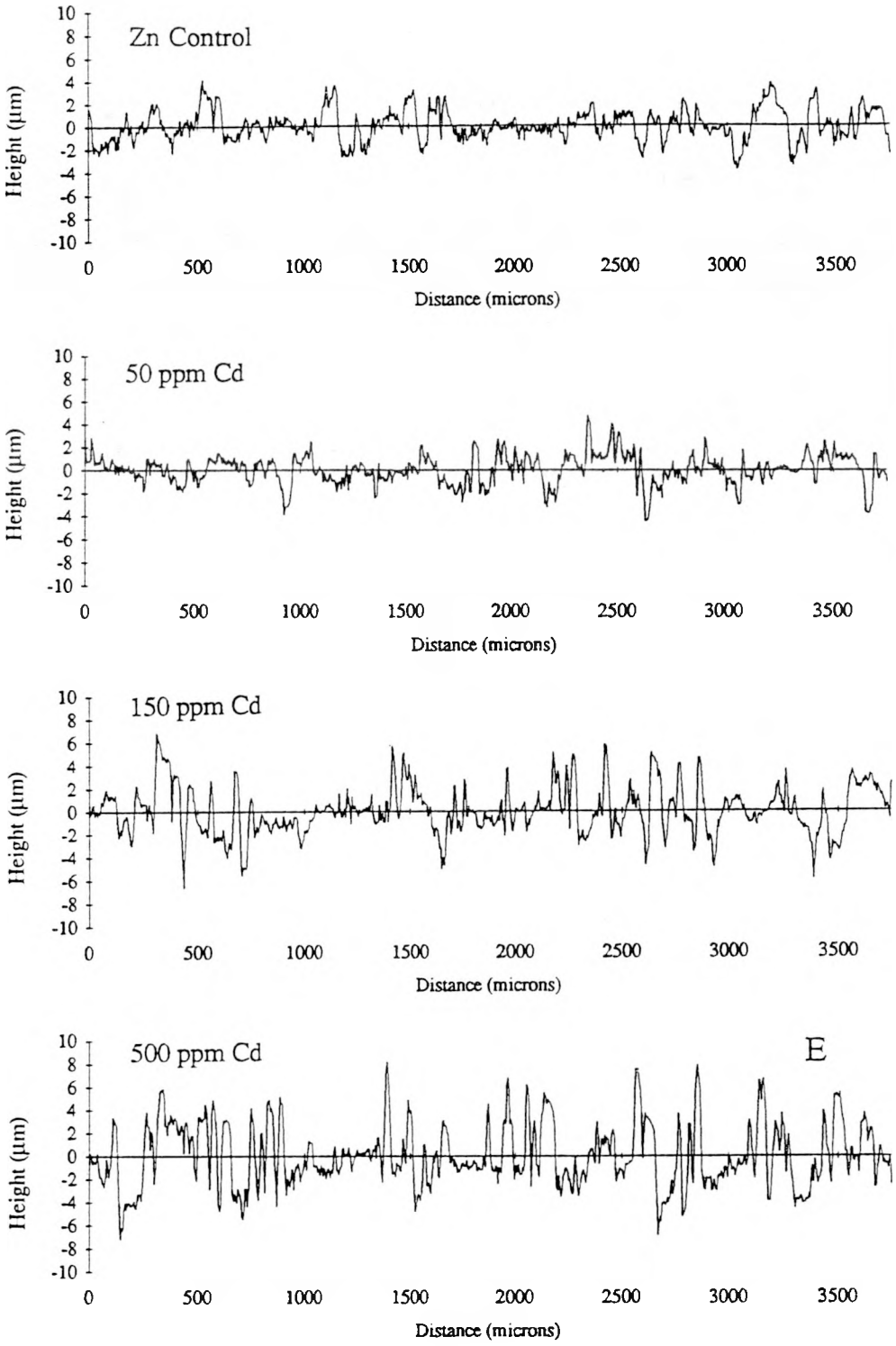

Figure D5b) Surface profilometry traces of laboratory EG samples of the Cd added series, with an increase in both prism texture and roughness.

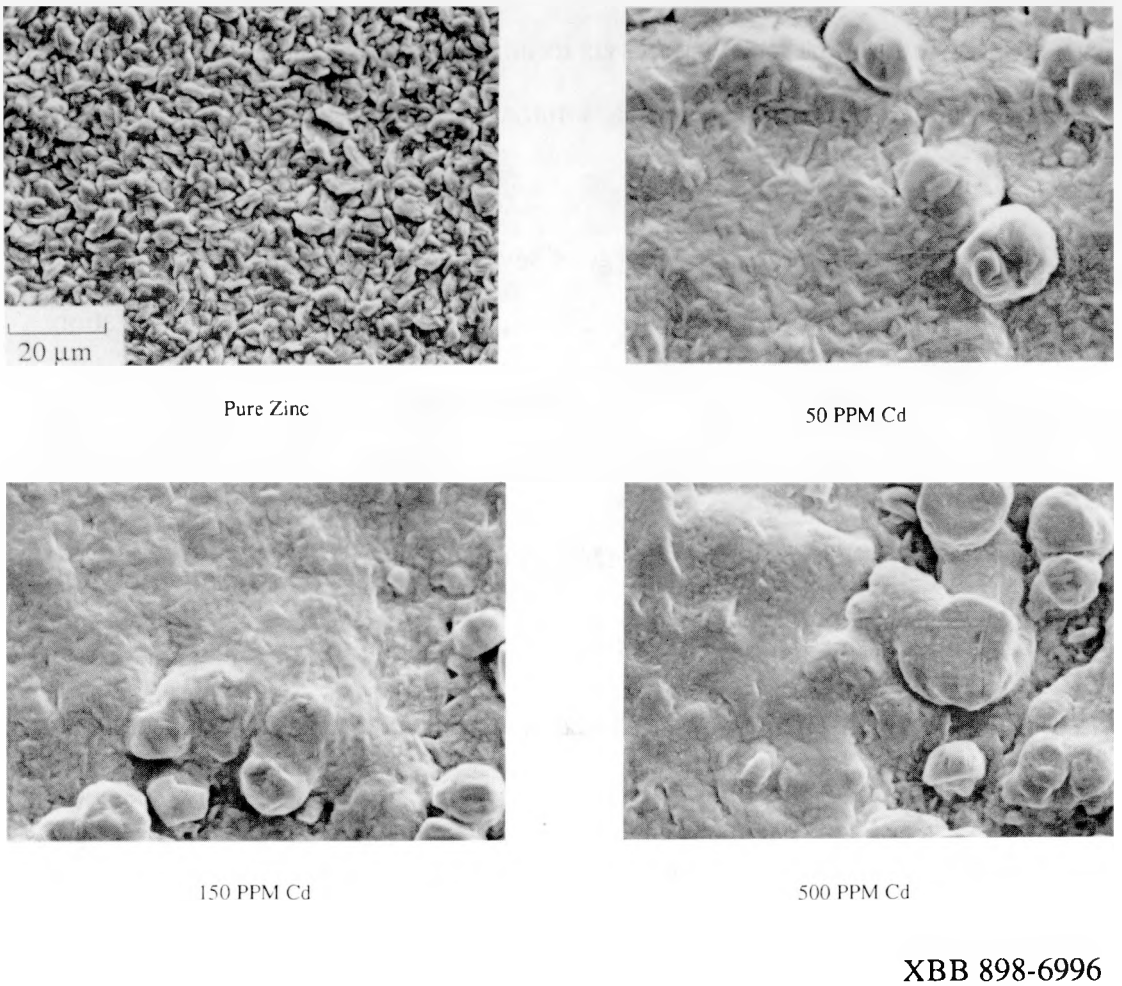

Figure D6) SEM micrographs of the surfaces of the Cd addition series showing nodules which give rise to significant change in surface roughness.

V CONCLUDING REMARKS

1 CONCLUSIONS

Based on the results of this work the following conclusions have been drawn:

1) The texture of the zinc coating, via its anisotropic mechanical response to plastic deformation, does NOT play a dominant role in determining friction in strip drawing tests.

2) The zinc at the surface undergoes severe local deformation, approaching a similar final texture with evidence of twinning and possible recrystallization.

3) DBS-μ correlates correlates well with contact area fraction in pure zinc EG steels, hence those factors which control contact area fraction control friction.

2 IMPLICATIONS and RECOMMENDATIONS

From the second conclusion :

a) Models which predict basal textured zinc to have low friction coefficient via its easy slip are inappropriate.

b) Basal oriented zinc can give rise to very high friction, due to the ease of shear and possible transfer of zinc to the tooling. As such, basal oriented deposits should be avoided.

c) Transfer / retransfer of zinc from the sheet to the tooling and back may be important, especially in fine grained basal textured specimens.

From the Third Conclusion :

Factors which control contact area fraction :

a) Initial surface roughness

b) coating hardness

i) prism texture (possible surface layer in duplex structure)

ii) alloy additions

c) possible substrate properties : r- value via change in surface roughness

d) lubricant rheology

3 DIRECTIONS for FUTURE WORK

The above list of factors which control contact area fraction should provide the directions for future research in the area of controlling friction in EG steels. Based on these implications, as well as some of the things encountered in this investigation, the following directions for continued research in the field of EG friction and formability are proposed.

1 Studies with controlled surface roughness variations - same zinc coating (laboratory deposited).

2 Studies with controlled hardness variations - same roughness (via thick deposits which are mechanically smoothed or post-coating "embossed").

3 Studies of r-value effect on contact area (and friction) from surface roughening due to stretching and bending.

4 Studies with variations of sliding distance in straight stripdraw tests.

5 Lubricant studies - rheology and additives (boundary compounds for anti-sticking).

6 Computer simulations of different combinations of shear vs. compression (α).

REFERENCES

INTRODUCTION

I1 M.G. Fontana & N.D. Greene, **Corrosion Engineering**, McGGraw Hill, New York, (1978), pp. 266-267.

I2 C.R. Barrett, W.D. Nix, & A.S. Tetelman, **The Principles of Engineering Materials**, Prentice-Hall, Inc., Englewood Cliffs, New Jersey, (1973), pp. 185-187.

I3 S. J. Shaffer, A.M. Phillip, & J.W. Morris, Jr., "The Micromechanisms of Surface Friction in Zinc Electrogalvanized Steel Sheets", in **Proc. GALVATECH '89, International Conference of Zinc and Zinc Alloy Coated Steel Sheet**, (September 5-7, 1989), Tokyo, ISIJ, pp. 338-344.

I4 T.R. Roberts, F.H. Guzzetta, & R.Y. Lin, "Morphology of High Rate Electrozinc", *Plating and Surface Finishing*, v.75, (September 1988), pp. 53-58.

I5 I. Tomov, Chr. Cvetkova, V. Velinov, A. Riesenkampf, & B. Pawlik, "Factors influencing the preferential orientations in zinc coatings electrodeposited from chloride baths", *J. Appl. Electrochemistry*, v.19, (1989), pp. 377-382.

I6 A. Weymeersch, R. Winand, & L. Renard, "Zinc Electrodeposition at High Current Densities, Part 2: Characteristics of Deposits", *Plating and Surface Finishing*, (May 1981), pp. 115-117.

I7 R.D. Naybour, "Morphologies of Zinc Electrodeposited from Zinc-Saturated Aqueous Alkaline Solutions", *Electrochimica Acta*, v.13, (1968), pp. 763-769.

I8 N. Izworski, Personal Communication, Ford Motor Company Data, April, 1988.

I9 S.P. Keeler & T.E. Dwyer, "Frictional Characteristics of Galvanized Steels Evaluated with a Draw Bead Simulator", **SAE Technical Paper # 860433**, (1986).

I10 H.D. Nine, "Drawbead Forces in Sheet Metal Forming", in **Mechanics of Sheet Metal Forming**, D.P. Koistinen and N.M. Wang, eds., Plenum Press, New York, (1978), pp. 179-211.

I11 P. Urcheck, Ford Motor Company, Personal Communication, May, 1989.

I12 John A. Schey, **Tribology in Metalworking, Friction, Lubrication, and Wear**, published by Amer. Soc. for Metals, 1983, Metals Park, OH, p.31.

I13 D.H. Buckley, **Surface Effects in Adhesion, Friction, Wear, and Lubrication**, Elsivier, Amsterdam, (1981).

I14 J.M. Challen & P.L. Oxley, "An Explanation of the Different Regimes of Friction and Wear Using Asperity Deformation Models", *Wear*, v.53, (1979), pp. 229-243.

I15 C.M. Edwards & J. Halling, "An Analysis of the Plastic Interaction of Surface Asperities and its Relevance to the Value of the Coefficient of Friction", *J. Mech. Eng. Sci.*, v.10, (1968), pp. 101-110.

I16 K. Komvopoulos, N. Saka, & N.P. Suh, "The Mechanism of Friction in Boundary Lubrication", *J. Tribology, Trans. ASME*, v. 107, (1985), pp. 452-462.

I17 T. Wanheim & N. Bay, "A Model for Friction in Metal Forming Processes", Ann. of CIRP., V.27, (1978), pp. 189-194.

I18 D.H. Buckley & R.L. Johnson, "The Influence of Crystal Structure and Some Properties of Hexagonal Metals on Friction and Adhesion", *Wear,* v.2, (1968), pp. 405-419.

I19 D.H. Buckley, "Influence of Crystal Orientation on Frictional Characteristics of Titanium Single Crystals in Vacuum", **NASA TN D-2988**, (1965).

I20 V. Rangarajan, D.K. Matlock, & G. Krauss, "Effects of Coating Properties on the Friction Response of Zinc Coated Sheet Steels", in **Zinc-Based Steel Coating Systems: Metallurgy and Performance**, G. Krauss & D. K. Matlock, eds., TMS, Warrendale, PA, (1990), pp. 263-280.

I21 J.H. Lindsay, R.F. Paluch, H.D. Nine, V.R. Miller, and T.J. O'Keefe, "The Interaction Between Electrogalvanized Zinc Deposit Structure and the Forming Properties of Sheet Steel", *Plat. and Surf. Finishing*, v.76, (1989), no.3, pp. 62-69.

I22 S.J. Shaffer, W.E. Nojima, P.N. Skarpelos, & J.W. Morris, Jr., "Research on the Metallurgical Determinants of Formability in Electrogalvanized Sheet", in **Zinc-Based Steel Coating Systems: Metallurgy and Performance**, G. Krauss & D. K. Matlock, eds., TMS, Warrendale, PA, (1990), pp. 251-262.

I23 T. Nakamori & A. Shibuya, "Effects of Galvannealling Conditions and Coating Weight on Powdering Resistance of Galvannealled Steel Sheet", **Corrosion Resistant Automotive Sheet Steel**, ed. L. Allegra, ASM, Metals Park, OH, (1988), pp. 139-149.

I24 Y. Hisamatsu, "Science and Technology of Zinc and Zinc Alloy Coated Steel Sheet", in **Proc. GALVATECH '89, International Conference of Zinc and Zinc Alloy Coated Steel Sheet**, September 5-7, Tokyo, ISIJ, (1989), pp. 3-12.

I25 S.-W. Pak, & M. Meshii, "Structure-Mechanical Property Relation in Zinc Electrogalvanized Coatings", in **Zinc-Based Steel Coating Systems: Metallurgy and Performance**, G. Krauss & D. K. Matlock, eds., TMS, Warrendale, PA, 1990, pp. 357-369.

I26 V. Rangarajan, N.M. Giallonrakis, D.K. Matlock, & G. Krauss, "The Effect of Texture and Microstructure on Deformation of Zinc Coatings", *J. Mater. Shap. Tech.*, v.6, no.4, (1989), pp. 217-227.

I27 S. Nakamura, M. Yoshida, & A. Nishimoto, "Frictional Characteristics of Coated Steel Sheets", in **Controlling Sheet Metal Forming Processes**, Proc. 15th Biennial IDDRG Congress, May 16-18, Dearborn, ASM Int., (1988), pp. 77-83.

EXPERIMENTAL DETAILS

E1 H. Leidheiser, Jr. and D.K. Kim, "Crystallographic Factors Affecting the Adherence of Paint to Deformed Galvanized Steels", *J. of Metals*, (Nov. 1976), pp. 19-25.

E2 Cited in ref (I26), p.217.

E3 L.G. Schultz, "A Direct Method for Determining Preferred Orientation of a Flat Reflection Sample Using a Geiger Counter X-ray Spectrometer", *J. Appl. Phys.*, v.20, (1949), pp. 1033-1036.

E4 H.-R. Wenk, "Measurement of Pole Figures" in **Preferred Orientation in Deformed Metals and Rocks: An Introduction to Modern Texture Analysis**, H.-R. Wenk, editor, Academic Press, Inc., New York, (1985), pp.11-47.

E5 J.S. Kallend, U.F. Kocks, A.D. Rollett, & H.-R. Wenk, : **popLA: the Preferred Orientation Package from Los Alamos**, University of California, Los Alamos National Laboratory, 1990. Documented in : "Operational Texture Analysis", *Mat. Sci. and Engin,* (in press).

E6 H.D. Nine, "The Applicability of Coulombs's Friction Law to Drawbeads in Sheet Metal Forming", *J. Applied Metalworking*, Vol.2., No.3, (1982), pp. 200-210.

E7 H.D. Nine, "New Drawbead Concepts for Sheet Metal Forming", *J. Applied Metalworking*, Vol.2., No.3, (1982), pp. 185-191.

E8 H.D. Nine, "Testing Lubricants For Sheet Metal Forming", **Proc. of The Metallurgical Society of AIME**, St. Louis, MO, (1982).

E9 E. Leitz, "Instructions for MINILOAD Hardness Tester", (1972), p.9.

E10 J. Hisamoto, personal discussion following presentation of "The Effect of Coating Hardness on the Peeling-Off Behavior of Electrogalvanized Steel Sheets and SOme Aspects of Their Press Formability", TMS Symposium on **Zinc-Based Steel Coating Systems: Metallurgy and Performance**, October 8, 1990.

E11 F.W. Daniels & C.G. Dunn, "The Effect of Orientation on Knoop Hardness of Single Crystals of Zinc and Silicon Ferrite", *Trans. ASM*, v. 41, (1949), pp. 419-442.

E12 G. Arrigoni & M. Sarracino, "Influence of Sheet Surface Roughness on the Top-Coat Appearance in Autobodies Painting Processes", Proc. IDDRG Congress, (1986), pp. 305-313.

E13 **Surface Texture (Surface Roughness, Waviness, and Lay)**, ANSI/ASME B46.1-1985, pub. by Am. Soc. of Mech. Engrs., New York, (1985).

E14 T. R. Thomas, ed. **Rough Surfaces**, Longman, London, (1982).

E15 J.F. Archard, "Surface Topography and Tribology", *Tribology*, v.7, (1974), pp. 213-220.

E16 E.J. Abbott & E.A. Firestone, "Specifying Surface Quality", *Mech. Engng.*, v.55, (1933), pp. 569-572.

E17 **Surface Topography in Engineering: A State of the Art**, review and bibliography T.R. Thomas & M. King, BHRA Fluid Engineering, Cransfield, England, (1977).

E18 Proceedings from the various : **Metrology and Properties of Engineering Surfaces**, 1st Int Conference, Leicester, (1979), 2nd Int. Conf., Leicester, (1982), 3rd Int. Conf., Teeside, (1985), 4th Int. Conf., Washington D.C., (1988).

RESULTS

R1 G. Sachs, "Zur Ableitung einer Fleissbedingung", *Z. Ver. Dtsch. Ing.*, v.72, (1928), pp. 734-736.

R2 R.K.W. Honeycombe, "Deformation of Hexagonal Metal Crystals", in **The Plastic Deformation of Metals**, 2nd edition, published by Amer. Soc. for Metals, Metals Park, (1982), p.114.

R3 J.K. Vennard, "Liquid Flow in Open Channels" in **Elementary Fluid Mechanics**, J.Wiley & Sons, Inc. New York, (1961), pp. 348-392.

DISCUSSION

D1 H.D. Nine, Personal Communication, GM Research Labs, April 1989.

D2 J.A. Schey, Personal Communication, Spring 1990 NADDRG Meeting, Ann Arbor, May, 1990.

D3 R.L. Bell & R.W. Cahn, "The Dynamics of Twinning and the Interrelation of Slip and Twinning in Zinc Crystals", *Proc. Roy. Soc. London,* v.A239, (1957), pp.494-521.

D4 V. Caglioti, G. Sachs, & M.A. Valouch, *Metallwirtschaft*, v.11, (1932), pp.165-166.

D5 C. Barrett & T.B. Massalski, **Structure of Metals**, 3rd edition (1980), Pergamon Press, Oxford, p. 561.

D6 W. Hofmann & B. Trautmann, *Z. Metallkde*, v.30, (1938).

D7 G. Wasserman & J. Grewen, **Texturen Metallischer Werkstoffe**, Springer, Berlin, (1962), p.152.

D8 A. Hargreaves, *J. Inst. Metals*, v.71, (1945), p.73.

D9 G. Gottstein & H. Mecking, "Recrystallization", in **Preferred Orientation in Deformed Metals and Rocks: An Introduction to Modern Texture Analysis**, H.-R. Wenk, editor, Academic Press, Inc., New York, (1985), pp. 183-214.

D10 H.J. Read, W.H. Smith, & W.B. Joseph, *"The Strength and Ductility of Zinc Electrodeposited from Acid Baths"*, Proc. Amer. Electroplaters Soc., v.51, (1964), pp. 61-65.

D11 E. Rabinowicz,"The Temperature of Sliding Surfaces", in **Friction and Wear of Materials**, J. Wiley & Sons, Inc., New York, (1965), pp. 86-94.

D12 C.H. Mathewson, in : **Zinc - The Science and Technology of the Metal, Its Alloys and Compounds**, Reinhold Pub. Co, New York, (1959), pp. 411-419.

D13 P.J. Alison & H. Wilman, "The Different Behaviour of Hexagonal and Cubic Metals in their Friction, Wear and Work Hardening During Abrasion", *Brit. J. Appl. Phys.*, v. 15, (1964), pp. 281-289.

D14 A.D. Sarkar, **Friction and Wear**, Academic Press, London, (1980), p.71.

D15 E. Rabinowicz, "Material Properties Which Influence Surface Interactions", in **Friction and Wear of Materials**, J. Wiley & Sons, Inc., New York, p.27, (1965).

D16 Y. Numakura, Nippon Steel Corporation, Personal Communication at Lawrence Berkeley Laboratory, March 7, 1990.

D17 S. Shima & N. Yamamoto, "Effect of Tool-Workpiece Contact Length on Friction Coefficient in Metal Forming", in **Advanced Technology of Plasticity** 1987, K. Lange, editor, Springer-Verlag, Berlin, pp. 901-908.

D18 J. von Stebut & D. Perry, "Strip Drawing of Boundary Lubricated Uncoated and Precoated Steel Sheets: Friction Response and Metal Transfer as a Function of Tool Surface Parameters", presented at the 15th IDDRG Congress, Dearborn, MI. May, 1988.

APPENDIX A

FRICTION REGIMES, MODELS, and THEORIES

Brief Review of Friction

Friction entails the interaction of a multicomponent system and depends on many variables within the system. In the measurement and description of friction, it has become common to refer to the constant of linear dependance of the resistance to sliding motion (i.e. the pulling force - F) on the normal load (N) as the coefficient of friction; μ, or $F=\mu N$. Bowden and Tabor[A1], among others, in order to put this into a microscopic view of local contact at an asperity, divide each of these forces by the local area of contact and write: $\tau = \mu P$. Where τ is the local shear stress and P is the local pressure.

1 Friction Regimes

To circumvent the monumental task of accounting for all the interacting variables, early tribologists have, in an attempt to simplify the situation, divided friction up into a number of regimes. Each regime of friction has a characteristic range of μ and is dependant upon particular variables. Noting that "nominally flat" contacting surfaces are microscopically very rough, and are composed of many peaks and valleys, one can see that the three regimes are broadly distinguished by the relative amount of contact between the asperities on the two surfaces, combined with the chemical nature of the surfaces.

1.1 Hydrodynamic Lubrication

Complete hydrodynamic lubrication requires a special geometry, such as that found in journal bearings, and depends on the formation of a converging wedge of lubricant, in which the viscosity increases with pressure, and completely separates the two surfaces. The key feature is the absence of metal to metal contact. μ_h (where the subscript h refers to hydrodynamic) in this case lies in the range of .001 to .01 and can be accurately predicted knowing the lubricant type, and the temperature, geometry, and speed of the moving bearing. Quasihyrdodynamic lubrication refers to a regime where only portions of the surface are completely separated by a lubricant film.

1.2 Boundary Lubrication

In boundary lubrication the loads and geometry are such that there is some contact between surfaces at the tips of the asperities on the tooling and the workpiece. However chemical additives to the lubricant react with one or both surfaces to form an interfacial boundary film, whose role is the prevention of metal to metal contact and subsequent formation of welded junctions. Normally the interfacial film has a lower shear strength than that of the lower strength metal. In boundary lubrication the coefficient of friction depends on the strength of the interfacial film formed by the boundary compound and the ability of the boundary compound forming additive to rapidly react and reform if it is scraped off and virgin metal is exposed. In the ideal case, μ_b (b stands for boundary) does not depend on the carrier lubricant properties and lies in the ranges of .01 to 0.1.

1.3 "Dry" Lubrication

In dry, or unlubricated sliding, or cases where the loads are high enough to produce metal-to-metal contact, μ_m (m stands for metal-to-metal) depends on the shear strength of the softer metal. In some cases, cold welded junctions are formed and subsequently sheared. In the case where all surface films have been removed, μ_m has been measured in the ranges of 0.1 to greater than 1.0[A2].

For the case of sheet metal forming, friction in all three regimes is simultaneously taking place in localized regions and the overall coefficient has been described as a linear function of the three : $\mu = a\mu_h + b\mu_b + c\mu_m$ where a, b, and c represent the area fractions for each of the hydrodynamic, boundary, and metal-to-metal coefficients of friction, respectively (figure A1)[A3]. This is sometimes known as a mixed lubrication regime. It is clear that one wishes to maximize a (or b) while minimizing c.

2 Friction Models

The simplest macroscopic model of friction is owed to Coulomb[A4] or Amontons[A5], which implies that that the frictional resistance to a pulling load is linearly proportional to the normal load and independent of contact area; $f=\mu N$. The constant of proportionality is known as the coefficient of friction, μ. This was more of an observation than a model, but essentially comprises an elastically deformed area of contact mechanism model.

Another method similar to the use of μ as the coefficient of friction has been to use a "friction factor" ; m (essentially a "sticking" parameter), in the equation $\tau=mk$. This is also known as the constant friction stress model, due originally to Orowan[A6], and later refined by Shaw, et al.[A7], and is used for cases of high contact pressures where plastic flow occurs. Here m, which can vary between 0 and 1 represents the fraction of shear strength of the softer material, and encompasses both the real contact area fraction as well as the reduction in strength due to any surface films. Most of the recent work on friction between contacting solids uses an approach similar to this and attempts to delineate factors from which m can be predicted.

3 Mechanistic Theories for Friction due to Plastic Deformation

Attempts by investigators to explain friction in terms of fundamental mechanisms have given rise to such concepts as the "molecular attraction" theory of friction of Tomlinson[A8], and the surface energy approach of Machlin and Rabinowicz [A9,A10]. These early theories did not receive much in the way of experimental confirmation or support and have more recently been replaced by physical models in which plastic deformation is seen to be paramount.

Such recent models recognize the contributions from several mechanisms. In addition to hydrodynamic components, recent theories attribute frictional resistance to 1) junction formation and shearing, and 2) plowing. Asperity deformation has been modelled by Edwards and Halling[A11] using both slip-line field and upper bound analysis of a single deforming asperity. Challen and Oxley[A12] use similar analysis to explain different regimes of friction and wear. Wanheim, et al.[A13], make use of the interaction between adjacent slip-line fields and predict that both the growth of real area of contact and the

nominal friction stress are asymptotic functions of the normal pressure and the yield stress of the softer material in pure shear. All such models involving asperity deformation assume : 1) that welded junctions form and are sheared, and 2) that such a junction has isotropic properties, making use of an average (based on isotropy) interfacial shear strength. This type of slip line analysis cannot be applied to strongly textured anisotropic materials.

Recent work by Komvopolous, et al.[A14] on aluminum, copper, and chromium promotes the importance of an additional factor, plowing, as the predominant contributor to the coefficient of friction. Plowing is described by the grooving of the surface of one material by either the hard asperities of another or by the "work hardened" debris particles (possible sheared off welded junctions) accumulated during sliding over the surface, hence adhesion is given a less predominant role. Here again isotropic "shear" properties are assumed. It is interesting to note that, while they have performed rather elegant mathematical calculations for the cases of plowing by both a cone and a hemisphere, the agreement between their predictions and experiments is not very good (figure A2). This simply illustrates how difficult simplified modelling of friction can be.

Schey[A15] has written a condensed review on the "laws" of friction in which he concludes that, due to the complicated interactions of the many variables involved, simple laws will never be found. Rigney and Hirth[A16] try to model steady state sliding of metals in terms of work hardening, recovery and microstructure. This is the most realistic approach this author has found, in that it addresses many of the interactions involved, and makes use of microstructural features. However, they note that of the 5 factors required to predict friction, ω, t, and L (the width and depth of the highly deformed region, and the load, respectively) are directly measurable "for a given sliding situation", and that τ, the shear stress of "the highly deformed region" can be estimated from "appropriate tests on severely cold-rolled material with similarly textured cell microstructures". Unfortunately, there are no experimental results in their work, only predicted trends. As is usual, and this is the reason the DBS test is so useful, each frictional situation is unique and "post-mortem" values (ω and t) are required for computation, hence the predictive value is clouded.

It clearly is not an easy task to model friction. For the case of EG steel, one has to additionally be concerned with the anisotropic slip characteristics of hcp zinc, the possibility of dynamic recrystallization, twinning, and zinc transfer to the tooling. As such no attempt will be made to predict friction in this work. Only to explore the micromechanisms and delineate which factors may be the most relevant.

REFERENCES

A1 F.P. Bowden & D. Tabor, "Adhesion, Surface Damage and the Mechanism of Friction", in : **Friction and Lubrication**, Butterworths, Inc., Washington D.C., (1965), pp. 20-32.

A2 Ibid, "The Breakdown of Oxide Films and the Friction of Clean Surfaces", pp. 33-43.

A3 John A. Schey, **Tribology in Metalworking, Friction, Lubrication, and Wear**, published by Amer. Soc. for Metals, (1983), Metals Park, OH, p.73.

A4 C.A. Coulomb, "Mémoires de Mathématique et de Physique de l'Académie Royale des Sciences", (1785), p.161.

A5 G. Amontons, "Histoire de l'Académie Royale des Sciences avec les Mémoires de Mathématique et de Physique, (1699), p.206.

A6 E. Orowan, *Proc. Instn. Mech. Eng.*, v.150, (1943), p.140.

A7 M.C. Shaw, A. Ber, & P.A. Maman, *J. Basic Eng.*, v.82, (1960), p.342.

A8 G.A. Tomlinson, *Phil. Mag.*,(1929), v.7, p.905.

A9 E.S. Machlin & W.R. Yankee, *J. Appl Physics*, (1954), v.25, p.576.

A10 E. Rabinowicz, *Trans. ASLE*, v.1, (1958), p.96.

A11 C.M. Edwards & J. Halling, "An Analysis of the Plastic Interaction of Surface Asperities and its Relevance to the Value of the Coefficient of Friction", *J. Mech. Eng. Sci.*, v.10, n.2, (1968), pp. 101-110.

A12 J.M. Challen & P.L.B. Oxley, "An Explanation of the Different Regimes of Friction and Wear Using Asperity Deformation Models", *Wear*, v.53, (1979), pp. 229-243.

A13 T. Wanheim, N. Bay, & A.S. Petersen, "A Theoretically Determined Model for Friction an Metal Working Processes", *Wear*, v.28, (1974), pp. 251-258.

A14 K. Komvopolous, N. Saka, & N.P. Suh, "The Mechanism of Friction in Boundary Lubrication", *Trans ASME*, v.107, n.10, (1985), pp. 452-462.

A15 J. A. Schey, "Friction Laws in Metalforming Tribology", in **Proc. 2nd Int. Conf. on Technology of Plasticity**, Stuttgart, (August 24-28, 1987), Springer-Verlag, N.Y., pp. 873-882.

A16 D.A. Rigney and J.P. Hirth, "Plastic Deformation and Sliding Friction of Metals", *Wear*, v.53, (1979), pp. 345-370.

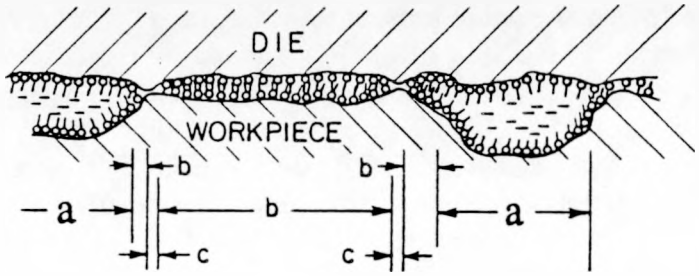

Figure A1) "Mixed" lubrication regime for sheet metal forming (adapted from ref. A3).

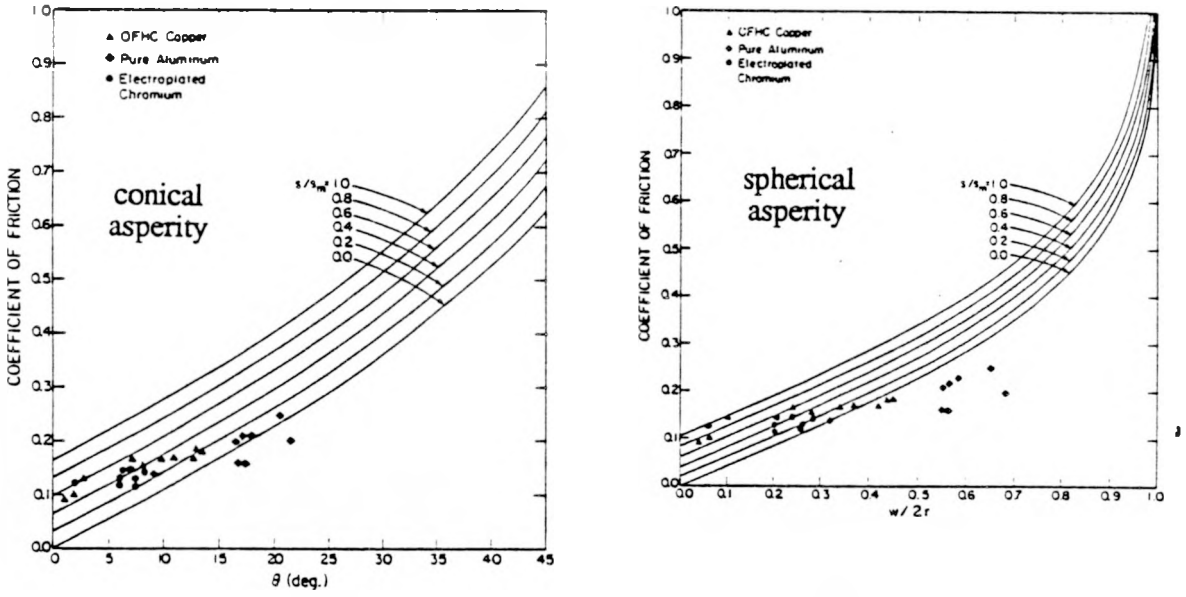

Figure A2) Difficulty in simplistic modelling of friction via single mechanism is illustrated in this work of Komvopolous, et al.[A14], for friction due to plowing.

APPENDIX B

In-Sheet-Plane Texture Measurement Method

Measurement The relative intensities of x-ray reflections from a polygranular sample without any texture (random orientation) can be theoretically predicted and/or experimentally measured. Note that in the so-called "powder method", care should be taken to maintain the zinc powder in a reducing atmosphere. Powder samples of zinc generally have extensive oxide present which change the relative intensity ratios due to oxide peak overlap. Fine zinc filings, compacted by isostatic compression (to prevent texture formation during compaction) can also be used. The measured values from the ASTM/JCPDS card #4-0831 can also be used. Alternatively the intensities may be calculated from crystal structure. See for example Cullity[B1] pages 107-143.

For non-random orientation distributions, these relative intensities are altered by the relative amounts of grains oriented with a particular plane parallel to the sheet. A commonly used and fairly rapid, simple technique for partial texture measurements makes use of normalization of measured intensities by the predicted intensities expected from a polygranular texture-free sample. An indication of the texture of the coating is obtained as follows:

Using a powder diffractometer (Cu K_α radiation was used in this work) with the sample in reflection geometry, a 2-theta scan is performed and the integrated intensities of several reflections is determined, these are termed I_{hkil} (where hkil refers to the Miller-Bravais indices of the reflecting plane). Note that integrated intensities require background subtraction. Additionally for zinc coatings on steel, one must be careful using the $11\bar{2}2$ reflection (there is an overlap with the iron 211 peak) and that the $10\bar{1}3$ and $11\bar{2}0$ reflections are properly deconvoluted.

Another caution is to exclude from the calculation higher order reflections such as 0004, $20\bar{2}0$, $20\bar{2}2$, etc. which are multiples of 0002, $10\bar{1}0$, $10\bar{1}1$ respectively and should have the same percentage. Each I_{hkil} is normalized by dividing it by its structure factor or "random" intensity, I^o_{hkil}, giving I^n_{hkil}. The values of I^o_{hkil} for zinc from the ASTM/JCPDS card for the 10 reflections used in this work are given in Table A1. The sum of these I^n_{hkil} is then computed, giving the total normalized intensity: I^n_{tot}. At this point one of two methods can be employed, however the results differ only by a scaling factor.

Table A1 X-Ray Intensities for Normalization

Number	Reflection	I/I_o	Number	Reflection	I/I_o
1	0002	53	6	$11\bar{2}0$	21
2	$10\bar{1}0$	40	7	$11\bar{2}2$	23
3	$10\bar{1}1$	100	8	$20\bar{2}1$	17
4	$10\bar{1}2$	28	9	$10\bar{1}1$	3
5	$10\bar{1}3$	25	10	$20\bar{2}3$	8

To obtain a "percentage of grains" with a particular orientation comparison, one divides each I^n_{hkil} by the I^n_{tot}) and multiplies by 100. For a random distribution of

orientations, each orientation would have the same percentage, equal to 100 divided by the number of reflections used in the calculation. For example 10% if 10 reflections are measured, and 12.5% if only 8 are used. This technique represents percentages of orientations only from those reflections used in the calculations. A limitation is that if too few peaks are used, the primary texture can be missed.

To obtain a "times random" comparison, one first divides I^n_{tot} by the number of reflections used in the calculation and uses this number to divide each I^n_{hkil}. Here, each reflection from a zinc coating with no texture would have a value equal to 1, while a preference of grains with a particular plane parallel to the sheet surface would have a value greater than one. Similarly an orientation "less than random" would have a value less than one. This may have a more physical appeal, but again the values are representative of only those reflections measured.

Representation For facilitating physical interpretation, the results are presented in a column chart with the orientations progressing from left to right, from basal through low angle pyramid, high angle pyramid, to the two prism planes, as shown schematically in the main text in Figure E3 (page 24). Applications for this technique include quick surveying of both commercial and experimentally deposited coatings as well as an indicator of the consistency of the production line characteristics.

Limitations Due to the geometry of a 2-theta scan, the above technique gives only an indication of a preference of grain orientations with a particular plane parallel to the sheet surface, without information about rotational distributions. Results of this technique therefore assume a fiber texture, or radial symmetry about the sheet normal (represented by the angle ψ in this work). For applications such as paint adhesion and corrosion resistance, this knowledge may be sufficient. In deformation modelling work however, calculations of resolved shear stresses (RSS), strains, and grain rotations depend not only on the orientation of the basal planes with respect to the sheet, but on the orientation of the a-axes about the c-axis, as well as the rotational distribution of the grains about ψ (Fig. R2, main text page 36).

References

B1 B.D. Cullity, "Diffraction II: Intensities of Diffracted Beams", in **Elements of X-Ray Diffraction**, Addison-Wesley, Menlo Park, 2nd Edition, (1978), pp. 107-145.

APPENDIX C

LISTING for RSS CALCULATIONS (Microsoft Basic for Macintosh)

```
REM  This program, written by Steve Shaffer and Armelle Philip (based on an
REM  FCC version written by Jean-Hubert Schmitt) will calculate the resolved
REM  shear stress on several slip systems and calculate the maximum.  The
REM  required input are the vectors "d" and "n", which are the slip direction
REM  and slip plane normals for a HEXAGONAL system.  These must be in a
REM  separate file called "zinc slips" and be in the form of unit vector components
REM  d1, d2, d3, n1, n2, n3 for each slip system.

DIM q(3,3), sig(11,3,3), sigrain(11,1,1,12,3,3), n(6,18), alpha(11)
DIM tau(18),psi(12),theta(1),phi(1)

pi=3.141592654#

REM  alpha is the fraction of compression (represented by k)
REM  (1-alpha) is the amount of shear  (alpha=1 is all compression, alpha=0
REM  is all "simple shear".
REM  phi is the rotation about the crystal c axis (represented by l: 0-50° by 10)
REM  theta is the rotation about the new crystal a-axis : a' (represented by m: 0, 35.5,
61.7)
REM  psi is the rotation about the normal to the sheet plane (represented by n: 0-165° by
15)
REM  q is the (3*3) transformation tensor matrix which depends on phi, theta, and psi
REM  sig are the (3*3) stress tensors in the sheet frame (3 of them)
REM  sigrain are the (3*3) stress tensors in the crystallographic frame
REM  n holds the (3+3=6) "slip system" unit vectors "d" and "n" for 18 slip systems
REM  tau is the resolved shear stress for each of the 18 slip systems

OPEN"I",#5,"zinc slips"
OPEN"O",#4,"calcRSS"
'OPEN "CLIP:TEXT" FOR OUTPUT AS 1
'open "LPT1:PROMPT" for output as 1

REM  this section sets the limits for alpha and the three parameters psi, theta, and phi
REM  (which are the Euler angles phi1, BIG PHI, and phi2).
REM
REM  ********************
REM  To compute RSS for a particular θ angle (tilt of basal plane from sheet plane)
REM   You must change the value of teh "active" theta(1) below.
REM  The program is currently set up for 11$\bar{2}$2 texture (61.7° from sheet plane).
REM  ******************

FOR k=1 TO 11: alpha(k)=(k-1!)/10!: NEXT k
'FOR l=1 TO 6: phi(l)=pi/18*(l-1) : NEXT l
'theta(1)=0.: phi(1)=0!
'theta(1)=35.5*pi/180!
theta(1)=61.7*pi/180!:phi(1)=30!*pi/180!
FOR n=1 TO 12: psi(n)=pi/12*(n-1) : NEXT n
```

```
REM  this section creates the 11 stress tensor matrices (depending on the
REM  fraction alpha) in the specimen sheet coordinate frame

FOR k=1 TO 11
sig(k,1,1)=0!: sig(k,1,2)=0!: sig(k,2,1)=0!: sig(k,2,3)=0!: sig(k,3,2)=0!: sig(k,2,2)=0!
sig(k,1,3)=1!-alpha(k): sig(k,3,1)=sig(k,1,3): sig(k,3,3)=alpha(k)
NEXT k

REM  the following subroutine transforms from the specimen coordinates into
REM  the crystallographic coordinate frame.

GOSUB Changebase

REM  this subroutine determines the resolved shear stress on each system
REM  and the maximum resolved shear stress amongst them.

GOSUB RSS
CLOSE#5
CLOSE#4
END

REM  this subroutine transforms coordinates from the specimen
REM  (sheet) system to the crystallographic coordinate system.

Changebase:

FOR l=1 TO 1: FOR m=1 TO 1 : FOR n=1 TO 12

REM  this section creates the 864 "Q" matrices,; 1 for each orientation of phi &theta &psi

q(1,1)=COS(phi(l))*COS(psi(n))-COS(theta(m))*SIN(phi(l))*SIN(psi(n))
q(1,2)=COS(phi(l))*SIN(psi(n))+COS(theta(m))*COS(psi(n))*SIN(phi(l))
q(1,3)=SIN(phi(l))*SIN(theta(m))
q(2,1)=-SIN(phi(l))*COS(psi(n))-SIN(psi(n))*COS(theta(m))*COS(phi(l))
q(2,2)=-SIN(phi(l))*SIN(psi(n))+COS(psi(n))*COS(phi(l))*COS(theta(m))
q(2,3)=SIN(theta(m))*COS(phi(l))
q(3,1)=SIN(psi(n))*SIN(theta(m)): q(3,2)=-SIN(theta(m))*COS(psi(n)):
q(3,3)=COS(theta(m))

REM  this section determines coordinates in the hexagonal system
REM  when phi,theta,psi are known

'phi1=phi(l)*180/pi
'theta1=theta(m)*180/pi
'psi1=psi(n)*180/pi

'WRITE#1, "phi,theta,psi";phi1,theta1,psi1
'WRITE#4, "phi,theta,psi";phi1,theta1,psi1
'PRINT#4," rolling direction, transverse, normal in hexagonal axes"
'FOR i=1 TO 3
'da1=q(i,1)+q(i,2)/SQR(3) : da2=2*q(i,2)/SQR(3) : da3=-(da1+da2) : dc=q(i,3)
'WRITE#4, da1,da2,da3,dc
```

```
'NEXT i

FOR k=1 TO 11
FOR i=1 TO 3: FOR j=1 TO 3
sigrain(k,l,m,n,i,j)=0!
FOR k1=1 TO 3: FOR l1=1 TO 3
sigrain(k,l,m,n,i,j)=sigrain(k,l,m,n,i,j)+q(i,l1)*q(j,k1)*sig(k,l1,k1)
NEXT l1: NEXT k1
NEXT j: NEXT i
NEXT k: NEXT n: NEXT m: NEXT l
RETURN

REM  this subroutine computes the resolved shear stress for each of the 3
REM  alphas, 6 phis, 3 thetas, and 12 psis on each of the 6 (soon to be 18) slip systems

RSS:

REM  This section imports the "slip systems" in the form of matricies of unit
REM  vectors of "n" the normal to the slip plane, and "d" the slip direction.
REM  These are in the crystallographic coordinate system.

FOR i=1 TO 6
INPUT#5,  n(i,1),n(i,2),n(i,3),n(i,4),n(i,5),n(i,6)
'PRINT "system :";i
'PRINT "normal : [";n(i,1);n(i,2);n(i,3);n(i,4);n(i,5);n(i,6);"]"
'WRITE #1, "system :";i
'WRITE#1, "system : [";n(i,1);n(i,2);n(i,3);n(i,4);n(i,5);n(i,6);"]"

WRITE #4, "system :"; i
WRITE #4, "system :";n(i,1);n(i,2);n(i,3);n(i,4);n(i,5);n(i,6)
NEXT i

FOR n=1 TO 12
psi(n)=psi(n)*180/3.14159268#
NEXT n

FOR l=1 TO 1
phi(l)=phi(l)*180/pi
NEXT l

FOR m=1 TO 1
theta(m)=theta(m)*180!/pi
NEXT m

 FOR k=1 TO 11
FOR l=1 TO 1: FOR m=1 TO 1 : FOR n=1 TO 12
'WRITE#1, "alpha,phi,theta,psi";alpha(k),phi(l),theta(m),psi(n)
WRITE#4, "alpha,phi,theta,psi";alpha(k),phi(l),theta(m),psi(n)

taumax=0!: ns=0!

REM this section determines the resolved shear stress
```

```
FOR i=1 TO 6
tau(i)=0!

FOR k1=1 TO 3
FOR l1=1 TO 3
tau(i)=tau(i)+n(i,k1)*n(i,l1+3)*sigrain(k,l,m,n,k1,l1)
NEXT l1:NEXT k1
'PRINT "Resolved shear stress : tau = "; tau(i)
WRITE #4, "Resolved shear stress : tau = "; tau(i)

REM  this section determines the maximum resolved shear stress between
REM  each slip system (use of absolute value accounts for positive and
REM  negative directions).

IF ABS(tau(i))>taumax THEN taumax = ABS(tau(i)):ns=i ELSE GOTO suite
suite:  NEXT i
'PRINT "Maximum resolved shear stress , on slip system # : ";taumax,ns
'WRITE#1, "Maximum resolved shear stress , on slip system # : ";taumax,ns
WRITE#4, "Maximum resolved shear stress , on slip system # : ";taumax,ns

FOR i=1 TO 6
IF (ABS(tau(i))=taumax) OR (ABS(tau(i))>.9*taumax) THEN  WRITE#4, tau(i),i ELSE
GOTO suite2
suite2: NEXT i

NEXT n: NEXT m: NEXT l: NEXT k

RETURN

REM  ****************************************************************
REM  Below is a sample of the file "Zinc slips" used by this program :

REM  1,0,0,0,0,1
REM  -.5,.866,0,0,0,1
REM  -.5,-.866,0,0,0,1
REM  1,0,0,0,1,0
REM  .5,-.866,0,-.866,-.5,0
REM  .5,.866,0,.866,-.5,0

REM   Note that this particular set is for basal (the top three)
REM  and prism slip (the bottom three) in the 11-20 direction only.
REM  ****************************************************************
```

APPENDIX D

Computation of Equivalent Loads and Pressures for the DBS and Stripdraw Tests

The average pressure over the surface of the DBS sample as it passes over the drawbead is computed by dividing the clamping load by the width and the sliding contact length of the specimen. At an average clamping load of 363 Kg_f (800 lbs.), over a specimen width of 1.5 inches, with a theoretical sliding distance of $\pi/2$ x .953 cm (3/8"), we arrive at a pressure of around 6.2 MPa (900 psi.).

The actual contact sliding length however is considerably less than the theoretical one due to non-conformity of the specimen to the exact geometry of the cylindrical bead. According to Harmon Nine(AD1), the inventor of the test and the equipment, the strip loses contact in places and a better estimate for the sliding length is $\pi/4$. This is shown in figure AD1. This will vary depending on the thickness and yield strength of the strip, but this is a reasonable estimate. Using this sliding distance, we arrive at a pressure of 12.4 MPa (1800 psi.).

For the same width sample, at a contact area of 1mm to 1.5 mm for the straight stripdraw test,we then arrive at an load for an equivalent pressure of about 50 to 75 Kg_f (110 to 170 lbs.).

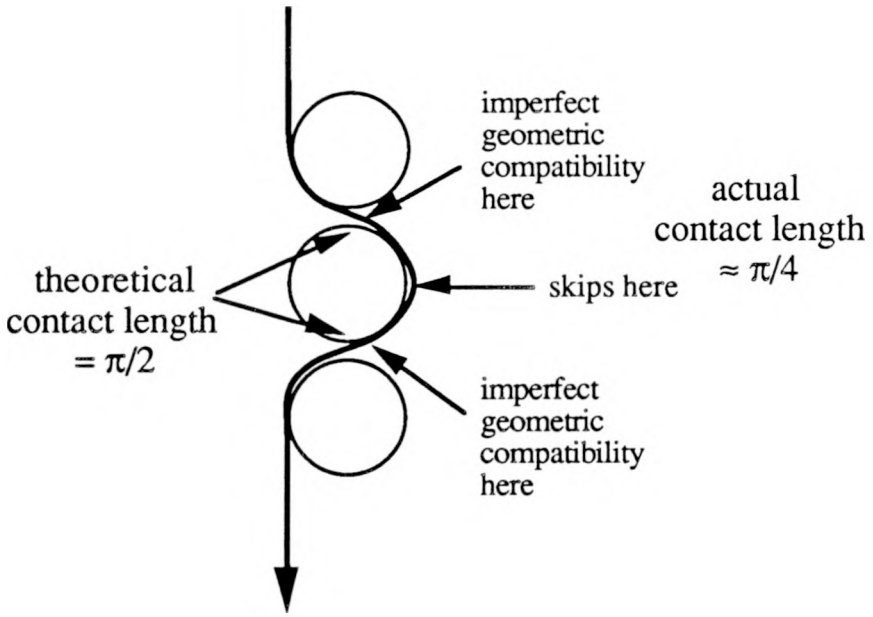

Figure AD1 Actual sliding distance is nearly half that of the theoretical value resulting from imperfect geometric compatibility due to unbending and skipping.

REFERENCES

AD1 H.D. Nine, personal communication, General Motors Research Center, (May, 1989).

APPENDIX E

A Proposed Technique for Deconvolution of Composite Textures as a Function of Depth.

INTRODUCTION

Several methods of metal processing result in a variation of texture with depth. In rolled aluminum-lithium sheets for example, it has been demonstrated that large differences in texture exist through the thickness, possibly affecting its fracture toughness[1]. In this case, the "layers" making up the composite texture are thick enough that it is possible to mechanically separate them (by cutting and grinding for example) in order to measure the texture of the individual layers themselves.

In other cases however, the thickness of the layers in which variations in texture take place is too small with respect to the penetration depth of x-rays for such mechanical separation techniques. In electrogalvanized (EG) steel for example, where a 5 to 10 μm thick coating of zinc is electrodeposited upon a 0.9 mm steel substrate, use of this technique on the thin zinc layer is not possible. Additionally, in friction tested EG sheets, the entire surface area in not deformed, only some 50 to 80%. This too must be accounted for if truly quantitative texture work regarding the deformed regions is desired.

Several instances arise where deconvolution of possible composite textures are desired. Work by Rangarajan, et al.[2] has indicated some question as to the homogeneity of texture with zinc coating thickness. In work involving surface friction studies of EG steel, a very thin surface layer of the zinc, on the order of less than one micron, is deformed by some combination of shear and compression due to friction testing[3].

Deformation modelling studies for surface friction require information solely from the deformed layer. In some friction tests, such as drawbead simulation, where there is alternating tensile and compressive deformation superimposed on top of the surface shearing and compression, the situation is much more complicated.

A technique involving alternating successive texture measurements and chemical surface layer removal, along with the formulation necessary to deconvolute the composite textures is being developed. This section will describe the principle of this technique.

METHOD

Let us take for example an idealized zinc coating, 10.3 μm thick, in which the top 1 micron has a texture T_1 and the lower 9.3 microns has a texture T_2 (figure AE1). Let us further assume that 75% (f^D) of the coating has this composite texture, while the remaining 25% (f^{1-D}) is undeformed, and hence has the original texture. Such a composite texture might be produced as a result of a surface friction test. After recording the undeformed texture (T_o), we then measure the texture of the "composite" coating resulting from the

friction test, followed by chemically etching away the top 1 μm and remeasuring the texture of the remaining coating. In a simplistic view, we can subtract the second texture (T_2) from the first ($T_1 + T_2$), accounting for the respective undeformed (1-D) and deformed (D) area fractions, and arrive at the texture of the deformed region from the layer which was chemically removed.

$$T_1 = [(T_1 + T_2) - (T_2)]f^D - (T_o)f^{1-D} \quad (1)$$

There are two problems which must be overcome. The first is that the intensity of the diffracting signal received at the detector (assuming perfect Bragg reflection) varies with depth. As the x-rays penetrate deeper into the material they are absorbed and hence the contribution from each successively deeper layer is decreased as measured by the exiting intensity. The second difficulty is how to account for this variation in intensity due to different thicknesses of samples using normalized pole figures. Additionally, we wish to exclude the portion of the coating which was not deformed at all. Proposed methods of accounting for both problems are described below.

SIGNAL CONTRIBUTION VARIATION WITH DEPTH

For a particular absorbing material and radiation used, one can calculate the attenuation of the incident intensity as a function of penetration depth using the relation[4] :

$$I/I_o = \exp^{-(\mu/\rho)\rho x} \quad (2)$$

where μ/ρ is the mass absorption coefficient, ρ is the density and x is the linear distance in cm (in this example : zinc - $\rho = 7.19$ gms/cm^3, $\mu/\rho = 109.6$ cm^2/gm for Fe K_α radiation). Further, assuming perfect Bragg scattering and knowing the angle of the particular reflection used, it is possible to compute the exiting intensity as a function of depth, substituting the relationship:

$$x = 2d/\sin\theta \quad (3)$$

in equation (2) above and plotting I/I_o as a function of depth, d. The geometry for this situation is shown in figure AE2 and the resulting intensity as a function of depth is shown in figure AE3a (same as figure R20, page 54 in the main body of this text) for the particular case of the (0002) reflection for zinc : 2θ=46.12°.

In order to properly weight the signals from different depths, one simply needs to integrate the I/I_o function. For example, it is found that 3.34, 2.74, 2.26, and 1.86 percent of the total signal reaches the detector from the material at the specific depths of 0.5, 1.0, 1.5, and 2.0 μm respectively. Making use of either analytical integration between fixed limits or, in our simple example, numerical integration using a step size of 0.1 μm, one

finds that 18.1, 32.9, 45.1, and 55.2 percent of the signal comes from the material down to a depth of 0.5, 1.0, 1.5, and 2.0 μm respectively. This is illustrated by the shaded regions in figure AE3b.

DIFFERENCE BETWEEN TWO NORMALIZED POLE FIGURES

While pole figures are generally normalized such that the total intensity of poles distributed over the specimen coordinate space is fixed[5], the perimeter region of such experimentally measured pole figures are generally not reliable and are often excluded from the normalization routine. This leads to a different total intensity than pole figures where reliable information at the periphery exists and hence can lead to complications in quantitative comparisons between the two types, or between experimentally measured, incomplete pole figures.

To overcome this, various methods exist for the computation of the orientation distribution function (ODF) from experimentally measured pole figures. The result of ODF calculations can be used to calculate complete, properly normalized pole figures from experimentally measured ones for comparative quantitative analysis. Further, such normalized, recalculated pole figures are useful for simple visual qualitative comparisons. In this work, the popLA[6] package was used.

The problem now remains to perform the subtraction between three previously normalized pole figures, taking into account the fact that the signal strengths should be different. This requires the modification of equation (1). We propose that this be done on a point by point basis between the two measured pole figures according to the following equation:

$$I^c = [(I^A - 1)f^{dA} + (I^B - 1)f^{dB}]f^D + [(I^{A+B} - 1)f^{1-D}] + 1 \qquad (4)$$

where I = normalized pole figure intensity at a given ϕ and χ , c = composite, A and B = upper and lower layers as defined in figure AE1, f^d = fraction from depth A or B as computed by the integration of equation 2, and D = deformed area fraction, respectively. We note that $I^{A+B} = I_o$, the intensity of the original undeformed sample.

What we have done here is to use a random intensity as the baseline, in this case 1, which is subtracted from each point in the normalized pole figure. This result is then multiplied by the fraction of the total signal from which the texture of interest comes. The final result must then be added back to the baseline, or random intensity. Solving equation (3) for I^A, the intensity of the chemically removed layer, we get :

$$I^A = 1 + (\{[(I^c - 1) - (I_o - 1)f^{1-D}] / f^D - (I^B - 1)f^{dB}\} / f^{dA}) \qquad (5)$$

from which the pole figure of the chemically removed layer can now be renormalized and replotted.

Once the techniques of controlled etching and thickness measurement are established for the particular material of interest, in principle, this technique can be applied to "chemically section", measure, and deconvolute textures from materials where the texture changes occur over thicknesses too small for other techniques. All of this work can be done on a personal computer, and the results of one preliminary example of such pole figure manipulations are shown in figure AE4.

CONCLUDING REMARKS

The development of a technique for deconvolution of textures from thin layers, which accounts for the variations in signal intensity due to depth as well as pole distribution normalization, should prove particularly useful for texture studies in thin films and surface layers. The proposed technique in this section is a start in this direction, however it has not yet been verified by other investigators. Additionally, for precisely quantitative work, one should also account for the change in signal intensity with tilt angle, ϕ. This has been neglected in this work.

REFERENCES

1) A.K. Vasudevan, W.G. Fricke, Jr., R.C. Malcolm, R.J. Bucci, M.A. Przystupa, & F. Barlat, "On Through Thickness Crystallographic Texture Gradient in Al-Li-Cu-Zr Alloy", *Metall. Trans.*, v. 19A, (March 1988), pp. 731-732.

2) V. Rangarajan, et. al., "The Effect of Texture and Microstructure on Deformation of Zinc Coatings", *J. Mater. Shap. Tech.*, v.6, no.4, (1989), pp. 217-227.

3) S.J. Shaffer, J.W. Morris, Jr., & H.-R. Wenk, "Textural Characterization and its Applications on Zinc Electrogalvanized Steels", in **Zinc-Based Steel Coating Systems: Metallurgy and Performance**, G. Krauss & D. K. Matlock, eds., TMS, Warrendale, PA, 1990, pp. 129-140.

4) B.D. Cullity, "Diffraction II: Intensities of Diffracted Beams", in **Elements of X-Ray Diffraction**, Addison-Wesley, Menlo Park, 2nd Edition, (1978), p. 13.

5) H.-R. Wenk, "Measurement of Pole Fugures", in **Preferred Orientation in Deformed Metals and Rocks: An Introduction to Modern Texture Analysis**, H.-R. Wenk, editor, Academic Press, Inc., New York, (1985), p.39.

6) J.S. Kallend, U.F. Kocks, A.D. Rollett, & H.-R. Wenk, : **popLA: the Preferred Orientation Package from Los Alamos**, University of California, Los Alamos National Laboratory, 1990. Documented in : "Operational Texture Analysis", *Mat. Sci. and Engin*, (in press).

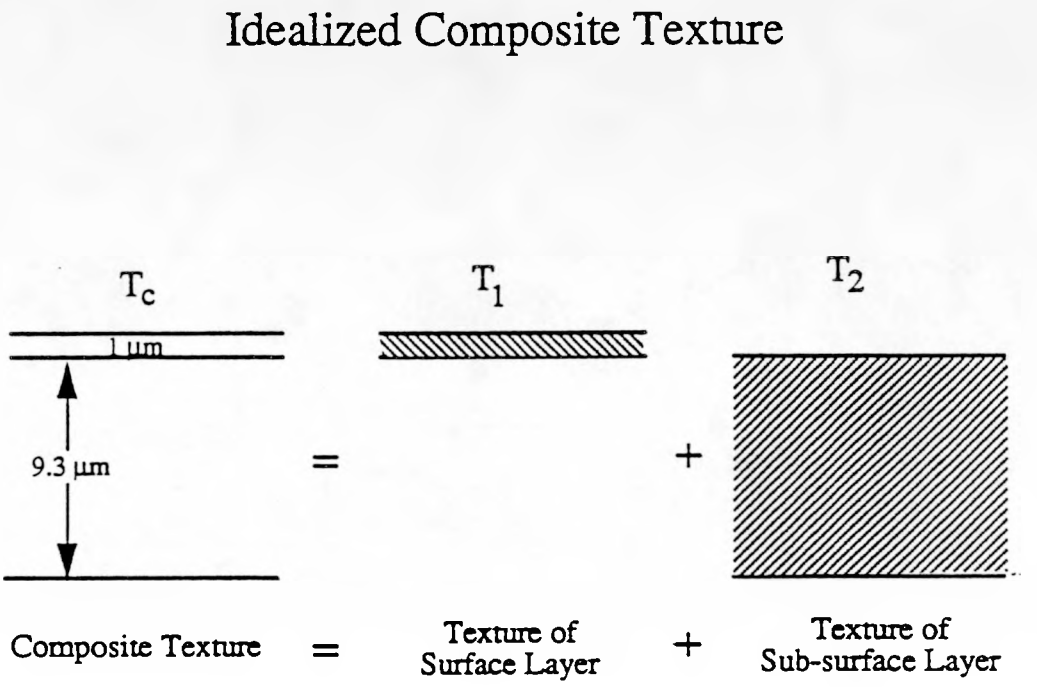

Figure AE1. Idealized composite texture of zinc coating. Top layer has developed different texture through surface friction testing.

ABSORPTION of X-RAYS

$$I/I_o = e^{-(\mu/\rho)\rho x}$$

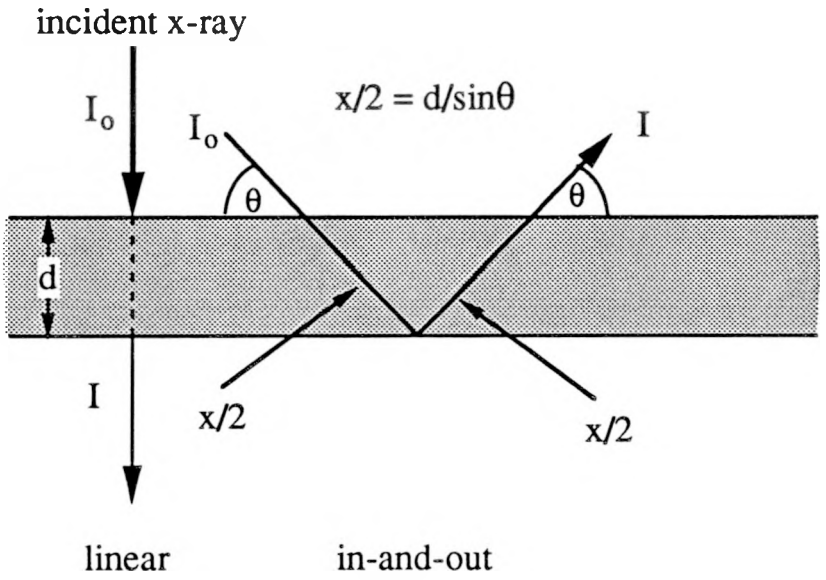

x = linear distance (cm)

μ/ρ = mass absorption coefficient (cm^2/gm)

ρ = density (gms/cm^3)

Figure AE2 Geometry of x-ray absorption, accounting for distance travelled through sample for a particular Bragg reflection angle, θ.

a)

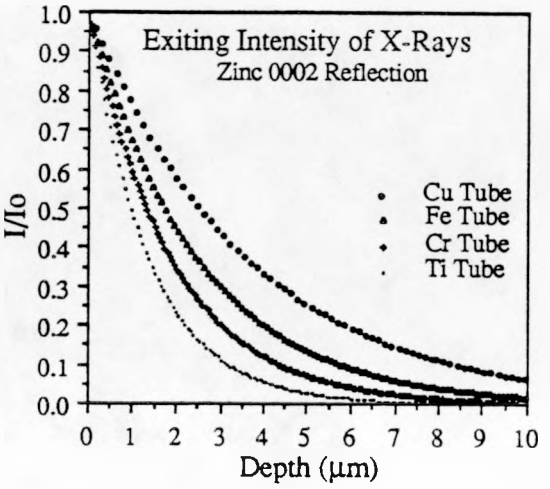

b)

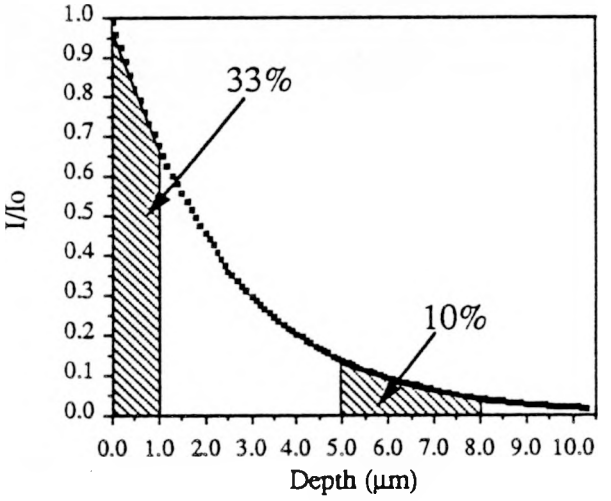

Figure AE3 a) Reduction in intensity of reflected signal due to absorption as a function of depth for several x-ray sources. b) Volume contributing to the signal is given by the area under the curve. Note, for example, that for an Fe x-ray tube, one third of the signal is due to the top 1 μm, while only 10% is contributed from the depth of 5 to 8 microns.

Deconvolution of Composite Textures

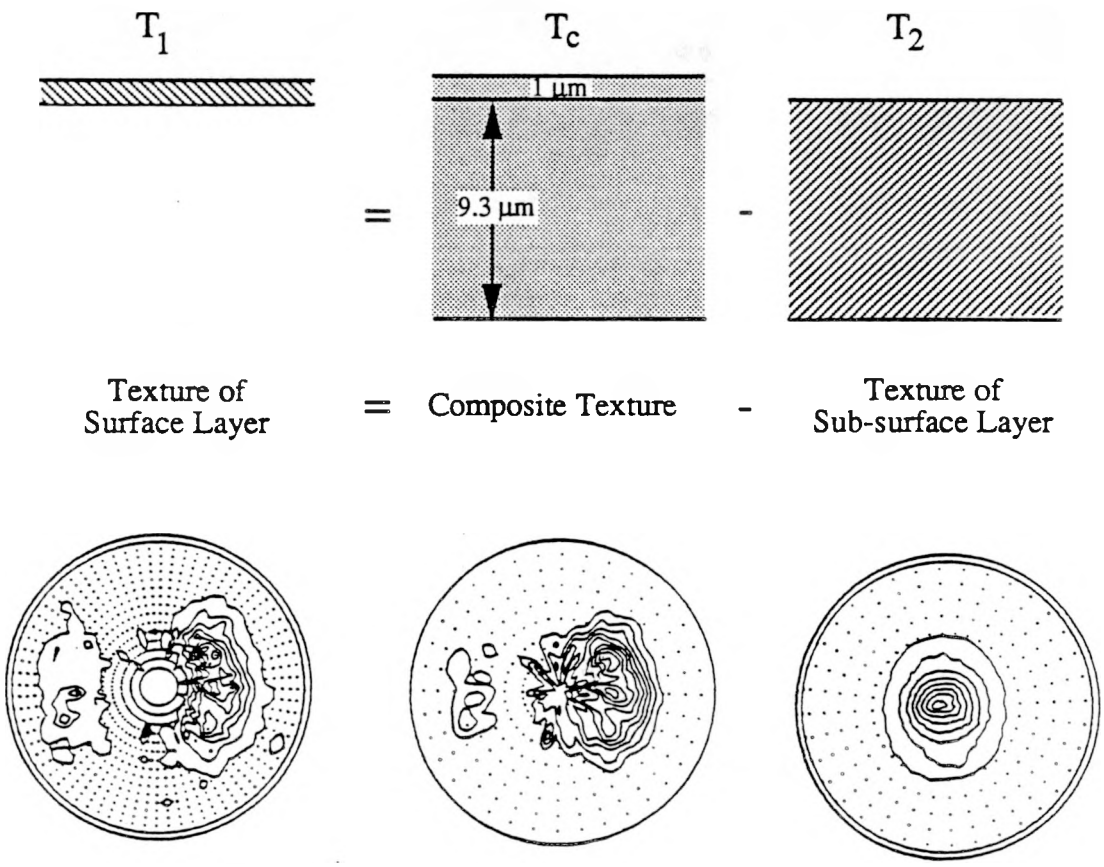

Figure AE4 Example of deconvolution of composite texures. Texture of surface is obtained by subtracting subsurface texture (measured after etching away surface layer) from composite texture. 0002 pole figures.